ABSTRACT

CRAIG, ELLEN J. Sugarloaf Mountain, Central Arizona: an Example of Miocene Andesitic Hybrid Magma Formed from Alkalic Basalt and Crustal Components. (Under the direction of Dr. R.V. Fodor.)

Sugarloaf Mountain is a 200-m high landform in central Arizona within the transition from the southern Basin and Range to the Colorado Plateau. It is composed of Miocene lavas that are alkalic basalt overlain by andesite and dacite. Sugarloaf offers an opportunity to evaluate the origin of andesite magmas with respect to coexisting basalt. Accordingly, sixteen samples were examined for petrography, major- and trace-element abundances, and mineral compositions.

Results: Basalts have 47.2 to 49.1 wt.% SiO_2 and 6.7 to 7.7 wt.% MgO, and they contain olivine (Fo_{73-86}) and clinopyroxene ($Fs_{8-13}Wo_{45-49}$; Mg# 78-84) phenocrysts. Three samples plot as alkalic basalt on a TAS diagram, and one sample plots as trachy-basalt. Regionally, Sugarloaf alkalic basalts are generally similar to the nearby (< 10 km) Stewart Mountain alkalic basalts but are slightly more enriched in incompatible trace elements. Andesites (and dacite) have 61.4 to 63.9 wt.% SiO_2 and 3.5 to 4.7 wt.% MgO. They also have olivine (Fo_{77-86}) and clinopyroxene ($Fs_{8-18}Wo_{35-45}$; Mg# 73-86) phenocrysts, and additionally have quartz (0.2-3.0 vol.%), Na-plagioclase (An_{28-47}; 3-6 vol.%), amphibole (Mg# 60-65), ± orthopyroxene ($Fs_{22-35}Wo_{2-3}$; Mg# 65-77), ± biotite (Mg# 60), ± Na,K feldspar ($Ab_{33-42}Or_{58-66}$). Notable for the andesites are (i) resorbed quartz, Na-plagioclase, and amphibole grains; (ii) spongy zones and margins in and on Na-plagioclase cores, some with thin, more calcic plagioclase rims (An_{48-53}), and (iii) most incompatible element abundances lower than those in the basalts (e.g., Ce 77-105 vs 114-166 ppm; Zr 149-173 vs 183-237; Nb 21-25 vs 34-42).

Conclusions: Fractional crystallization of Sugarloaf basalt cannot alone yield the andesites because (a) their 61.4 to 63.9 wt.% SiO_2 cannot be achieved at 3.5 to 4.7 wt.% MgO under any P or fO_2 conditions (e.g., modeling by MELTS; mass-balancing), and (b) their low incompatible element abundances cannot be achieved by fractionation trends from ≈7 wt.% MgO in basalt to 3.5-4.7 wt.% MgO. On the other hand, andesite mineral assemblages, textures, and compositions are all consistent with basaltic magma having mixed with rhyolitic magma or having assimilated crustal granitoid rock. Binary mixing (assimilation) calculations yield good results for producing andesite compositions. For example, best fit curves for calculated major element values versus actual major element values have $R^2 > 0.99$. In particular, a hybrid mix of 73% average upper-crust composition and 27% Sugarloaf basalt is one example of endmember proportions that create a model hybrid that resembles Sugarloaf andesite. While the mixing results suggest that Sugarloaf andesites are hybrids of basalt and SiO_2-rich crustal material, the low-trace elements in the andesite indicate that the crustal material had to be not only SiO_2-rich but also depleted in trace elements. It is possible for rock with such a composition to occur in continental crust. For example, a quartz- and feldspar-rich rock could have both high SiO_2 and low trace elements.

The coexisting Sugarloaf basalt types — alkalic and trachy — can be explained by equilibrium melting calculations showing that the higher incompatible trace element abundances in the trachy-basalt are likely due to a lower degree of partial melting from the same mantle source as for the alkalic basalts (e.g., Zr/Nb, Zr/Ba, La/Sm, and Th/La are similar).

This model for mixing between basaltic and rhyolitic magmas at Sugarloaf Mountain to produce hybrid intermediate magmas is consistent with models for the origins of intermediate lavas at Mount Hood, in the Ecuadorian Andes, and in New Zealand's Taupo Volcanic Zone. Sugarloaf Mountain represents a relatively small volcanic field that further supports the origin of andesites by magma mixing processes that are known to have operated in volcanic provinces on a global scale.

Sugarloaf Mountain, Central Arizona: an Example of Miocene Andesitic Hybrid Magma Formed from Alkalic Basalt and Crustal Components

by
Ellen J. Craig

A thesis submitted to the Graduate Faculty of
North Carolina State University
in partial fulfillment of the
requirements for the Degree of
Master of Science

Marine, Earth, and Atmospheric Sciences

Raleigh, North Carolina

2015

APPROVED BY:

_____	_____
Dr. R.V. Fodor Committee Chair	Dr. Karl Wegmann
_____	
Dr. David McConnell	

DEDICATION

This thesis is dedicated to my whole family and all the animals.

BIOGRAPHY

Ellen Craig was born in the Spruce Pine mining district of North Carolina and grew up on Rocky Knob, a landform composed of gneiss and quartzite. Favorite pastimes include waterfall hopping along the Blue Ridge Escarpment in North Carolina. Professors Arpita Nandi and Yongli Gao at East Tennessee State University shared their enthusiasm for geologic research with her through their terrific teaching and mentoring. In 2012, she came to NC State to work with Dr. Ronald Fodor for her masters project in igneous petrology and geochemistry.

ACKNOWLEDGMENTS

Thank you to my advisor, Dr. Ronald Fodor, for all of the expertise, work, and attention that he has given to this thesis. Thank you also to my committee members, Dr. David McConnell and Dr. Karl Wegmann, for their contributions of knowledge, time, and concern to my graduate program. Thank you to Laura Holland, Gary Lackmann, Connie Hockaday, and Martha Canizales for being so helpful and friendly at all times. Thank you to Katherine Ryker, Nathan Lyons, Bruce Riddell, April Grissom, Dough Cjazka, Steve Smith, Mike Pelch, and Hayley Smith for getting me through my TA assignment. Thank you to my fellow petrologists and geochemists, Chao Li, Mike Mohr, Stephen Hughes, and Kelly Johnson for always being available to talk rocks. Last but not least, thank you to Sandra Yuter, Gabriel Zilnik, and Brian Langerhans for their mentorship as scientists outside the classroom.

Special thanks to the Geological Society of America for a graduate student research grant and to R.S. Jacobs of Caird Energy for financial support for analyses and thin sections for this project.

TABLE OF CONTENTS

LIST OF TABLES

LIST OF FIGURES

GEOLOGIC SETTING

RESULTS

DISCUSSION

INTRODUCTION

Several processes have been identified for the origins of intermediate-composition magmas, such as those represented by andesitic lavas. Intermediate magmas can be direct melts of upper mantle lherzolite or amphibolite, differentiated from basalts, or hybrid mixes of basalts and continental crust (Anderson, 1976; Eichelberger, 1978; Rudnick, 1995; Annen *et al.*, 2006; Reubi, 2009; Kent *et al.*, 2010; Eichelberger, 2010). Because intermediate-magma origins are varied and complex, and often represent multiple processes, it is important to geochemically and mineralogically examine andesite occurrences not yet studied in petrologic detail. Sugarloaf Mountain, a volcanic field in central Arizona (Fig. 1A) is one such candidate for the study of andesite origins. It is a small (≈2 km^2) field composed of Miocene basaltic lavas with overlying lavas described as intermediate in composition based on their amphibole and quartz phenocrysts (Skotnicki, 1991; Skotnicki & Leighty, 1997). The coexisting basaltic and intermediate lavas at Sugarloaf Mountain make it a reasonable volcanic field at which to evaluate how intermediate-composition lavas may be related to basaltic magmas.

In order to explore this relationship between basaltic and hornblende- and quartz-bearing lavas, I collected 16 lava samples that represent Sugarloaf Mountain from its base to its peak, about 200 vertical meters. My objectives were to determine if the intermediate lavas formed by (i) differentiation of basaltic magma; (ii) hybridization of basaltic magma through mixing with rhyolitic magmas or through assimilation of continental crust; (iii) a

combination of these processes; or (iv) by a process independent of the coexisting basaltic lavas. My objectives were addressed by determining the petrographic details and the major and trace element whole-rock compositions of all 16 samples, as well as mineral compositions in representative samples. Additionally, I explored the relationship between the intermediate and basaltic lavas through mass balancing model calculations, MELTS software modeling, and calculations that represent simple mixing between Sugarloaf Mountain basaltic magma and various proportions of crustal material. Finally, I evaluated the basalts in terms of how they compare to nearby basalt and how they compare within the Sugarloaf Mountain volcanic field.

GEOLOGIC SETTING

Sugarloaf Mountain is a small (≈2 km^2) (Fig. 1B) volcanic field approximately 10 km north of the large (≈8000 km^2) Goldfield-Superstition volcanic province (G-SVP) in central Arizona (Fig. 1A). Both volcanic fields are part of a volcanic region near the northern boundary of the southern Basin and Range physiographic province at the transition to the Colorado Plateau (Fig. 1A). The nearest basalt field is Stewart Mountain (Fig. 1A; Singer & Fodor, 2013), ≈10 km southwest of Sugarloaf Mountain.

Ages of 20.53 to 15.92 Ma ($^{40}Ar/^{39}Ar$ for sanidine) were determined by McIntosh & Ferguson (1998) for silicic lavas and tuffs of the G-SVP. Shafiqullah *et al.* (1980) determined an age of ≈15.53 Ma for the nearby Stewart Mountain volcanics and also determined an age

of ≈14.78 Ma for andesite from the area of Bartlett Dam, which is ≈15 km NNW of Sugarloaf. Based on these ages for nearby volcanic fields, Sugarloaf Mountain lavas are inferred to represent Miocene volcanism and to have been deposited ≈20–15 Ma. No age-dating has been conducted for the Sugarloaf lavas themselves. Detailed geologic mapping of Sugarloaf Mountain was conducted by Skotnicki (1992) as part of an M.S. thesis project and later by the Arizona Geologic Survey (Skotnicki & Leighty, 1997).

Crustal shortening occurred in western North America due to the subduction of the Farallon plate from approximately 155 to 60 Ma (Liu, 2001). Subduction slowed and ended from ≈50–20 Ma as the Farallon plate foundered beneath North America (Burchfiel *et al.,* 1992; Humphreys, 1995). This event was followed by extensional tectonics and magmatism in western North America (Lipman, 1992). Following the end of active subduction of the Farallon plate, Eocene to early Miocene magmatism occurred in regions across the Cordillera of southwestern North America (Christiansen & Yeats, 1992; Liu, 2001). The magmatism in the southern Basin and Range province and the transition zone in central Arizona ≈29–15 Ma corresponds to this wave of post-Farallon extensional activity (Glazner & Bartley, 1984; Christiansen & Yeats, 1992; Spencer *et al.*, 1995). Given the relative dating that places Sugarloaf at ≈20–15 Ma, Sugarloaf Mountain lavas would have been emplaced during the final episodes of this extension-related volcanism in central Arizona.

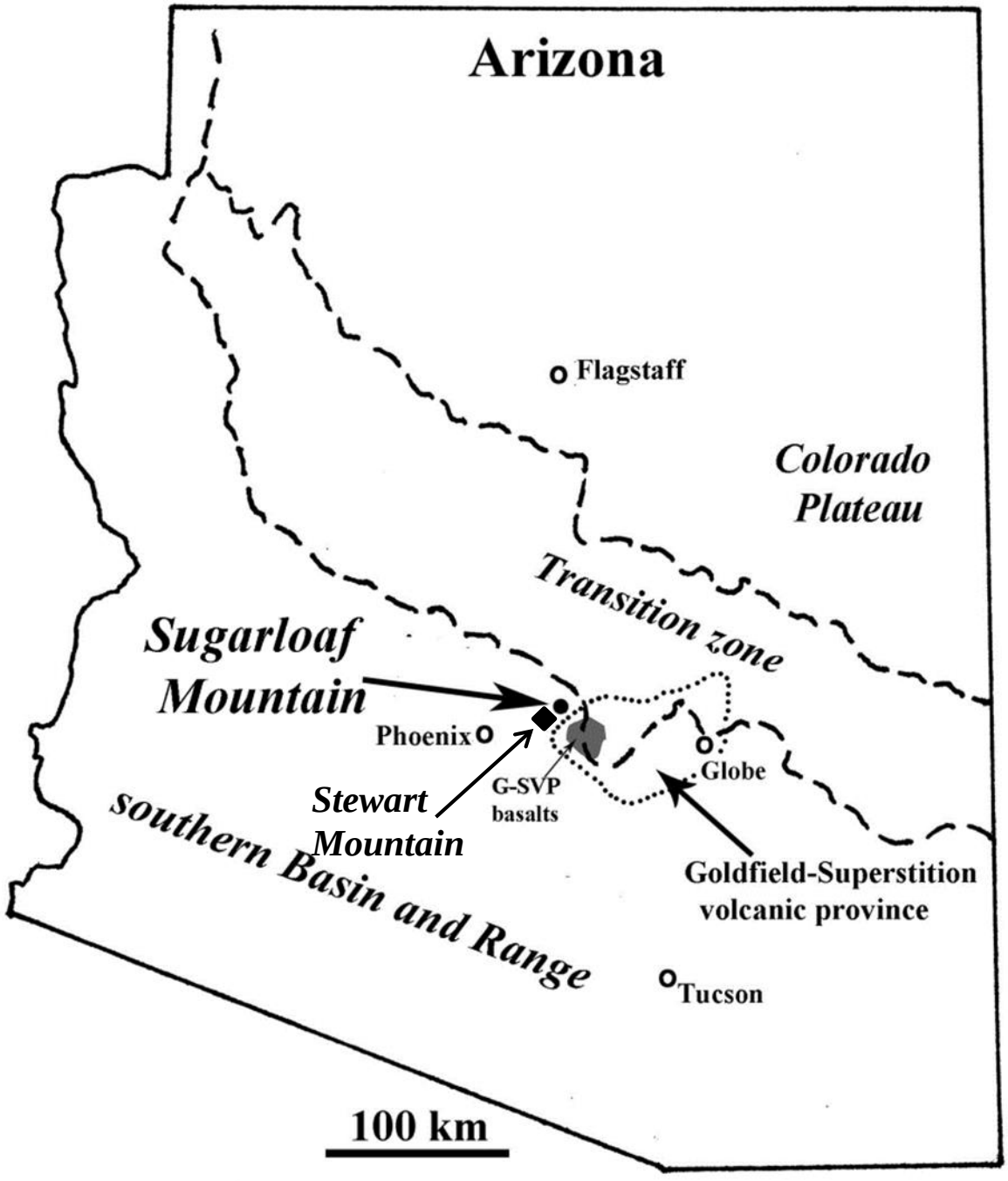

Fig. 1A. Map of Arizona showing the location of Sugarloaf Mountain and the Goldfield-Superstition volcanic province in relation to Phoenix and three major physiographic provinces: the Colorado Plateau, transition zone, and southern Basin and Range. Modified from Singer & Fodor (2013).

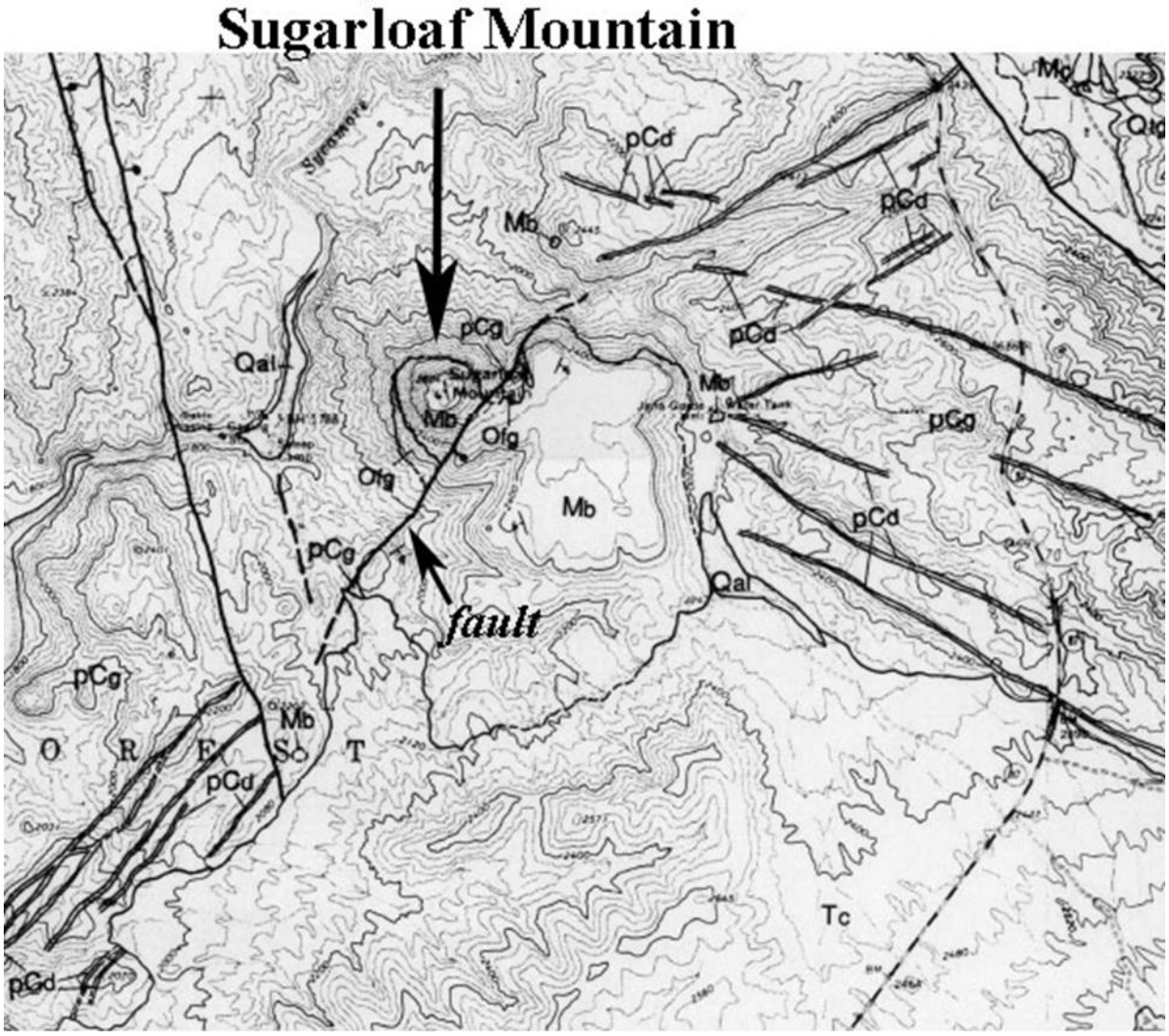

Fig. 1B. Geologic map showing Sugarloaf Mountain (after Skotnicki, 1992) and a northeast-striking normal fault (arrow) southeast of the peak.

Field geology and sampling

Sugarloaf Mountain lavas are distinct in appearance by varying degrees of blockiness, platiness, visicularity, and modal phenocryst minerals. The mountain is also distinguished by its profile of stacked lavas, its mesa, and its peak rising above the mesa (Fig. 2A–B). The mesa is a broad, flat shelf that occurs midway up Sugarloaf (Fig. 3A) and could be the result of normal faulting as mapped by Skotnicki (1992) (Fig. 1B). While intermediate lavas on Sugarloaf are stratigraphically above basaltic lavas, basalts on the peak are found above the intermediate lavas on the mesa, as seen in Fig. 3B. The normal fault transecting Sugarloaf (Fig. 1B) could account for this stratigraphic offset. Therefore, lavas on the mesa may correlate with those near or at the peak. The samples for this study, however, do not attempt to represent every lava flow on Sugarloaf Mountain. Furthermore, the original extent and vent source of the Sugarloaf lavas is unknown. Additional geochemical data for lava flows from the area surrounding Sugarloaf would be necessary to determine whether any remnants of the Sugarloaf lava flows exist apart from Sugarloaf Mountain.

Fig. 2A. Photograph taken from the Sugarloaf mesa (foreground) showing the peak of Sugarloaf in the background. Sugarloaf is ≈200 m high, and the peak rises ≈60 m above the mesa from the location at which this photograph was taken.

Fig. 2B. Photograph by Baldy (2014) of Sugarloaf Mountain facing its south side. This view shows ≈200 m of topographic relief from the base of Sugarloaf to the peak.

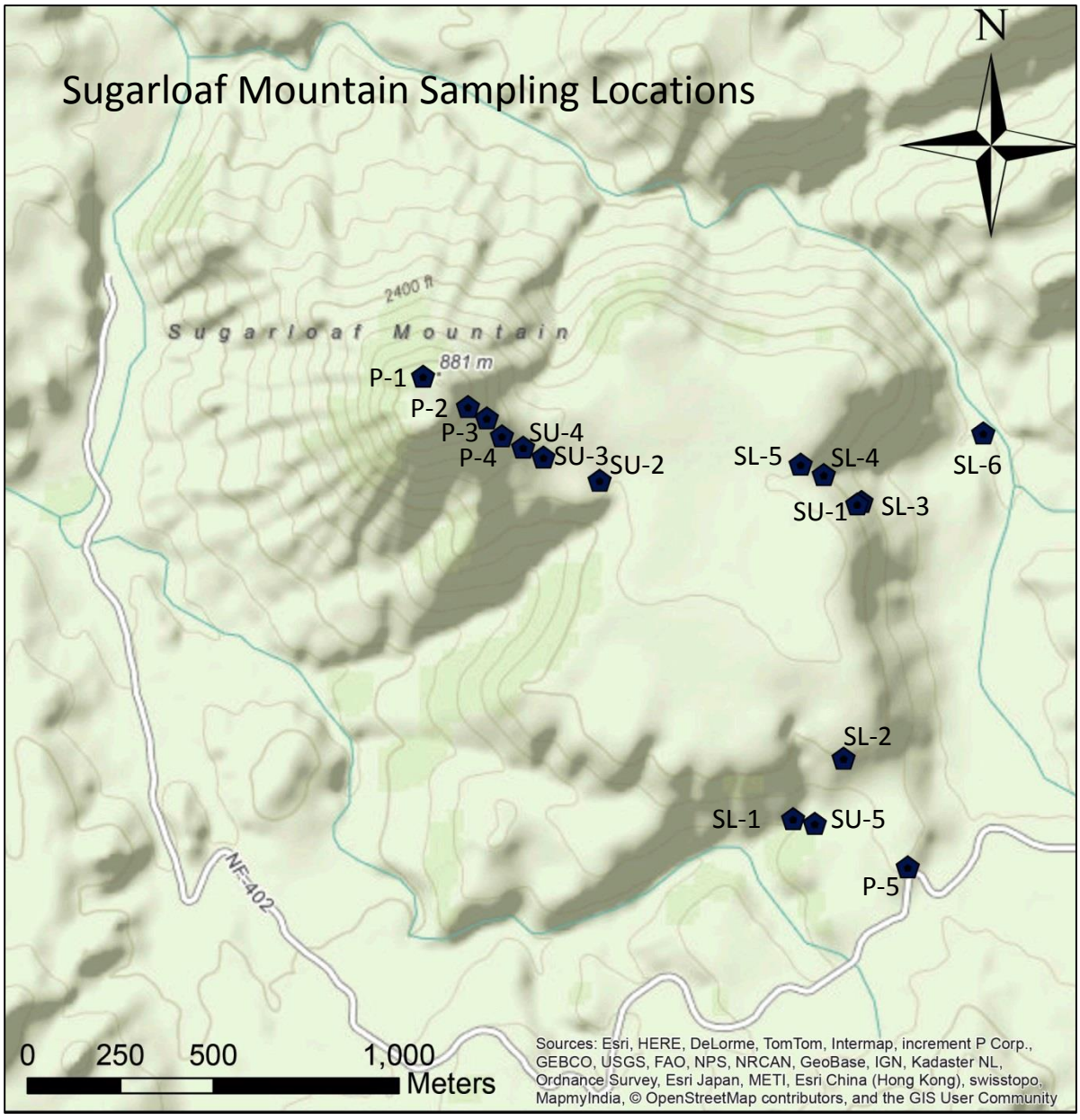

Fig. 3A. Topographic map showing locations where samples were collected from Sugarloaf Mountain.

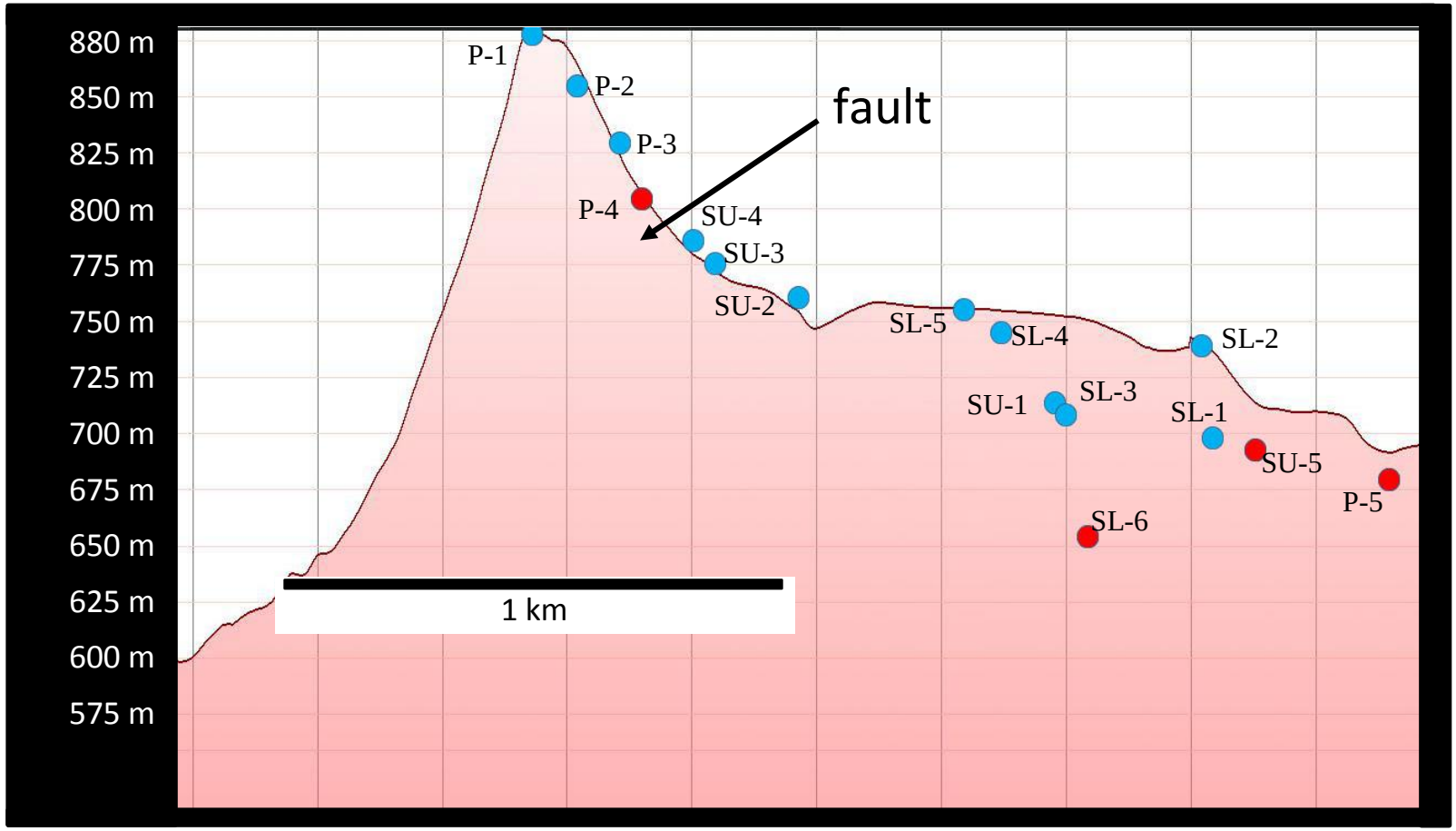

Fig. 3B. Topographic profile of Sugarloaf Mountain created by using Google Earth (2015). Sample locations are shown as red (basalts) and blue dots (intermediate lavas). Lavas near the base may correlate with those near the peak due to the normal fault (arrow).

METHODS

Sixteen samples were collected from the peak of Sugarloaf down to the lowest outcroppings at its base. This represents ≈200 m of relief. Sample locations were selected to represent lava flows on the basis of least weathering and are labeled on the topographic map in Fig. 3A. GPS coordinates are listed in Appendix B.

Analytical Techniques

One thin section of each hand sample was studied using a petrographic microscope. Modal percentages were determined by counting 1500–2000 points on each thin section. Whole-rock major element compositions were determined by X-ray fluorescence on fused glass discs, and trace element compositions were determined by inductively coupled plasma mass spectrometry on rock powders. Each analytical technique was performed by Acme Analytical Laboratories in Vancouver, BC. Mineral compositions were determined using an ARL-SEMQ electron microprobe in the Department of Marine, Earth, and Atmospheric Sciences at North Carolina State University. Analytical conditions were 15 keV, 0.015 μA sample current, and 10-second peak and background counting times. Mineral standards used were olivine, clinopyroxene, orthopyroxene, microcline, plagioclase, albite, ilmenite, and magnetite, all obtained from the Smithsonian Institution.

RESULTS

Petrography

The basalts are samples P-5, SU-5, SL-6, and P-4. The modal compositions are in Table 1. All four samples are porphyritic and have phenocrysts of clinopyroxene (9–15 vol. %) and olivine (2–7 vol. %) (Table 1, Figs. 4, 5K–L). Additionally, P-4 has ≈3 vol. % Fe-Ti oxide phenocrysts. Clinopyroxene grains are subhedral and ≈1 mm in size or less. Olivine is subhedral and ranges in size from 0.5–2.5 mm, and many grains have iddingsite rims or are completely iddingsitized. Fe-Ti oxide is subhedral to anhedral and ≈1 mm in size. Except for SL-6, each sample has an intergranular groundmass of plagioclase laths, olivine as iddingsite, clinopyroxene, Fe-Ti oxides, and interstitial feldspar (Fig. 5K–L). SL-6 has a micro-hyaloophitic groundmass with plagioclase and Fe-Ti oxide microlites.

The andesitic samples are SL-4, SL-1, P-3, SU-2, SU-1, SL-2, SU-4, SU-3, SL-3, P-1, P-2, and SL-5. All of these samples are porphyritic and have phenocrysts of plagioclase (2–7 vol. %), clinopyroxene (1–9 vol. %), quartz (0.2–3 vol. %), amphibole (0.1–3 vol. %), and olivine (0.1–2 vol. %), and some have trace amounts of alkali feldspar, orthopyroxene, and biotite phenocrysts (Table 1, Figs. 4–5). Additionally, there is a lithic fragment in SL-3. Plagioclase is generally subhedral and ranges in size from 0.5–4 mm. Notable about almost all plagioclase phenocrysts are spongy zones—some surrounded by thin (<10 microns) plagioclase rims—and smooth resorbed margins (Fig. 5A–D). Olivine is subhedral to euhedral, 1–2 mm in size, and many grains have iddingsite rims or are completely

Table 1: Modal compositions (in volume %) of basaltic, andesitic, and dacitic rocks from Sugarloaf Mountain, central Arizona

	Basalt				Andesite											Dacite
	P-5	SU-5	SL-6	P-4	SL-4	SL-1	P-3	SU-2	SU-1	SL-2	SU-4	SU-3	SL-3	P-1	P-2	SL-5
Olivine	5.4	7.2	2.1	6.7	1.3	2.4	1.6	2.1	–	1.1	–	–	0.4	1.6	–	1.2
Clinopyroxene	10.8	11.1	9.5	15.6	2.0	1.4	7.4	7.9	1.5	0.9	5.0	8.6	3.3	1.4	1.0	0.5
Plagioclase	–	–	–	–	2.2	3.3	2.9	2.8	5.7	4.7	5.2	5.5	6.1	2.8	1.8	6.4
Amphibole	–	–	–	–	0.8	1.2	2.3	1.7	3.1	1.0	0.8	2.6	1.1	1.1	1.2	0.9
Quartz	–	–	–	–	1.6	0.7	1.2	0.2	0.7	3.3	1.8	1.8	–	–	0.2	0.8
Orthopyroxene	–	–	–	–	–	0.1	–	–	–	–	–	–	–	–	–	–
Biotite	–	–	–	–	–	–	–	–	–	–	–	–	–	–	–	0.1
Opaques	–	–	–	2.8	–	–	–	–	–	–	–	–	0.8	–	–	–
Lithic Fragment	–	–	–	–	–	–	–	–	–	–	–	–	2.7	–	–	–
Grndmass	83.8	81.7	88.4	74.8	92.1	90.8	84.6	85.2	89.0	88.9	87.2	81.5	85.7	93.1	95.8	90.1

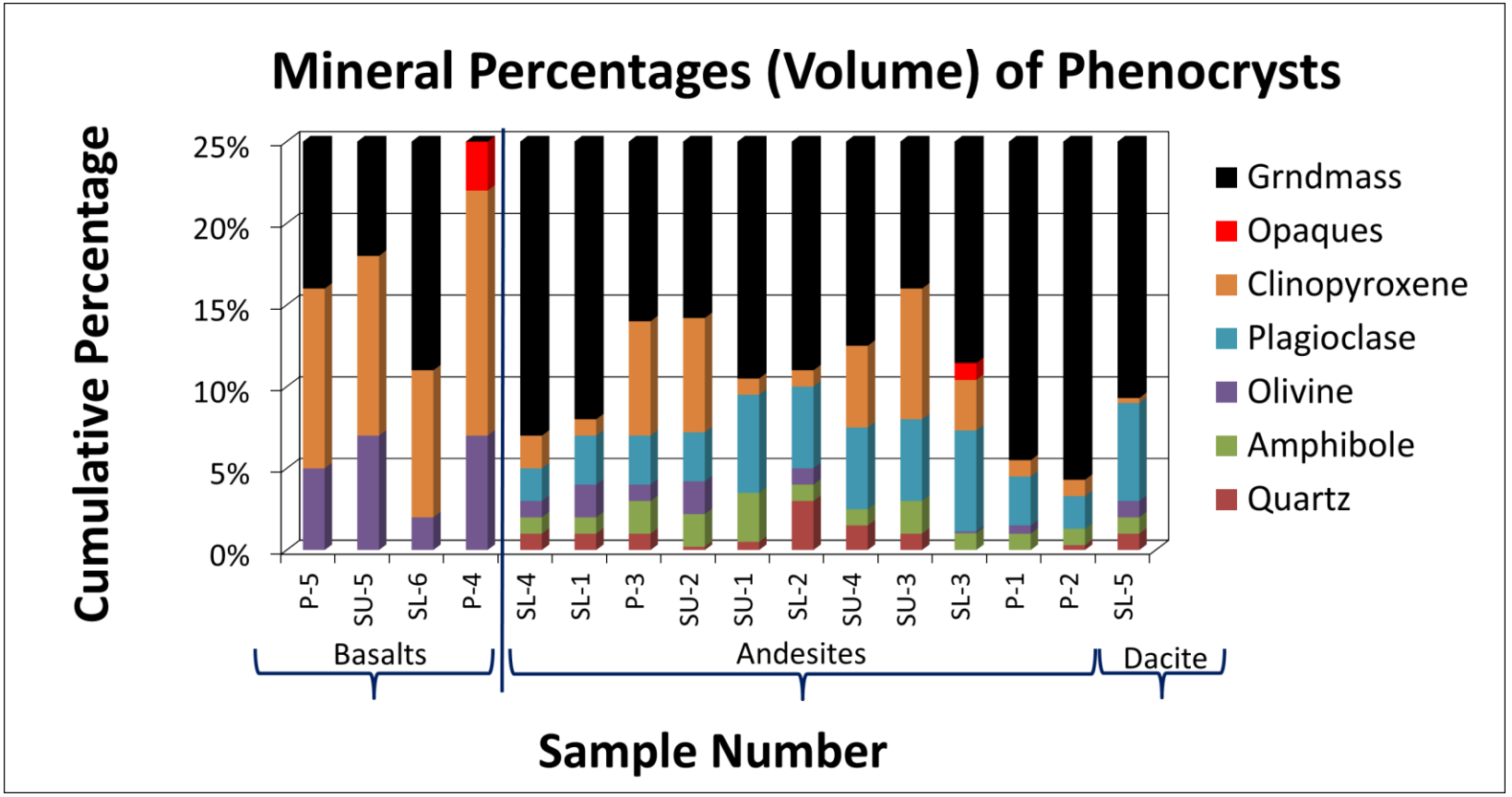

Fig. 4. Graph showing the modal percentages of phenocrysts in Sugarloaf thin sections. Groundmass accounts for 75% or more of each sample, therefore the cumulative percentage axis is cut off at 25%. Lithic fragment is counted as groundmass for this diagram.

Fig. 5. Photomicrographs of minerals in Sugarloaf andesites, dacite, and basalts. All are viewed in cross polarized light except panel H, which is in plane polarized light. All scale bars are 1 mm. Plagioclase with a spongy core surrounded by a reaction zone and thin plagioclase rim in andesite SL-4 (panel A); rounded, spongy plagioclase in andesite P-3 (panel B); rounded plagioclase with spongy center in andesite SL-4 (panel C); spongy plagioclase with a strained quartz (top center) and a small clinopyroxene grain (left center) in andesite P-3 (Panel D); partially resorbed amphibole in andesite SU-4 (panel E); clinopyroxene in andesite SL-4 (panel F); dipyramidal olivine in andesite SL-1 (panel G); arrow pointing to biotite grain next to vesicle in dacite SL-5 (panel H); assemblage of subrounded, resorbed quartz grains in andesite SL-2 (panel I); quartz with reaction rim in andesite SL-4 (panel J); clinopyroxene glomerocryst in basalt P-5 (panel K); two iddingsitized olivine grains in basalt P-4, and a fresh core (blue) in one grain (panel L).

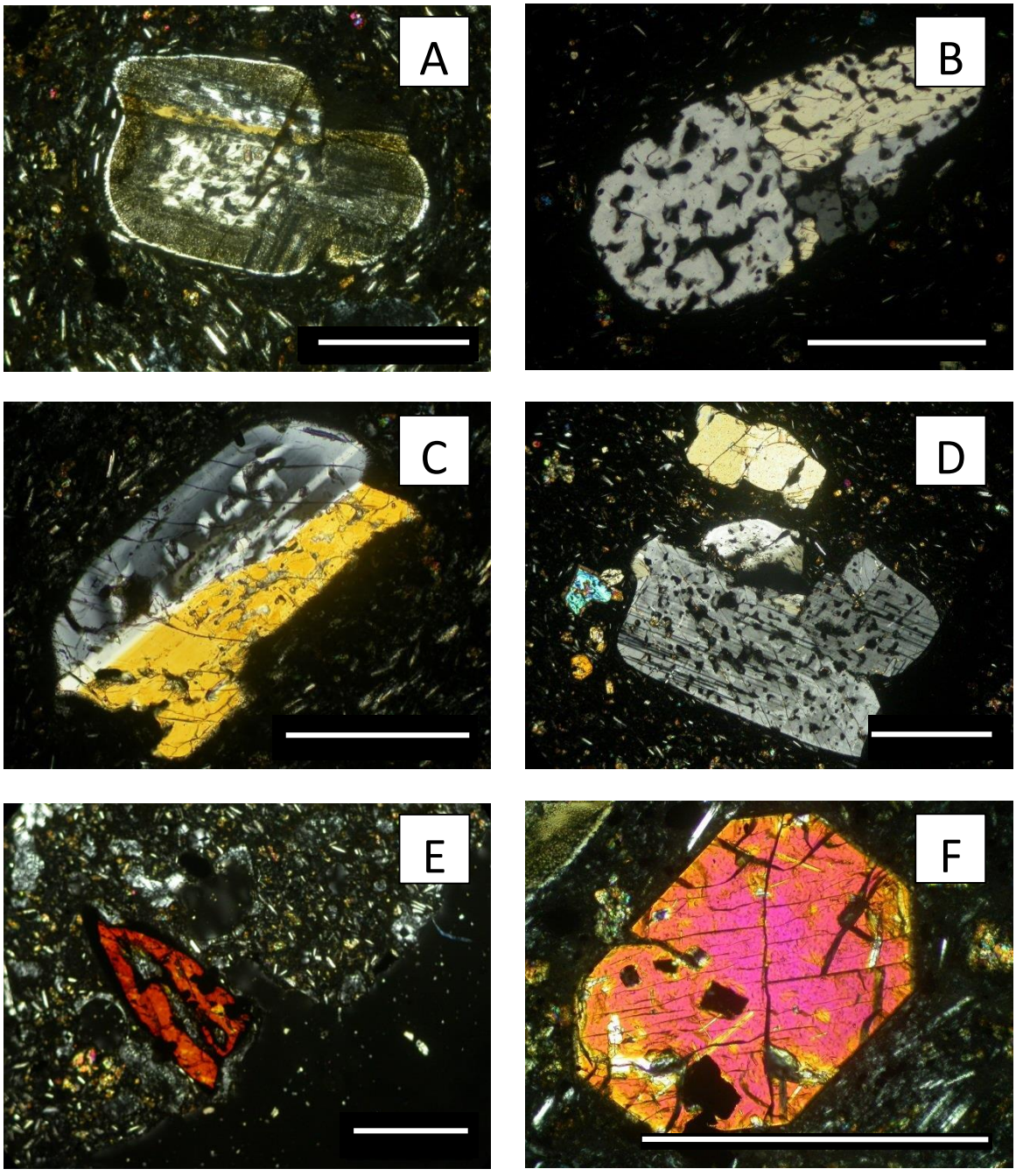
A
B
C
D
E
F

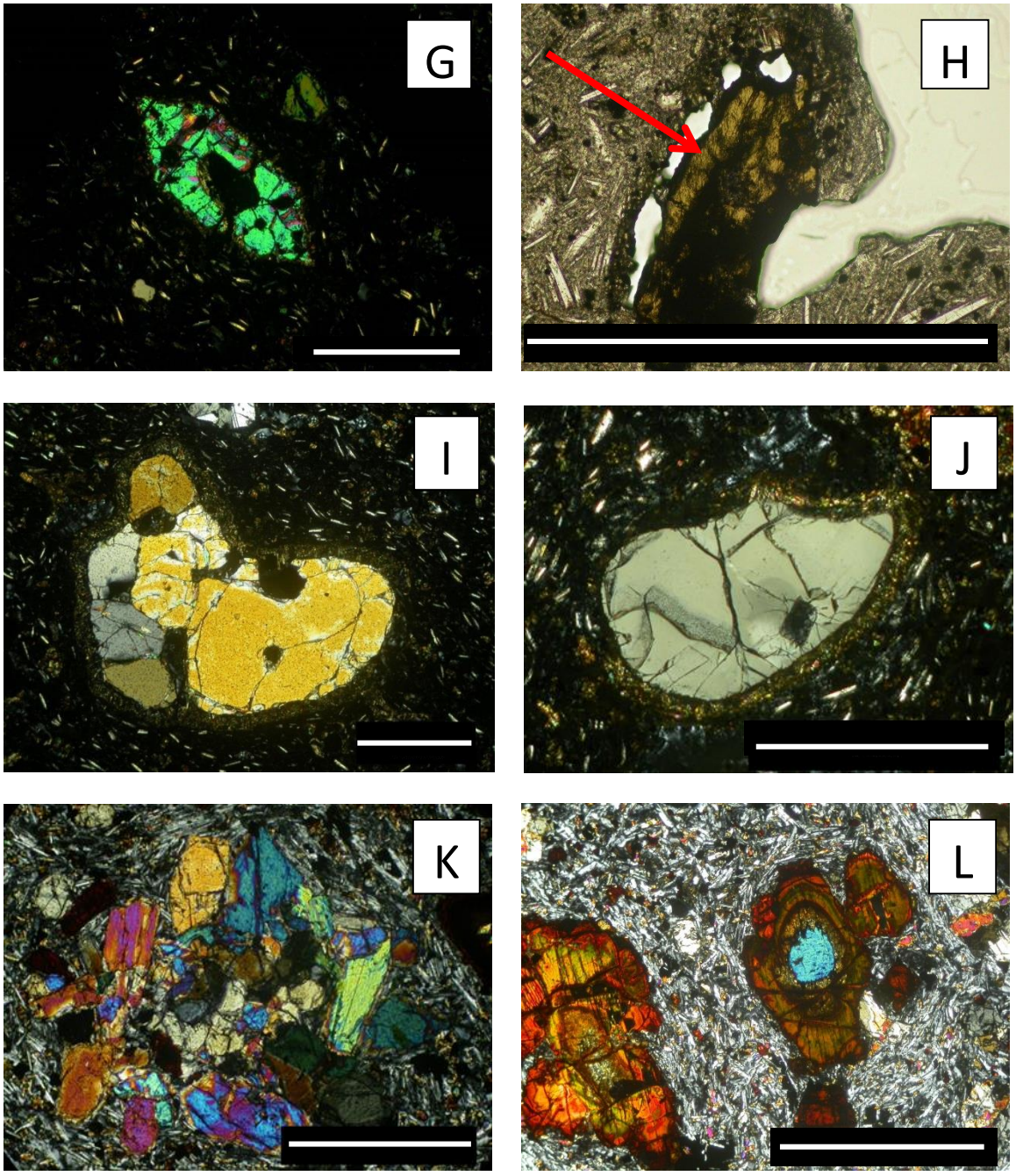
G
H
I
J
K
L

iddingsitized (Fig. 5G). Clinopyroxene is subhedral, ranges in size from 0.5–3 mm, and occurs as single grains and as glomerocrysts (Fig. 5F). Amphibole can be subhedral (Fig. 5E) or can occur as subrounded grains and ranges in size most often from 1–2 mm. Quartz grains are 1–2 mm in size, subrounded, and anhedral, with many grains having smooth resorbed margins and reaction rims of clinopyroxene (Fig. 5I–J). Trace orthopyroxene is subhedral and ≈1.5–2.5 mm in size. Trace biotite is subhedral and ≈1 mm in size (Fig. 5H). The lithic fragment contains iddingsitized olivine, clinopyroxene, and feldspar laths. All andesitic samples have groundmasses that are glassy and contain microlites of plagioclase and Fe-Ti oxides (Fig. 5A–J).

Geochemical results

Whole-rock major and trace element compositions were determined for sixteen Sugarloaf Mountain samples. The results are presented in Table 2, and they are expressed in SiO_2 and MgO variation diagrams (Figs. 6–8). Included on the variation diagrams are basalts from Stewart Mountain, a volcanic field 9.85 km south of Sugarloaf (Singer & Fodor, 2013). Emplaced ≈15.5 Ma (Shafiqullah *et al.,* 1980), Stewart Mountain lavas are the closest basalts of comparable age to Sugarloaf lavas. They therefore offer an appropriate comparative reference for Sugarloaf basaltic lavas. Average compositions for minerals in eight Sugarloaf lavas are presented in Tables 3–7 and illustrated in variation diagrams (Figs. 11–15).

Table 2: Whole-rock major and trace element compositions listed in order of decreasing MgO for basalts, andesites, and dacite from Sugarloaf Mountain, central Arizona

	Basalts				Andesites											Dacite
	P-5	SU-5	SL-6	P-4	SL-4	SL-1	P-3	SU-2	SU-1	SL-2	SU-4	SU-3	SL-3	P-1	P-2	SL-5
SiO_2	49.02	49.13	47.23	49.13	61.81	61.59	61.68	61.62	62.00	62.50	62.47	62.94	62.52	62.68	61.37	63.89
TiO_2	2.01	2.02	2.41	2.08	1.18	1.27	1.25	1.17	1.22	1.09	1.11	1.12	1.22	1.06	1.29	1.02
Al_2O_3	14.02	13.93	14.29	14.30	13.74	13.61	13.72	13.53	13.90	13.17	13.86	13.66	13.94	13.42	13.71	13.72
Fe_2O_3	11.20	11.50	11.78	11.64	6.33	6.86	6.62	6.47	6.50	6.09	6.00	6.20	6.57	5.68	6.91	5.68
MnO	0.17	0.17	0.17	0.16	0.09	0.10	0.10	0.09	0.09	0.09	0.09	0.09	0.09	0.09	0.11	0.09
MgO	7.72	7.55	7.13	6.74	4.69	4.38	4.37	4.37	4.20	4.14	4.06	4.01	3.78	3.69	3.52	3.45
CaO	10.55	10.42	10.56	10.48	5.74	6.21	5.43	5.45	5.70	5.97	5.29	5.18	5.25	6.04	5.52	4.82
Na_2O	3.07	3.11	3.06	3.21	3.24	3.59	3.68	3.64	3.31	3.57	3.86	3.70	3.80	3.53	3.74	3.47
K_2O	1.41	1.43	2.07	1.49	2.27	2.45	2.64	2.62	2.62	2.50	2.35	2.66	2.65	2.69	2.65	2.98
P_2O_5	0.71	0.70	1.00	0.77	0.59	0.45	0.44	0.39	0.42	0.38	0.39	0.39	0.42	0.37	0.44	0.32
Total	99.88	99.96	99.70	100.00	99.68	100.51	99.93	99.35	99.96	99.50	99.48	99.95	100.24	99.25	99.26	99.44
Mg#	60.3	59.1	57.1	56.0	62.0	58.4	59.2	59.8	58.7	59.9	59.8	58.7	55.9	58.8	52.9	57.2
LOI	1.75	1.51	1.04	1.27	2.51	1.77	1.25	1.12	2.30	2.13	1.47	1.36	0.69	2.72	0.91	1.32
Rb	20.90	21.30	34.70	23.90	28.00	34.60	34.80	33.00	31.20	37.10	29.10	37.00	25.70	33.30	29.30	25.70
Ba	942	900	1262	1076	2314	2150	2196	2101	2266	2009	2011	2242	1997	2535	2572	2250
Sr	969	979	1384	1016	850	861	836	793	822	781	779	837	795	763	881	692
Zr	183	184	237	203	165	165	169	168	156	156	160	173	171	149	175	151
Y	22.20	22.00	25.40	24.40	16.50	15.60	14.80	13.80	16.70	14.00	13.70	14.70	13.90	13.00	18.40	12.30
Nb	33.73	34.22	41.47	36.28	22.33	23.90	24.03	22.69	22.40	21.44	21.38	23.42	23.90	20.85	24.62	21.00
Th	7.30	7.20	10.40	7.90	6.40	6.40	7.00	6.40	6.40	6.20	6.60	7.00	5.90	7.10	6.30	5.70
Hf	4.88	4.56	6.10	5.09	4.29	4.33	4.26	4.25	4.08	4.03	4.21	3.94	4.47	4.06	4.51	3.78
Ta	1.80	1.80	2.10	1.90	1.20	1.40	1.40	1.30	1.30	1.30	1.30	1.30	1.30	1.30	1.50	1.20
U	1.70	1.60	2.40	1.90	1.40	1.80	1.80	1.70	1.70	1.70	1.70	1.90	1.70	2.00	1.90	1.50
Pb	7.82	9.24	10.58	8.35	14.23	13.44	16.83	13.59	13.91	13.82	14.75	16.42	14.83	20.41	14.68	15.51
Zn	107	106	117	109	70.50	81.60	88.10	75.40	72.60	71.70	74.30	83.40	79.70	68.40	79.10	65.10
Ni	148	158	89.00	161	84.60	97.40	102	98.80	80.60	81.50	82.80	82.30	96.50	68.80	104	80.30
Co	50.40	46.50	39.70	48.90	22.90	25.40	29.00	25.30	23.80	22.10	22.80	23.30	23.20	19.10	30.30	19.60
Cu	90.60	91.56	85.69	96.21	42.80	59.58	44.50	46.85	42.90	44.05	45.08	39.80	42.89	40.06	48.84	35.46
V	210	208	252	226	101	116	117	109	112	99.00	100	105	113	96.00	125	92.00
Cr	211	229	159	252	153	173	171	156	148	139	140	142	151	135	182	120
Sc	19.90	19.40	19.50	20.00	9.80	10.30	10.40	9.40	9.90	8.80	8.40	9.30	10.10	8.40	9.80	8.10

Table 2, continued

	Basalts				Andesites											Dacite
	P-5	SU-5	SL-6	P-4	SL-4	SL-1	P-3	SU-2	SU-1	SL-2	SU-4	SU-3	SL-3	P-1	P-2	SL-5
La	55.90	57.10	83.00	62.40	56.30	49.60	53.20	51.30	53.00	46.60	49.30	51.80	46.20	48.00	54.00	38.90
Ce	116	114	166	122	95.75	95.17	105	96.40	101	88.72	89.88	98.06	91.95	90.95	96.88	76.88
Pr	13.80	13.30	18.30	14.30	10.30	10.10	10.40	9.50	10.80	9.10	9.60	10.10	9.50	8.90	11.00	7.60
Nd	52.60	54.40	82.20	56.10	42.30	39.80	38.20	34.90	40.90	35.10	35.80	38.40	36.70	33.90	41.70	30.20
Sm	8.70	8.80	12.80	10.60	6.00	5.90	6.70	5.60	6.20	5.10	4.90	6.30	6.10	4.90	6.60	4.00
Eu	2.50	2.70	3.10	2.90	1.20	1.40	1.50	1.10	1.40	1.40	1.20	1.40	1.40	1.20	1.40	1.10
Gd	6.90	6.10	9.30	7.80	4.00	4.80	4.10	3.80	5.00	4.00	3.90	5.80	4.20	4.20	4.90	4.50
Tb	0.80	0.80	0.90	1.00	0.60	0.50	0.50	0.40	0.60	0.50	0.50	0.50	0.60	0.40	0.60	0.50
Dy	4.20	4.50	5.80	4.80	3.60	3.10	3.00	2.40	3.40	2.90	3.30	3.00	3.00	2.90	3.50	2.50
Ho	0.70	0.70	0.70	0.80	0.60	0.50	0.40	0.40	0.50	0.50	0.40	0.40	0.50	0.40	0.60	0.40
Er	2.20	2.10	2.40	2.10	1.60	1.30	1.40	1.30	1.40	1.30	1.40	1.40	1.40	1.30	1.50	1.20
Tm	0.20	0.20	0.30	0.30	0.20	0.20	0.20	0.10	0.20	0.20	0.20	0.20	0.10	0.20	0.20	0.20
Yb	1.90	1.90	2.10	2.00	1.60	1.60	1.50	1.20	1.50	1.30	1.40	1.40	1.40	1.40	1.90	1.30
Lu	0.20	0.20	0.20	0.30	0.20	0.20	0.10	0.20	0.20	0.20	0.20	0.20	0.10	0.20	0.20	0.30

Mg# = mol. MgO/(MgO+FeO)

LOI = loss on ignition at 1,000°C

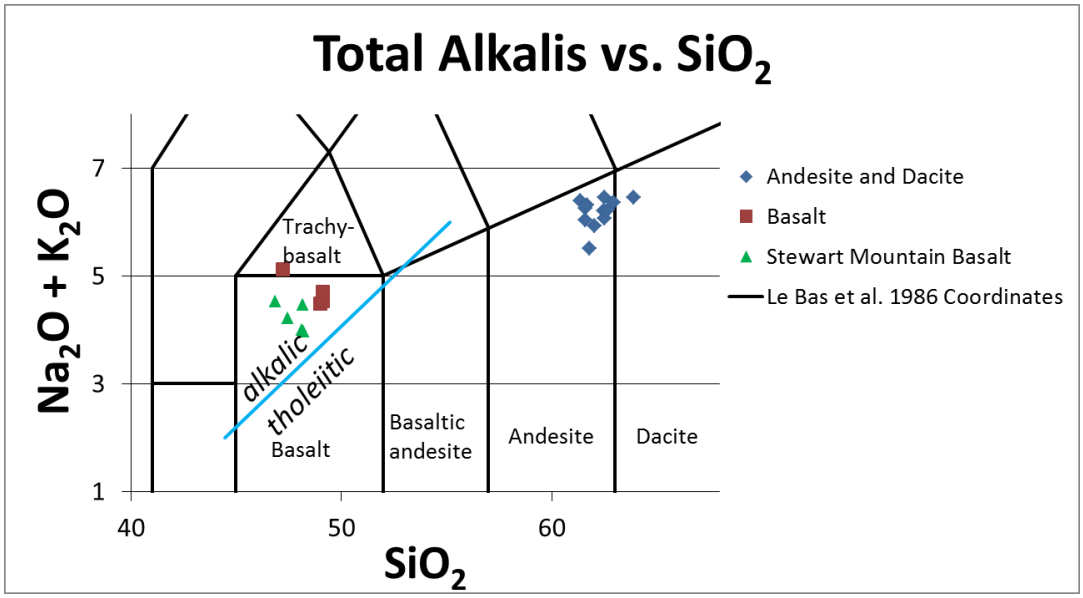

Fig. 6. Whole-rock compositions for Sugarloaf Mountain basalts, andesites, and dacite plotted in weight percent on a total alkali-silica (TAS) diagram. Stewart Mountain alkalic basalts are also shown. Coordinates and rock types for TAS classification are from the IUGS Subcomission on the Systematics of Igneous Rocks (Le Bas *et al.,* 1986). A reference line for alkalic and tholeiitic basalts is included (Macdonald & Katsura, 1964).

Fig. 7. Major element MgO variation diagrams for Sugarloaf basalt samples, Sugarloaf andesite and dacite samples, and alkalic basalt samples from Stewart Mountain, central Arizona (Singer & Fodor, 2013). Trachy-basalt SL-6 is labeled in some panels in order for it to be easily distinguished from the alkalic basalts.

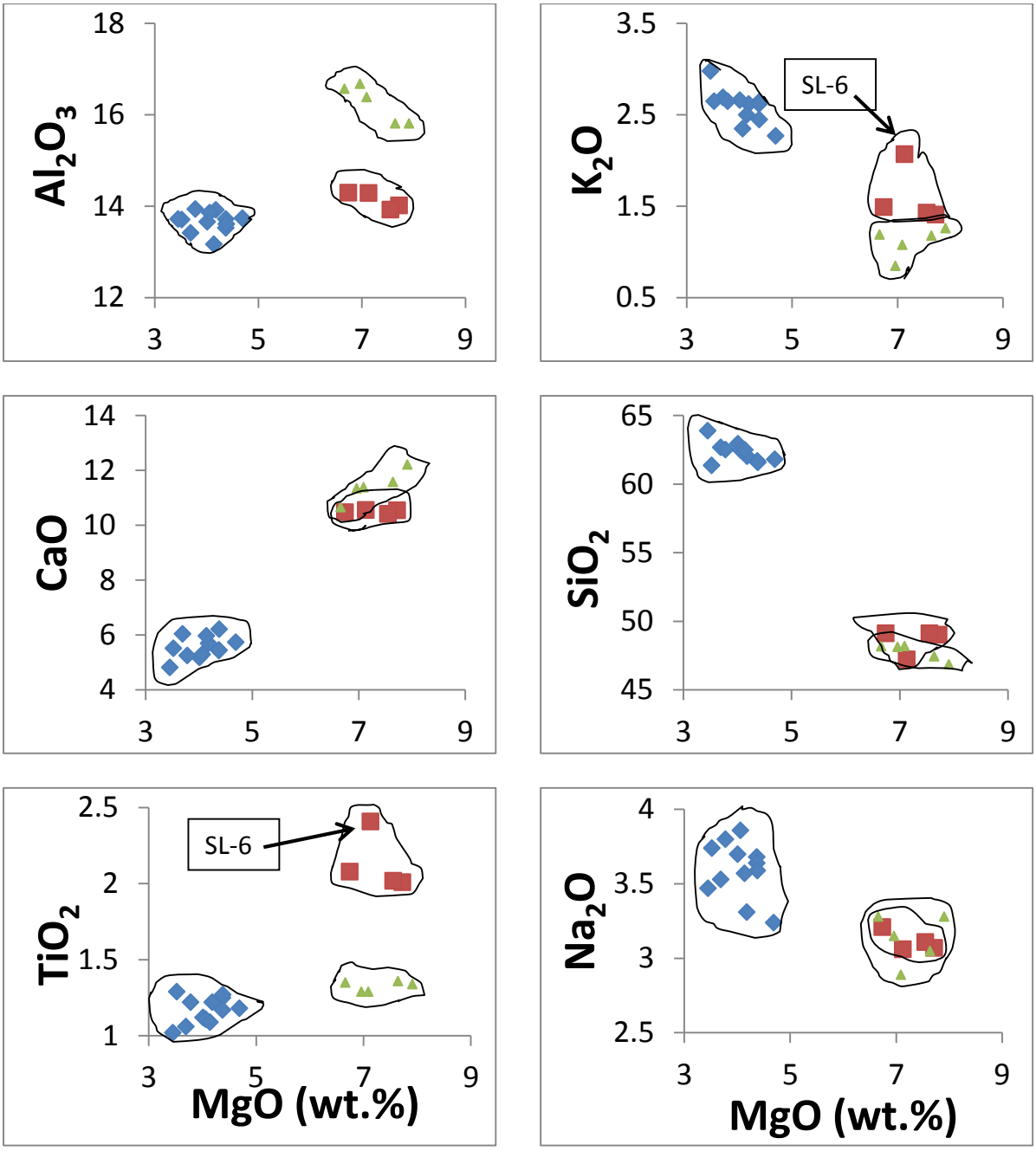
Al2O3
18
16
14
12
3
5
7
9
K2O
3.5
2.5
1.5
0.5
SL-6
CaO
14
12
10
8
6
4
SiO2
65
60
55
50
45
TiO2
2.5
2
1.5
1
SL-6
Na2O
4
3.5
3
2.5
MgO (wt.%)
MgO (wt.%)

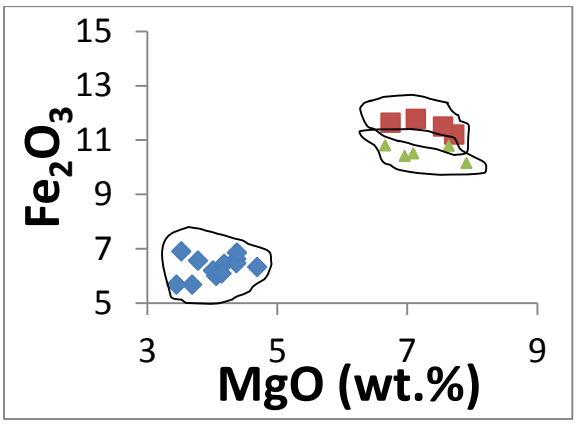

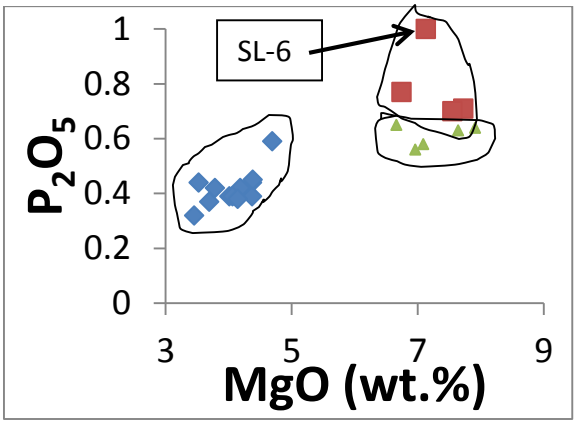

Andesites and Dacite

Basalts

Stewart Mountain Basalts

Major element compositions

Sugarloaf Mountain samples are basalts (47.2–49.1 wt. % SiO_2), andesites (61.4–62.9 wt. % SiO_2), and one dacite (63.9 wt. % SiO_2) according to the total alkali-silica (TAS) diagram (Fig. 6). The basalts are all alkalic according to the Hawaiian reference line for alkalic and tholeiitic basalts (Fig. 6). The lowest-SiO_2 basalt has slightly higher total $Na_2O + K_2O$ abundance than the other basalt samples and plots as a trachy-basalt in Fig. 6. For comparison, Stewart Mountain basalts generally overlap Sugarloaf basalts in SiO_2 (46.5–49 wt. %) but are slightly lower in total $Na_2O + K_2O$ (Fig. 6).

Basalts

MgO abundances in the basalts range from 6.7 wt. % to 7.7 wt. %. Among major elements that are incompatible—TiO_2, K_2O, Na_2O, and P_2O_5—the trachy-basalt (SL-6) is relatively enriched compared to the other three basalt samples, which generally overlap one another. For other major elements, including CaO, Al_2O_3, and Fe_2O_3, there are no distinctions among the four basalt samples. The Stewart Mountain basalts have MgO similar to Sugarloaf basalt but are lower in incompatible major elements and have higher CaO and Al_2O_3. Additionally, Stewart basalts and Sugarloaf basalts have overlapping Na_2O (Fig. 7).

Andesites and dacite

The Sugarloaf andesites and dacite have MgO abundances from 3.5 to 4.7 wt. %. Within the small MgO range, there are weak positive correlations for incompatible major elements P_2O_5 and TiO_2 versus MgO, and there are weak negative correlations for SiO_2 and incompatible major element K_2O versus MgO. All other major elements show little or no correlation with MgO. Compared to the basalts, Sugarloaf andesites and dacite have higher incompatible alkali elements Na_2O and K_2O but have lower abundances of incompatible elements P_2O_5, TiO_2, CaO and Fe_2O_3 (Fig. 7).

Trace element compositions

Basalts

Among three basalts, abundances for incompatible elements Zr, Nb, Th, La, and Ta show weak negative correlations with MgO over the small range 6.7–7.7 wt. % MgO. The trachy-basalt, SL-6, is enriched in these trace elements relative to their abundances in the other three basalts. For example, the Zr abundance is 237 ppm for SL-6 but 183–203 ppm for all other basalts (Fig. 8).

The MgO diagrams for compatible elements show that three of the four basaltic samples have similar Ni, Cr, and Sc. The compatible trace elements Ni and Cr are notably

Fig. 8. Trace element MgO variation diagrams for Sugarloaf high-magnesium samples (basalts), Sugarloaf evolved samples (andesites and dacite), and alkalic basalts from Stewart Mountain, central Arizona (Singer & Fodor, 2013).

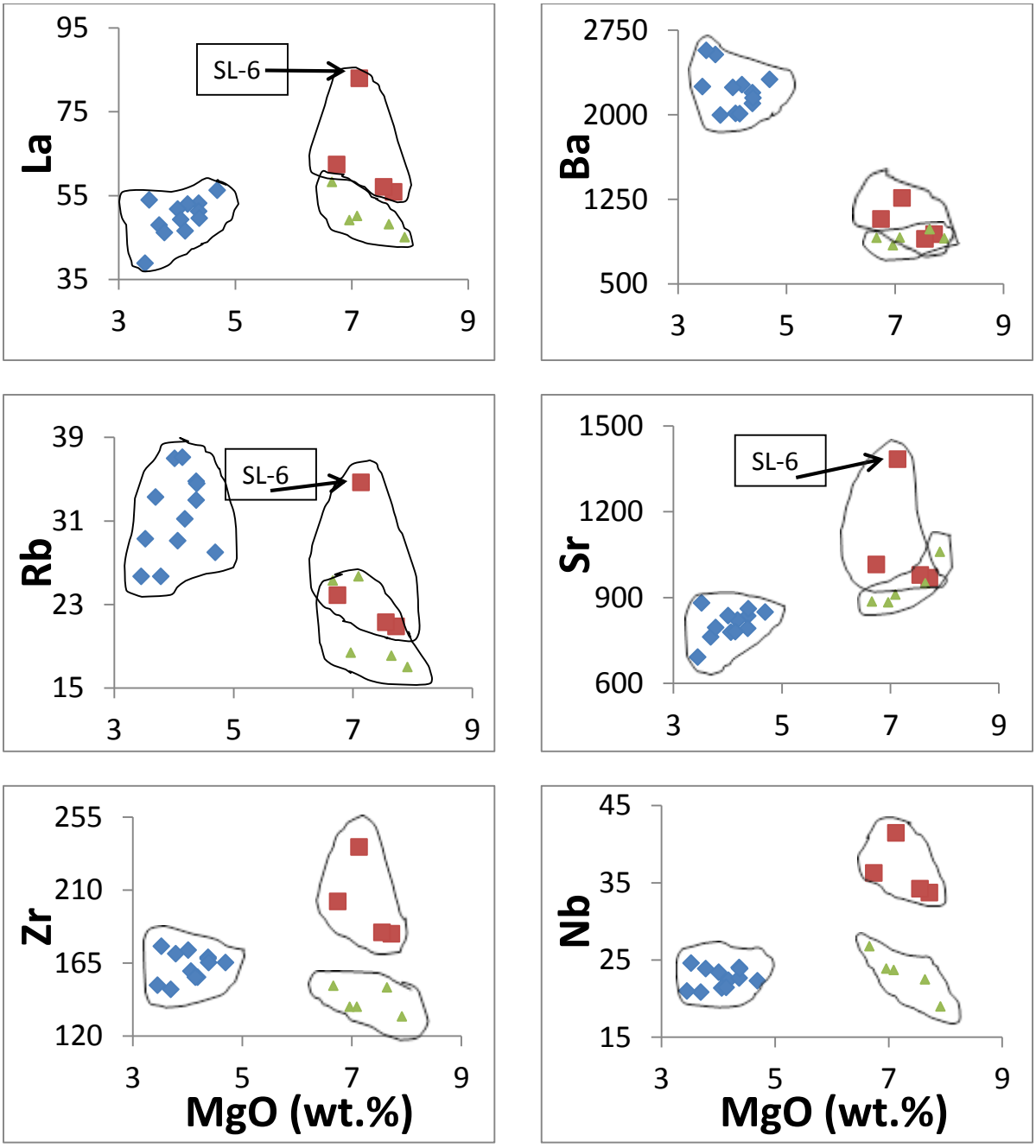
La
95
75
55
35
3
5
7
9
SL-6
Ba
2750
2000
1250
500
Rb
39
31
23
15
Sr
1500
1200
900
600
Zr
255
210
165
120
Nb
45
35
25
15
MgO (wt.%)
MgO (wt.%)

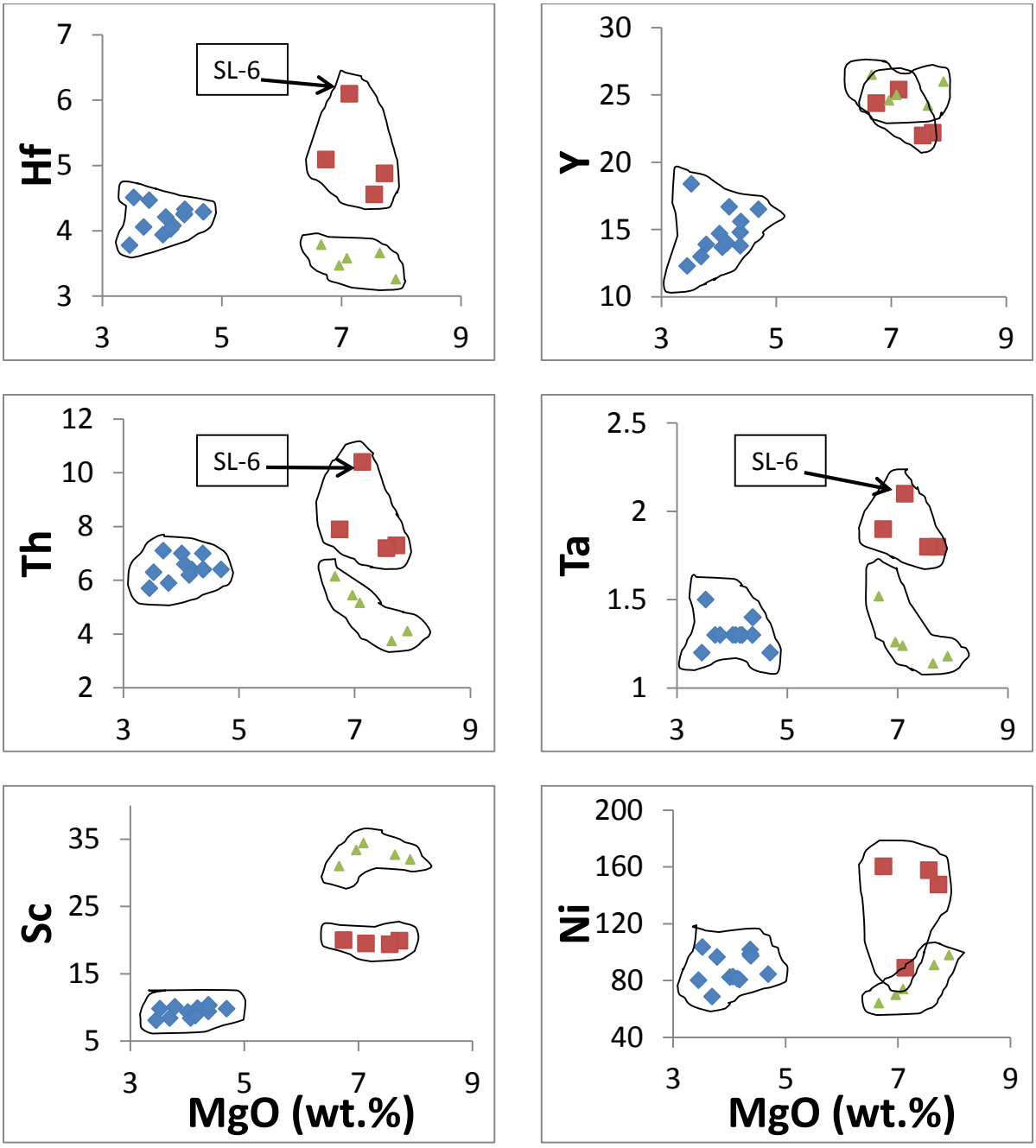
Hf
SL-6
Y
Th
SL-6
Ta
SL-6
Sc
MgO (wt.%)
Ni
MgO (wt.%)

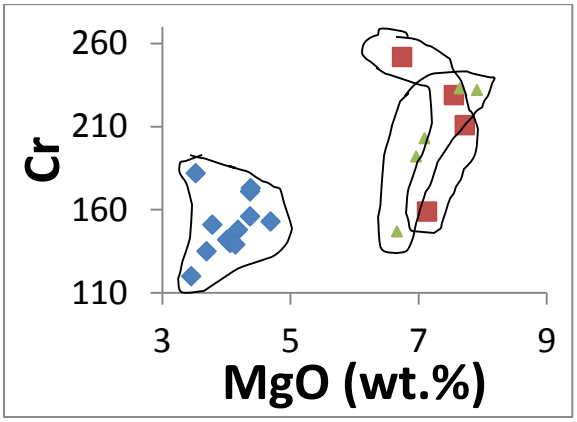

Andesites and Dacite

Basalts

Stewart Mountain Basalts

lower in the trachy-basalt (SL-6) when compared to the other three basalts, but for the compatible trace element Sc, all four basalts have similar abundances (19.4–20.0 ppm) (Fig. 8).

Compared to the Sugarloaf Mountain basalts, the Stewart Mountain basalts have lower Ni, similar Cr, and higher Sc. The exception to these observations is the SL-6 Ni abundance (89 ppm) which plots within the field for Stewart basalts (64–98 ppm Ni) and notably farther from the other three Sugarloaf basalts (148–161 ppm Ni) (Fig. 8).

Chondrite-normalized rare earth element (REE) patterns are displayed in Fig. 9A. All Sugarloaf basaltic rocks are enriched in light rare earth elements (LREE) and the trachy-basalt (SL-6) is the most LREE-enriched. For example, three basalts have $La_{(n)}$ = 180–201, while SL-6 has $La_{(n)}$ = 268. This is consistent with SL-6 showing enrichment in incompatible elements in the MgO diagrams.

Primitive mantle-normalized patterns are displayed in Fig. 10A. SL-6 is more enriched than the other three basalts in the most incompatible elements, which is similar to the enrichment observed for SL-6 in the LREEs. However, the shapes of all four basaltic patterns are similar. All four basaltic patterns peak at Ba and exhibit negative anomalies for Nb-Ta and P and a weak negative anomaly for Ti. Additionally, they all appear to have a slight negative K anomaly.

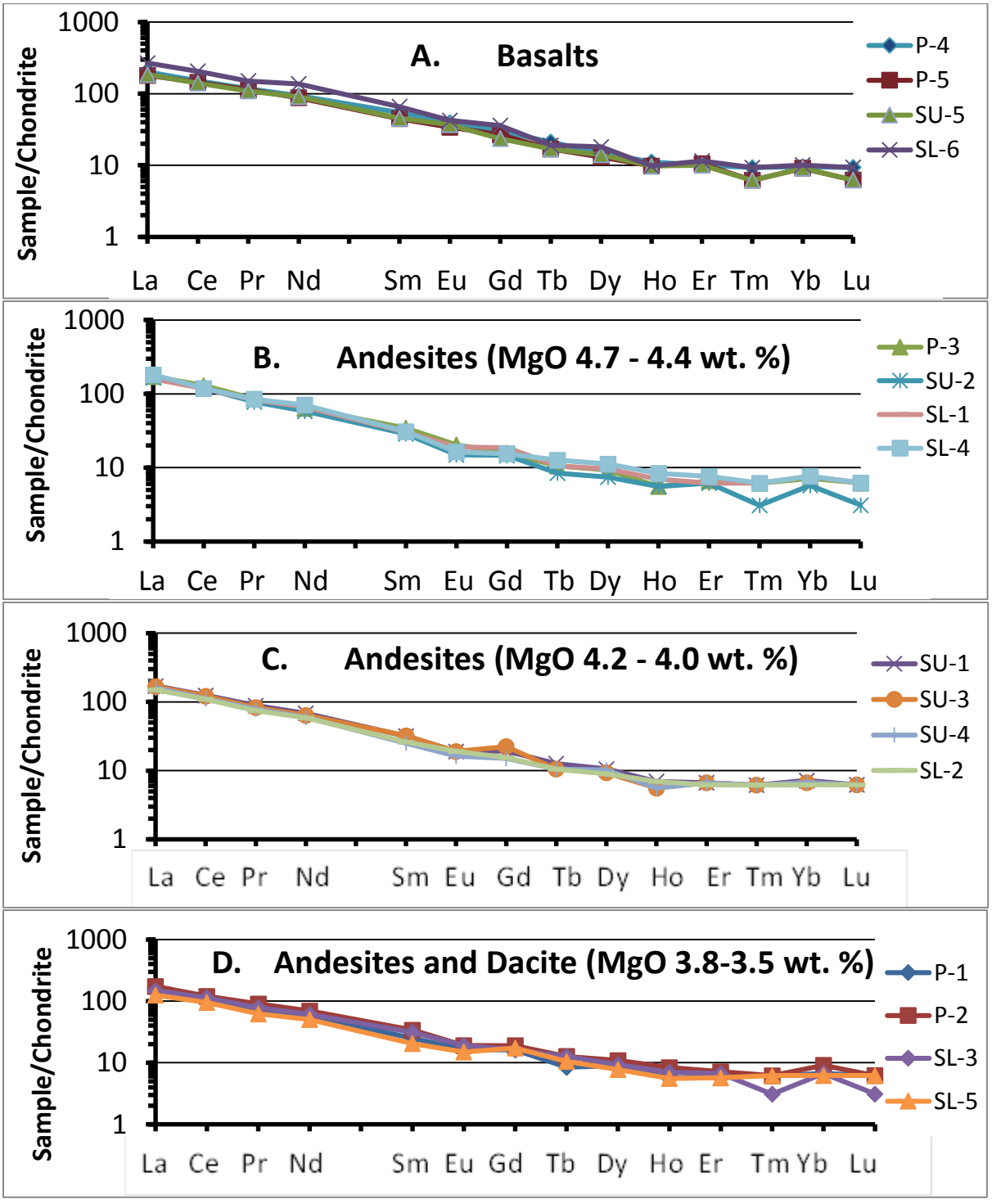

Fig. 9. Rare earth element diagrams for Sugarloaf Mountain basalts (panel A); four highest-MgO andesites (panel B); four next-highest-MgO andesites (panel C); three lowest-MgO andesites and the Sugarloaf dacite (panel D).

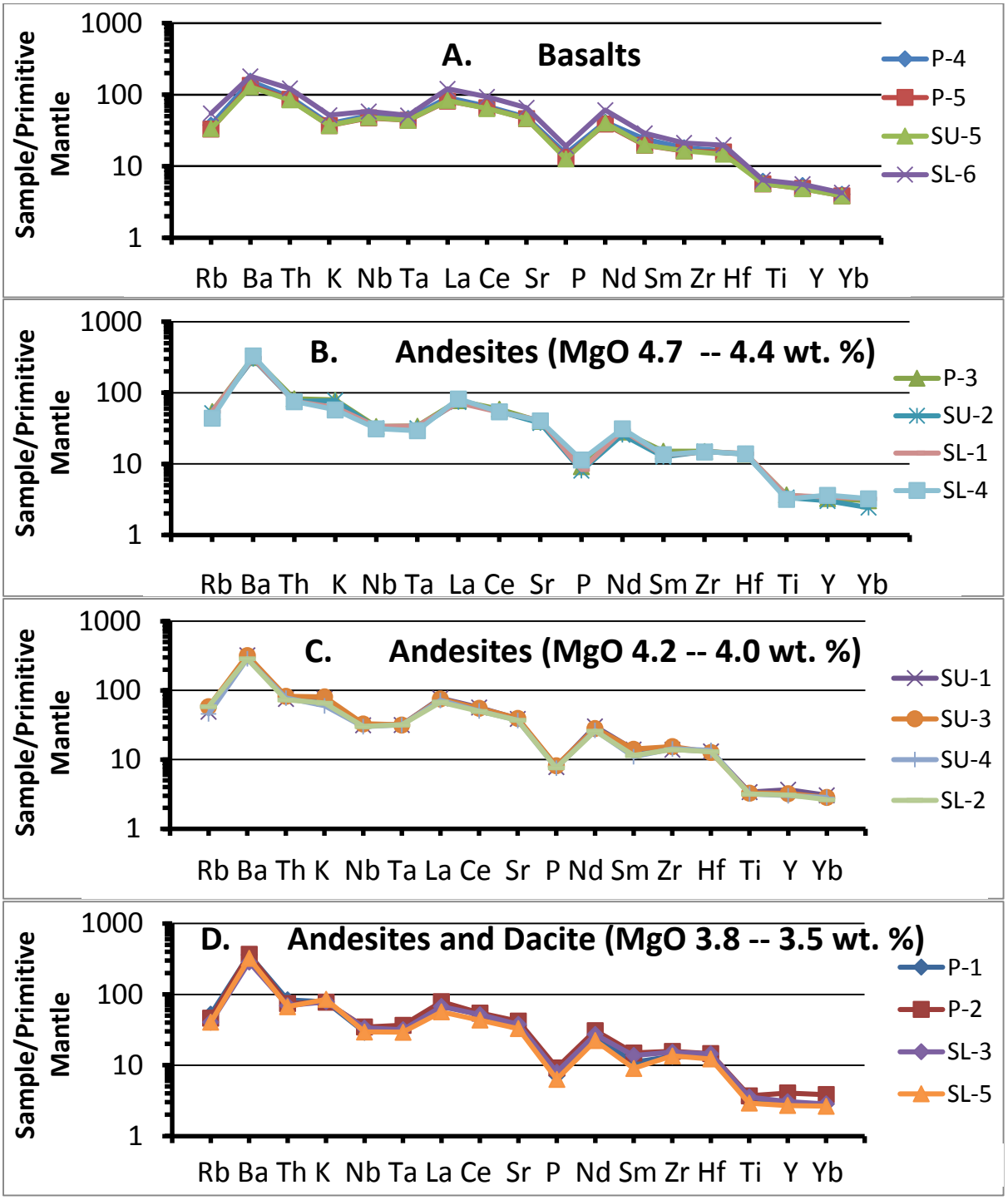

Fig. 10. Primitive mantle normalized diagrams for Sugarloaf Mountain basalts (panel A); four highest-MgO andesites (panel B); four next-highest-MgO andesites (panel C); three lowest-MgO andesites and the Sugarloaf dacite (panel D).

Andesites and dacite

Among the incompatible trace elements in the andesites and dacite, La and Sr show weak positive correlations versus MgO. Other incompatible elements plot versus MgO as scattered fields. Many incompatible element concentrations in the andesites and dacite—such as those for Sr, Zr, Nb, Th, Ta, La, and Ce—are lower than or barely overlapping with the same element concentrations in the basalts. However, Ba in the andesites and dacite is clearly enriched relative to Ba in the basalts, and Rb is higher in the andesites and dacite than in any of the basalts except the trachy-basalt (SL-6) (Figs. 8–9).

On the MgO variation diagrams for compatible elements Ni and Cr, Sugarloaf andesites and dacite partially overlap the basalts but have lower abundances on average. The Sc abundances in the andesites and dacite are distinctly lower than the Sc abundances in basalts. These evolved lavas do not show trends for compatible trace elements versus MgO (Fig. 8).

Chondrite-normalized trace element patterns for andesite and dacite are presented in Fig. 9, and these samples are grouped into three different plots (Fig. 9B–D) based on MgO concentrations. Panel B shows andesites with 4.7–4.4 wt. % MgO; panel C shows andesites with 4.2–4.0 wt. % MgO; panel D shows andesites and dacite with 3. 8–3.5 wt. % MgO. The andesite patterns generally overlap each other. For example, among LREEs, normalized La values ($La_{(n)}$) all fall within ≈150–180 (Fig. 9B–D) whereas the dacite (SL-5) which has the lowest MgO (3.5 wt. %) and highest SiO_2, has the lowest $La_{(n)}$, ≈126. Similarly, all andesites

fall within a range of $Ce_{(n)}$ = 110–130, but the dacite has $Ce_{(n)}$ = 95. Also, the slopes of the patterns are similar for all andesites, where $Ce/Yb_{(n)} \approx$ 14–22 (Table 2). The slope for the dacite pattern, $Ce/Yb_{(n)}$ = 16.4, is at the low end of the range for andesite pattern slopes. The dacite and most of the andesites have weak Eu anomalies of similar magnitude.

The patterns for trace elements normalized to primitive mantle for andesites and dacite are shown in Fig. 10, where panels B–D show the patterns in groups based on MgO concentrations. These patterns overlap each other and retain the shapes of the basaltic patterns. As with the basalts, Ba is the most enriched, P is strongly depleted, and there are weak Ti negative anomalies. All andesites and the dacite exhibit Nb-Ta negative anomalies that are "deeper" than those for the basalts (Fig. 10A–D).

Mineral compositions

Mineral compositions for representative phenocrysts of feldspar, clinopyroxene and orthopyroxene, olivine, amphibole, and one biotite as well as groundmass feldspar are tabulated (Tables 3–7). Also presented are ternary and quadrilateral diagrams for feldspar and clinopyroxene compositions, plots comparing TiO_2 and SiO_2 to Mg# for average amphibole compositions, and plots comparing FeO and TiO_2 to MgO concentrations for Sugarloaf and G-SVP biotite compositions (Figs. 11–16).

Feldspar

Analyses were performed on plagioclase and alkali feldspar phenocrysts, one alkalic feldspar xenocryst, and on groundmass feldspar laths, microlites, and interstitial material in nine samples of basalt and andesite (Fig. 11A–B; Table 3). In Sugarloaf basalts, feldspar in three samples (SU-5, SL-6, and P-4) occurs only as groundmass plagioclase laths, largely labradorite, with compositions ranging from $An_{34.8–61.8}$ $Or_{1.3–10.3}$ (Fig. 11B). Two samples have interstitial alkali feldspar $An_{5.8–29.6}$ $Or_{7.1–47.7}$ that is nearly a compositional continuum from the groundmass plagioclase laths. In SL-6, a xenocryst of sanidine has the composition $An_{10}Ab_{30}Or_{60}$ (Fig. 11B).

Feldspar in Sugarloaf andesites occurs as phenocrysts of plagioclase, some with discrete rims around spongy zones, as rare alkali feldspar grains, and as groundmass plagioclase laths (Fig. 11A; Table 3). The plagioclase phenocrysts, many spongy-textured and subrounded, have compositions that are almost entirely andesine but include some oligoclase ($An_{24.7–48.6}Or_{1.3–7.7}$). In SU-4, core compositions range from oligoclase to labradorite ($An_{26.2–55.3}Or_{1.3–7.7}$). Thin rims on andesine phenocrysts in SL-1 and SU-3 are more calcic than the cores they surround, having andesine-labradorite compositions of $An_{44.9–56.-0}$ $Or_{2.3–3.6}$. Two alkali feldspar grains in one andesite (SU-1) are largely sanidine in composition, mainly ranging over Or_{60-83}, but include a few Na-rich points (e.g., $Or_{20-54}Ab_{46-79}$). Groundmass microlites in two samples overlap the andesine cores but are on average

more calcic than the cores ($An_{42.3–50.2}Or_{1.9–4.9}$). In sample SL-1, both the groundmass and rim compositions overlap and are distinctly more calcic (An_{50-60}) than the core (Fig. 11A).

Table 3: Average compositions of representative plagioclase phenocrysts, alkali feldspar phenocrysts and xenocryst, and groundmass plagioclase and interstitial alkali feldspar in basalts and andesites of Sugarloaf Mountain, central Arizona

	Basalt				Andesite					
	SU-5	SL-6		P-4	SU-2	SU-1				
	Grndmss	Xenocryst	Grndmss	Grndmss	Ph	Ph-Kspar	Ph-Kspar	Ph	Ph	Grndmss
SiO_2	57.1	65.1	51.4	57.1	57.1	65.3	65.5	58.4	57.4	56.3
Al_2O_3	25.6	18.9	29.2	25.8	26.6	19.4	19.3	26.8	26.4	27.5
FeO	0.48	0.14	1.4	0.37	0.26	0.08	0.03	0.33	0.30	0.73
CaO	7.5	0.17	11.9	7.0	8.2	0.03	0.07	7.8	7.7	9.7
Na_2O	6.1	4.6	4.2	6.1	6.0	4.8	3.8	6.9	7.2	5.7
K_2O	1.9	10.0	0.40	2.3	0.41	10.0	11.4	0.40	0.45	0.41
Total	98.68	98.91	98.50	98.67	98.57	99.61	100.10	100.63	99.45	100.34
An	36.1	0.83	59.6	33.7	40.2	0.15	0.34	37.8	36.3	47.4
Or	10.9	58.4	2.4	13.2	2.4	57.7	72.2	2.3	2.5	50.3

	Andesite									
	SL-1						SU-4		SU-3	
	Ph	Ph	Rim	Ph	Rim	Grndmss	Ph	Ph	Ph	Rim
SiO_2	60.1	58.6	53.8	59.9	54.3	54.6	56.7	59.2	58.9	53.3
Al_2O_3	24.9	25.9	28.7	24.5	28.1	27.9	27.4	24.3	26.3	28.1
FeO	0.26	0.31	0.72	0.21	0.55	0.73	0.31	0.25	0.25	0.46
CaO	5.7	6.5	9.9	6.7	11.1	10.1	9.1	6.3	7.5	9.7
Na_2O	7.7	7.2	5.3	7.7	5.2	5.4	5.4	6.6	6.5	5.0
K_2O	0.78	0.60	0.48	0.62	0.47	0.51	0.34	0.77	0.47	0.38
Total	99.44	99.11	98.90	99.63	99.72	99.24	98.91	96.65	99.45	96.56
An	27.8	32.1	49.4	31.4	52.7	49.4	44.8	31.2	37.0	47.5
Or	4.5	3.5	2.8	3.5	2.7	3.0	2.0	4.5	2.7	2.2

Each column is the average of: 5-16 analytical points per grain for phenocrysts; 7-34 analytical points for groundmass; and 5-6 analytical points for rims

Table 3, continued

	Andesite				
	P-2				
	Ph	Ph	Ph	Ph	Grndmss
SiO_2	56.0	55.1	57.9	57.6	55.0
Al_2O_3	26.9	27.4	24.9	24.6	26.9
FeO	0.22	0.29	0.25	0.29	0.77
CaO	8.4	9.0	6.7	6.5	9.1
Na_2O	6.4	6.1	7.2	7.1	5.7
K_2O	0.38	0.26	0.57	0.54	0.62
Total	98.30	98.15	97.52	96.63	98.09
An	41.2	44.3	32.9	32.6	45.2
Or	2.2	1.5	3.3	3.2	3.7

Each column is the average of: 5-16 analytical points per grain for phenocrysts; 7-34 analytical points for groundmass; and 5-6 analytical points for rims

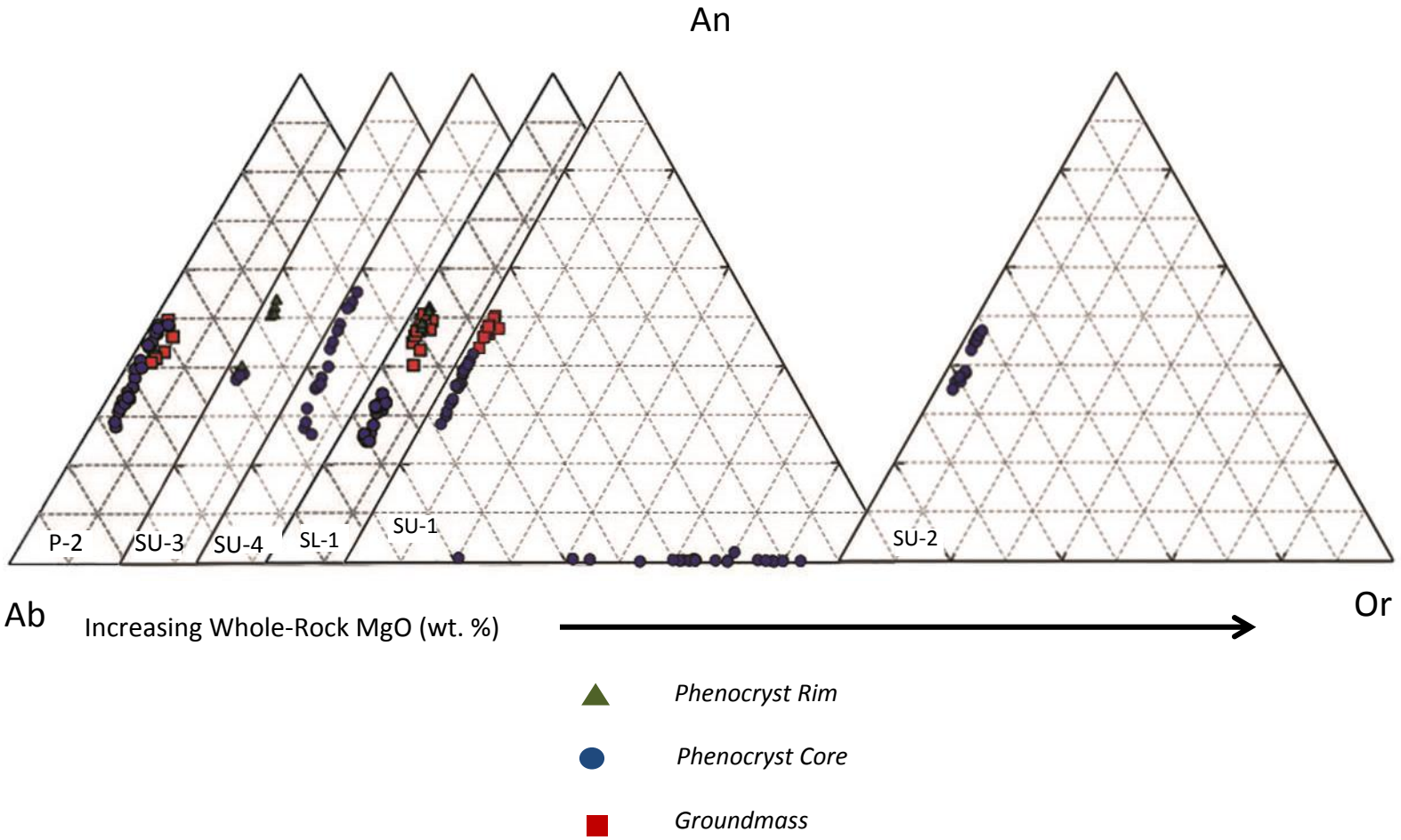

Fig. 11A. Feldspar ternary plots for plagioclase and alkali feldspar in Sugarloaf Mountain andesites. Each point represents an analysis on a feldspar grain by electron microprobe.

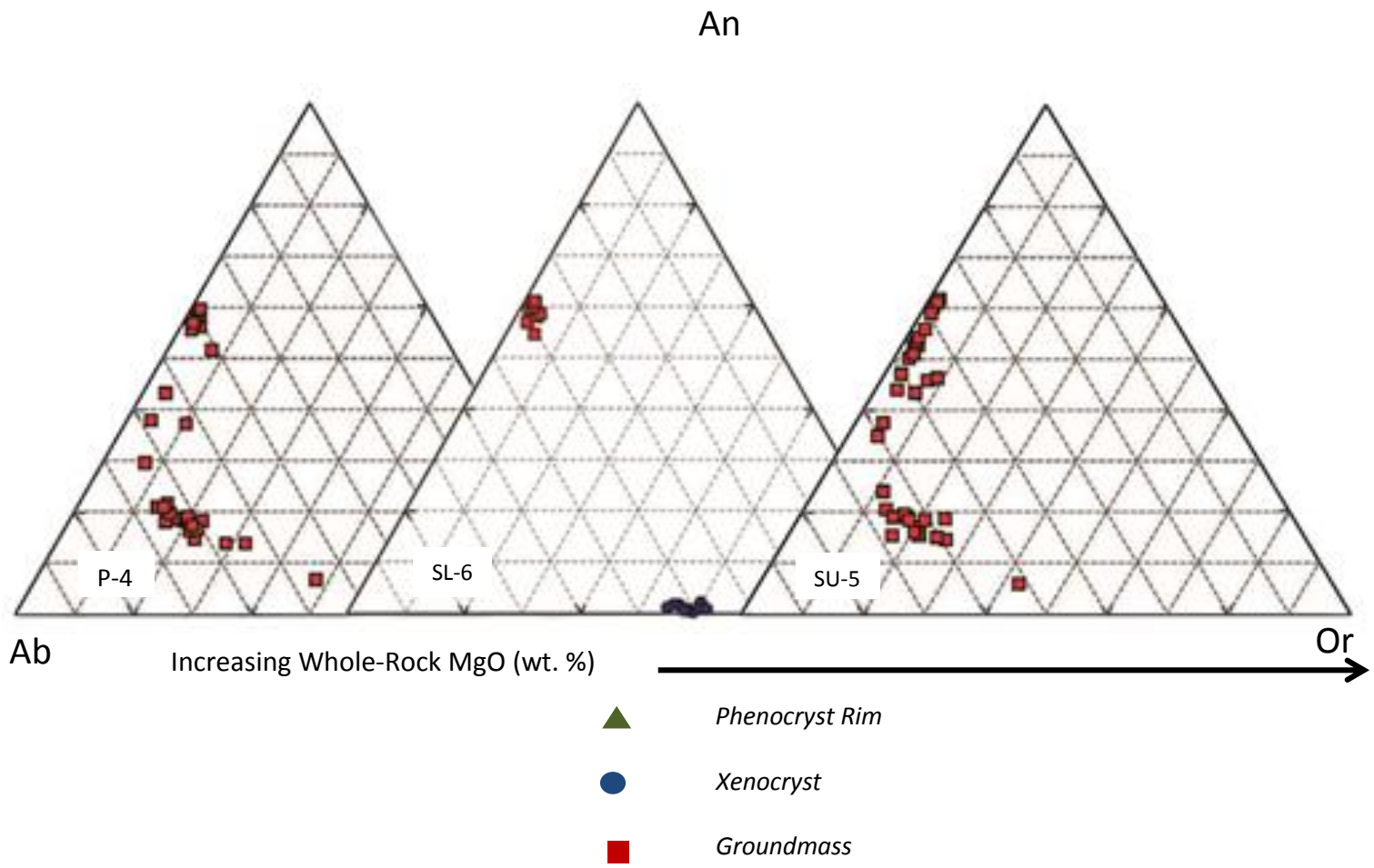

Fig. 11B. Feldspar ternary plots for plagioclase and alkali feldspar xenocryst and groundmass interstitial material in Sugarloaf Mountain basalts. Each point represents an analysis on a feldspar grain by electron microprobe.

Pyroxene

Analyses for clinopyroxene and orthopyroxene phenocrysts in each of ten samples of basalt, andesite, and dacite are in Fig. 12 and Table 4. Among the basalts, SU-5 and P-4 contain clinopyroxene with end-member ranges of $Wo_{45.3–49.2}Fs_{8.0–12.9}$. The trachy-basalt (SL-6) contains augite with slightly lower CaO (Wo ≈43–45 mol. %) at similar Fs (Fig. 12). Clinopyroxene Al_2O_3 ranges from 2.6–6.2 wt. % in the basalts (Table 4).

Sugarloaf andesite and dacite clinopyroxenes have generally lower Wo and higher Fs than Sugarloaf basalt clinopyroxenes (Fig. 12; Table 4). For example, andesites SL-1, P-3, SU-1, SU-4, SU-3, and P-2 and dacite SL-5 have clinopyroxene compositions within the range $Wo_{33.2–45.6}Fs_{7.0–18.4}$. The dacite (SL-5) clinopyroxene has the highest Wo content. Clinopyroxene Al_2O_3 ranges from 1.4–8.0 wt. % in the andesites. In addition, samples SL-1, SU-1, and P-2 all have orthopyroxene that is bronzite to hypersthene in composition ($Wo_{1.0–4.1}Fs_{20.5–35.1}$). Orthopyroxene Al_2O_3 ranges from 0.54 to ≈3.0 wt. % (Table 4).

For comparison, clinopyroxene Wo, Fs, and Al_2O_3 compositions for Sugarloaf alkalic basalts are similar to those reported for alkalic basalts in the nearby Stewart Mountain and G-SVP volcanic fields. At Stewart Mountain, clinopyroxene compositions have average end-member values within the range $Wo_{44.5–45.5}Fs_{10.6–11.9}$ and Al_2O_3 averages that range from 4.0–6.8 wt. % (Singer & Fodor, 2013). In the G-SVP, clinopyroxenes were reported as having end-member values within the range $Wo_{43.6–50.5}Fs_{6.3–12.1}$ and Al_2O_3 averages ranging from 3.4–6.5 wt. % (Fodor & Vetter, 2011). The only orthopyroxene reported for the comparison

areas is from a rhyolite in the G-SVP. This orthopyroxene is similar to Sugarloaf orthopyroxene with end-members $Wo_{2.5}Fs_{33.1}$ and an Al_2O_3 concentration of 1.5 wt. % (Dombroski, 2010).

Table 4: Average compositions for clinopyroxene and orthopyroxene phenocrysts in basalts, andesites, and dacite from Sugarloaf Mountain, central Arizona

	Basalt					Andesite								
	SU-5		SL-6	P-4		SL-1		P-3			SU-1			
	CPX	CPX	CPX	CPX	CPX	CPX	OPX	CPX	CPX	CPX	CPX	CPX	OPX	OPX
SiO_2	52.1	51.7	49.7	50.0	51.7	50.3	52.7	49.4	50.8	50.9	51.0	49.4	53.1	52.7
TiO_2	0.84	0.79	1.4	1.1	0.80	0.81	0.09	1.0	0.74	1.1	0.94	1.4	0.47	0.28
Al_2O_3	3.6	4.2	5.2	5.2	4.0	5.2	0.92	3.9	4.8	4.2	3.8	4.5	3.0	2.4
Cr_2O_3	0.26	0.58	0.27	0.28	0.29	0.17	0.01	0.03	0.03	0.42	0.61	0.18	0.06	0.07
FeO	6.5	5.7	6.6	6.6	6.1	7.1	21.6	8.5	9.7	6.9	6.1	7.5	14.5	15.1
MnO	0.17	0.13	0.11	0.16	0.15	0.18	1.3	0.19	0.22	0.15	0.12	0.15	0.26	0.27
MgO	14.8	14.6	15.2	13.9	14.6	15.1	22.5	15.6	14.9	15.8	16.6	15.7	27.3	27.7
CaO	22.7	23.1	21.0	22.4	22.1	20.2	0.77	19.2	18.2	19.9	21.0	20.1	1.7	1.3
Na_2O	0.24	0.29	0.58	0.23	0.30	0.56	0.01	0.55	0.52	0.52	0.53	0.53	0.04	0.04
Total	101.21	101.09	100.06	99.87	100.04	99.62	99.90	98.37	99.91	99.89	100.70	99.46	100.43	99.86
Wo	47.0	48.3	44.4	47.8	46.9	43.2	1.6	40.4	39.2	42.1	43.0	42.1	3.3	2.5
Fs	10.5	9.3	10.9	11.0	10.1	12.0	34.5	14.0	16.3	11.4	9.7	12.2	22.2	22.8
Mg#	80.3	82.1	80.5	79.0	81.0	79.0	64.9	76.5	73.3	80.4	83.0	78.9	77.1	76.6

Each column is the average of 3—10 analytical points per grain

Table 4, continued

	Andesite								Dacite		
	SU-4			SU-3	P-2				SL-5		
	CPX	OPX	OPX	CPX	CPX	CPX	OPX	OPX	CPX	CPX	CPX
SiO_2	51.6	53.3	52.6	51.6	51.7	51.5	54.3	53.7	50.2	50.3	51.2
TiO_2	0.51	0.07	0.08	0.87	0.63	0.90	0.13	0.20	1.6	1.0	1.1
Al_2O_3	3.2	0.94	1.1	4.1	3.0	3.5	0.86	1.7	3.7	3.4	3.7
Cr_2O_3	<0.01	<0.01	<0.01	0.46	0.12	0.60	<0.01	0.05	0.09	0.30	0.22
FeO	8.7	19.8	20.8	6.7	7.4	5.4	19.3	14.8	8.6	7.4	6.4
MnO	0.17	0.94	1.1	0.18	0.19	0.15	1.3	0.42	0.18	0.17	0.18
MgO	15.3	24.5	24.4	17.6	15.5	16.7	23.5	27.7	15.2	15.9	16.0
CaO	20.3	0.66	0.60	18.8	20.1	20.4	0.79	1.0	20.4	20.3	21.0
Na_2O	0.46	<0.01	<0.01	0.48	0.39	0.49	0.02	0.02	0.40	0.43	0.44
	100.24	100.21	100.68	100.79	99.03	99.64	100.20	99.59	100.37	99.20	100.07
Wo	42.0	1.4	1.2	38.8	42.4	42.7	1.6	2.0	42.3	42.1	43.5
Fs	14.0	30.8	32.0	10.8	12.2	8.8	31.0	22.6	13.9	12.0	10.4
Mg#	75.8	68.8	67.7	82.5	78.8	84.6	68.6	76.9	75.8	79.3	81.6

Each column is the average of 3—10 analytical points per grain

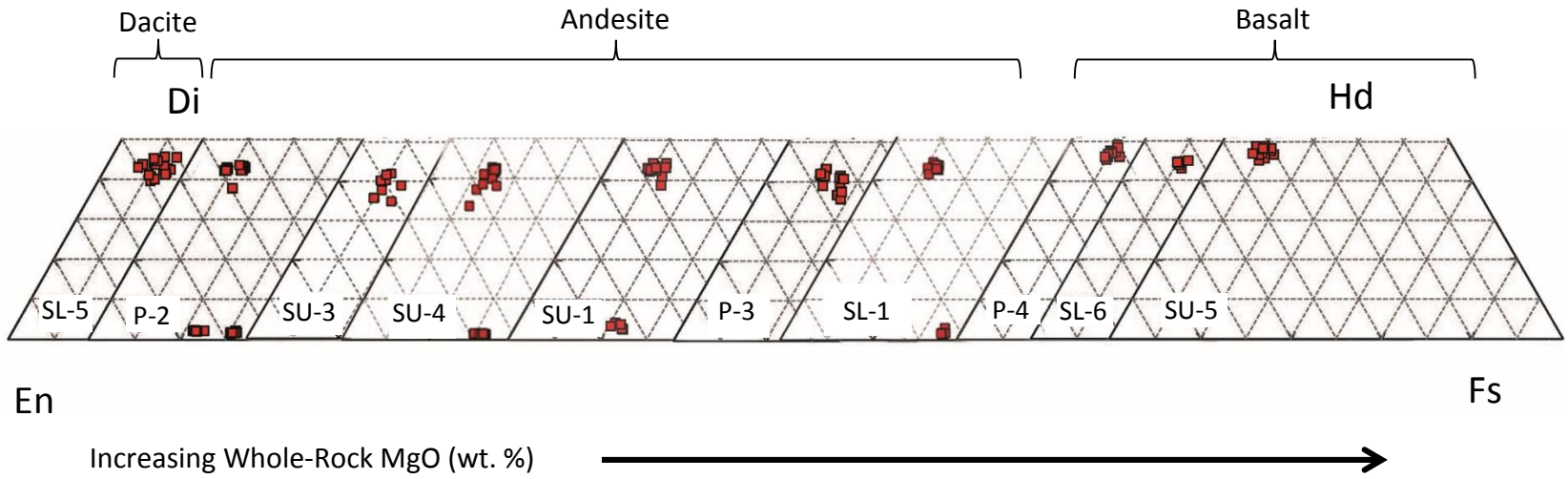

Fig. 12. Pyroxene quadrilaterals for clinopyroxene and orthopyroxene within the Sugarloaf Mountain alkalic basalts, andesites, and dacite. Each plotted point represents a point on a pyroxene grain analyzed by electron microprobe.

Olivine

Olivine phenocrysts in each of nine samples were analyzed. Average compositions for representative olivine grains are presented in Table 5, where they represent normal compositional zonation of highest Fo in cores to lowest Fo at the rims (Fig. 13). The average Fo concentrations for olivines in two basalts (SU-5 and SL-6) range from $Fo_{83.8–85.1}$, but P-4 has a much lower Fo concentration of $\approx Fo_{73}$. Average olivine in andesites SL-1, SU-4, and SU-3 has compositions $Fo_{83.8–85.5}$ and overlaps the Fo compositions for basalts SU-5 and SL-6, but Fo in two other andesites (P-3 and SU-1) and the dacite (SL-5) have lower average values of $Fo_{77.5–81.6}$.

The most Fo-rich core areas observed for each grain (Fig. 13) were used to evaluate whether or not the olivine represents equilibrium crystallization from liquids that are represented by the whole-rock host compositions. An olivine-liquid FeO/MgO partitioning coefficient of $K_D = 0.3 \pm 0.03$ represents equilibrium (Roeder & Emslie, 1970). Based on this standard, only the olivine grains in andesite SU-1 with $K_D \approx 0.32$, andesite SU-4 with $K_D \approx 0.27–0.29$ and the dacite (SL-5) with $K_D \approx 0.28–0.29$ (Table 5) crystallized at equilibrium with their surrounding host rocks. High olivine partition coefficients in samples P-4 and P-3 ($K_D \approx 0.34–0.47$) indicate that they crystallized from melts having lower MgO than their host rocks. Conversely, olivine in SU-5, SL-6, SL-1, and SU-3 ($K_D \approx 0.22–0.26$) crystallized from melts of higher MgO than their host rocks.

Table 5: Average compositions of olivine phenocrysts in basalts, andesites, and dacite from Sugarloaf Mountain, central Arizona

	Basalts				Andesites									Dacite	
	SU-5		SL-6	P-4	SL-1		P-3		SU-1	SU-4		SU-3		SL-5	
SiO_2	38.8	38.1	37.3	37.9	38.7	39.4	37.6	37.9	40.1	38.6	38.4	39.4	38.8	38.3	38.3
FeO	14.3	15.3	14.6	23.1	13.9	15.1	20.8	18.5	17.2	15.8	15.2	14.6	14.4	17.9	17.2
MnO	0.22	0.24	0.28	0.34	0.22	0.23	0.30	0.18	0.25	0.19	0.23	0.17	0.19	0.13	0.17
MgO	45.9	44.5	46.2	34.9	45.8	44.9	40.1	42.1	40.7	46.1	45.5	45.5	46.0	42.9	42.6
CaO	0.20	0.23	0.25	0.36	0.19	0.17	0.10	0.16	0.30	0.13	0.18	0.21	0.21	0.15	0.18
NiO	0.37	0.30	0.29	0.33	0.36	0.27	0.34	0.37	0.22	n.d.	n.d.	n.d.	n.d.	0.32	0.31
Total	99.79	98.67	98.92	96.93	99.17	100.07	99.24	99.21	98.77	100.82	99.51	99.88	99.60	99.70	98.76
Fo	85.1	83.8	85.0	72.9	85.5	84.1	77.5	80.3	80.9	83.8	84.2	84.7	84.9	81.0	81.6
$K_D^{Fe/Mg}$	0.23	0.25	0.22	0.47	0.22	0.26	0.40	0.34	0.32	0.29	0.27	0.24	0.24	0.28	0.29

Each column is the average of 4—11 analytical points per grain

$K_D^{Fe/Mg}$ represents the partitioning coefficient established for the most Mg-rich point (Fig. 13) with respect to its host sample FeO/MgO

n.d. : concentration of this element was not determined

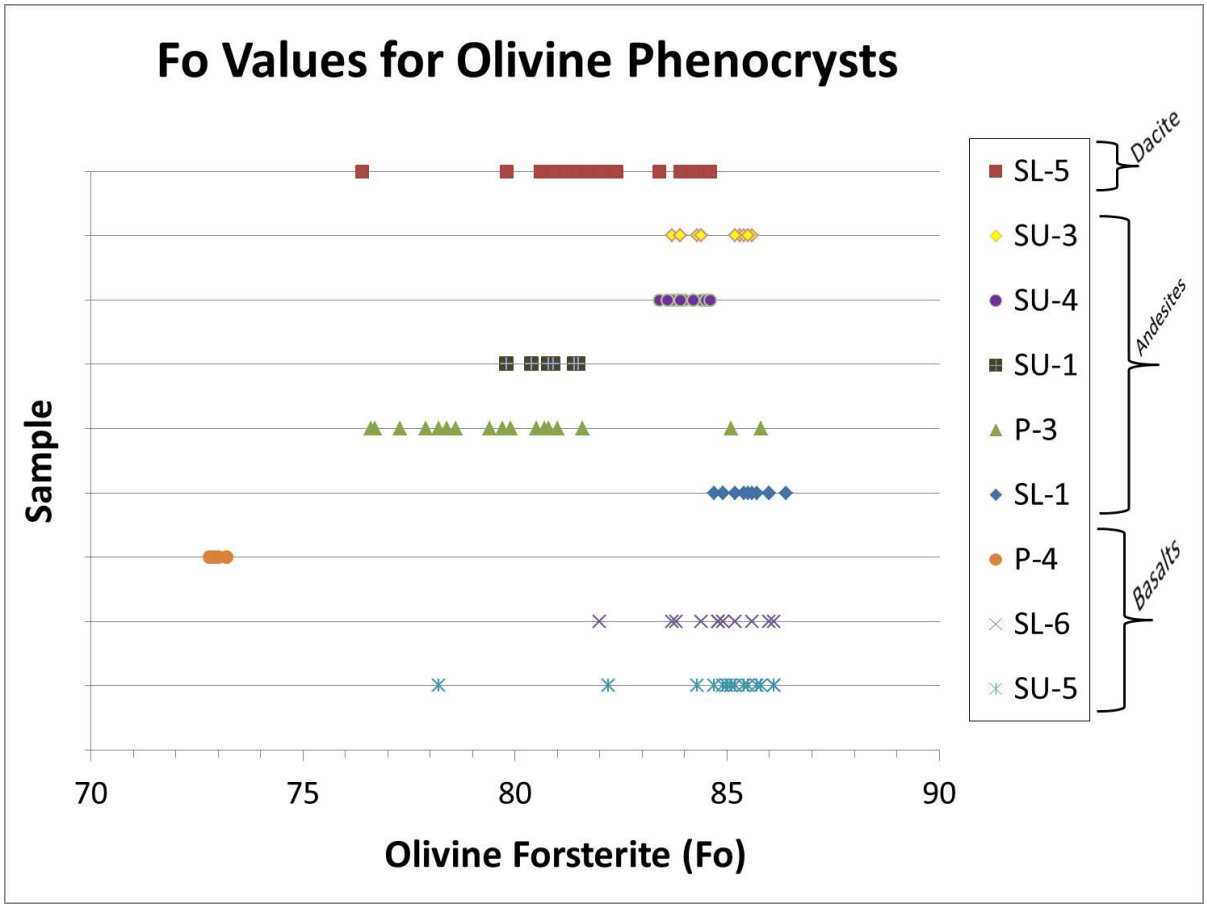

Fig. 13. Diagram showing the range of olivine forsterite (Fo) content determined by electron microprobe for representative Sugarloaf basalt, andesite, and dacite samples. Each plotted point represents a point on an olivine grain in the designated sample that was analyzed by electron microprobe.

Amphibole

Amphibole phenocrysts in each of seven andesite and dacite samples were analyzed. Average compositions for representative amphibole grains are presented in Table 6. In a plot of silica per formula unit (silica PFU) vs. Mg#, amphibole grains plot in a cluster as pargasite compositions with the exception of one of the four SU-3 grains, which plots as edenite (Fig. 14).

Amphibole FeO and TiO_2 are plotted versus MgO for each amphibole analytical point in Fig. 15. Average values for G-SVP amphiboles (Dombroski, 2010) are also plotted for comparison. The Sugarloaf amphiboles have a rather small range in MgO concentration, from 12.6–13.6 wt. %. Across this MgO range, some distinctions are apparent in FeO and TiO_2 among the amphiboles in different samples. For example, SU-1 has the highest TiO_2 concentration but among the lowest FeO concentrations (Fig. 15A–B). Similarly, SU-3 has among the highest FeO concentrations but comparatively low TiO_2. Also, SU-3 has MgO concentrations that extend the entire MgO range for all samples combined and shows a good negative correlation between TiO_2 and MgO (Fig. 15A–B). With the exception of a few of the analyzed points from SU-3 that have relatively low TiO_2, all Sugarloaf amphiboles are lower in MgO and higher in TiO_2 than any reported for the G-SVP, but the two locations have similar FeO (Fig. 15A–B).

Table 6: Average compositions and structural formulas of amphibole phenocrysts in andesites and dacite from Sugarloaf Mountain, central Arizona

	Andesites									Dacite
	SL-1	P-3	SU-1	SU-3				SU-4	P-2	SL-5
SiO_2	41.1	41.2	41.4	42.8	42.6	44.1	41.2	42.0	43.1	42.0
TiO_2	2.5	2.5	2.8	2.6	2.7	1.8	3.0	3.1	2.8	3.4
Al_2O_3	11.9	11.8	12.8	10.9	11.2	9.9	11.9	12.0	11.3	12.7
FeO	12.6	13.1	12.1	14.4	13.4	13.5	14.8	12.8	13.0	12.0
MnO	0.54	0.15	0.08	0.25	0.21	0.25	0.18	0.14	0.18	0.06
MgO	12.6	12.7	12.9	13.1	13.1	13.2	12.3	13.0	13.6	12.8
CaO	10.8	11.4	10.5	10.9	10.8	10.8	10.8	11.3	12.1	10.6
Na_2O	2.0	2.1	2.2	2.3	2.3	2.1	2.6	2.5	2.2	2.2
K_2O	0.53	0.39	0.52	0.55	0.57	0.49	0.59	0.65	0.37	0.62
Total	94.57	95.34	95.30	97.80	96.88	96.14	97.37	97.49	98.65	96.38

Each column is the average of 5—10 analytical points per grain

Totals are low due to the presence of H_2O, which cannot be analyzed by microprobe

Mg #	0.64	0.63	0.65	0.62	0.64	0.64	0.60	0.64	0.65	0.65
				Numbers of Cations on the basis of 23 (O)						
Si	6.235	6.266	6.253	6.357	6.346	6.604	6.180	6.230	6.305	6.251
Ti	0.315	0.284	0.381	0.290	0.303	0.203	0.338	0.346	0.305	0.290
Al	2.272	2.145	2.221	1.908	1.966	1.747	2.103	2.098	1.953	2.112
Fe	1.527	1.615	1.493	1.790	1.671	1.692	1.858	1.589	1.598	1.665
Mn	0.010	0.069	0.008	0.025	0.025	0.038	0.025	0.013	0.023	0.019
Mg	2.888	2.878	2.835	2.902	2.910	2.948	2.751	2.876	2.976	2.872
Ca	1.700	1.769	1.693	1.738	1.759	1.736	1.738	1.799	1.904	1.848
Na	0.635	0.601	0.628	0.662	0.664	0.610	0.756	0.719	0.633	0.619
K	0.099	0.103	0.118	0.114	0.114	0.096	0.115	0.132	0.069	0.075

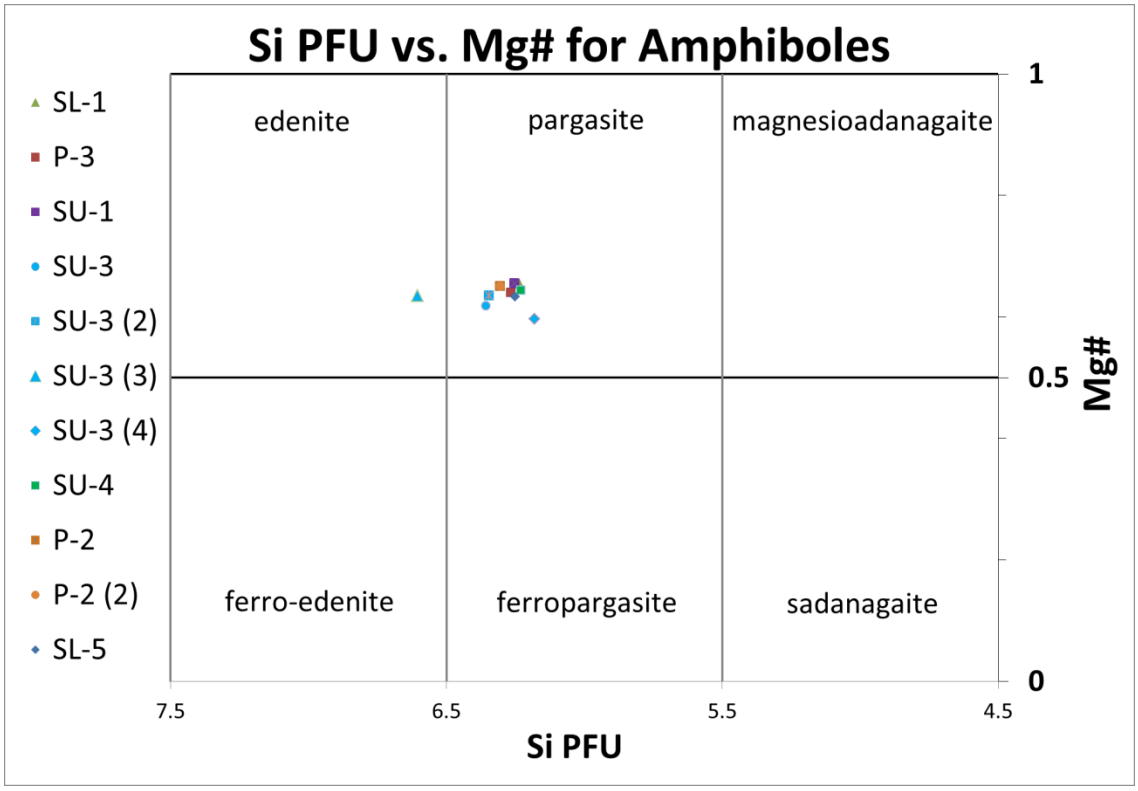

Fig. 14. Compositions of amphibole phenocrysts in Sugarloaf andesites and dacite plotted using the Mg# vs. Si per formula unit (PFU) diagram from Leake *et al*. (1997). Numbers in parentheses designate the second, third, and fourth amphibole grains analyzed from the same sample.

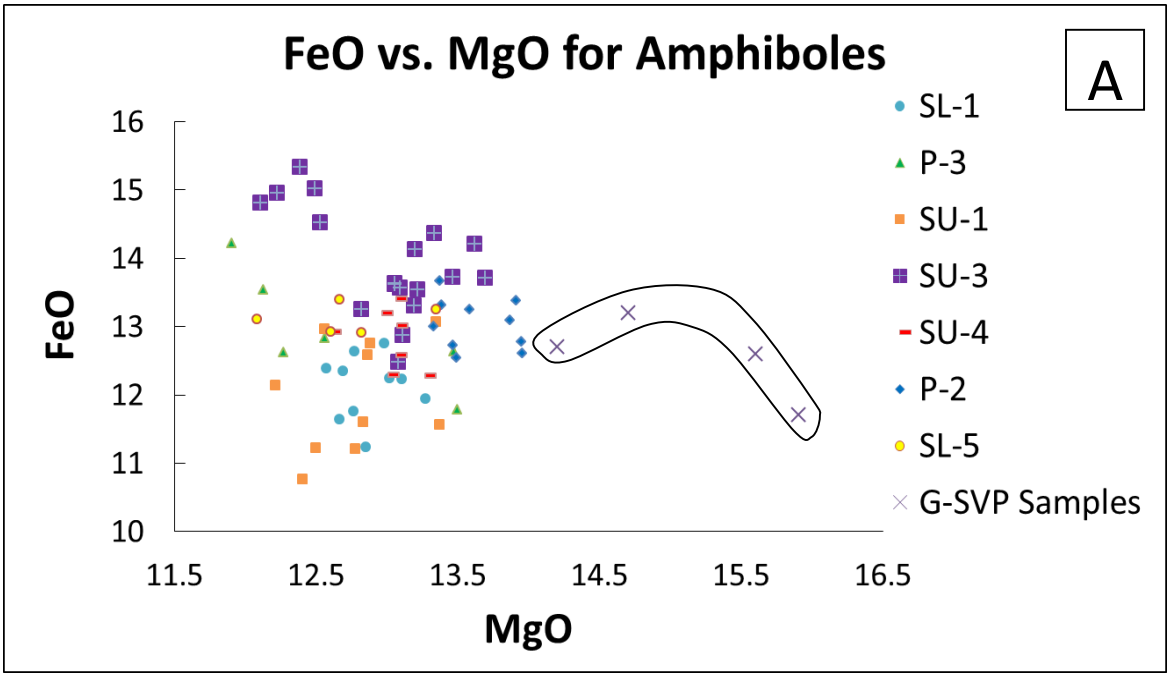

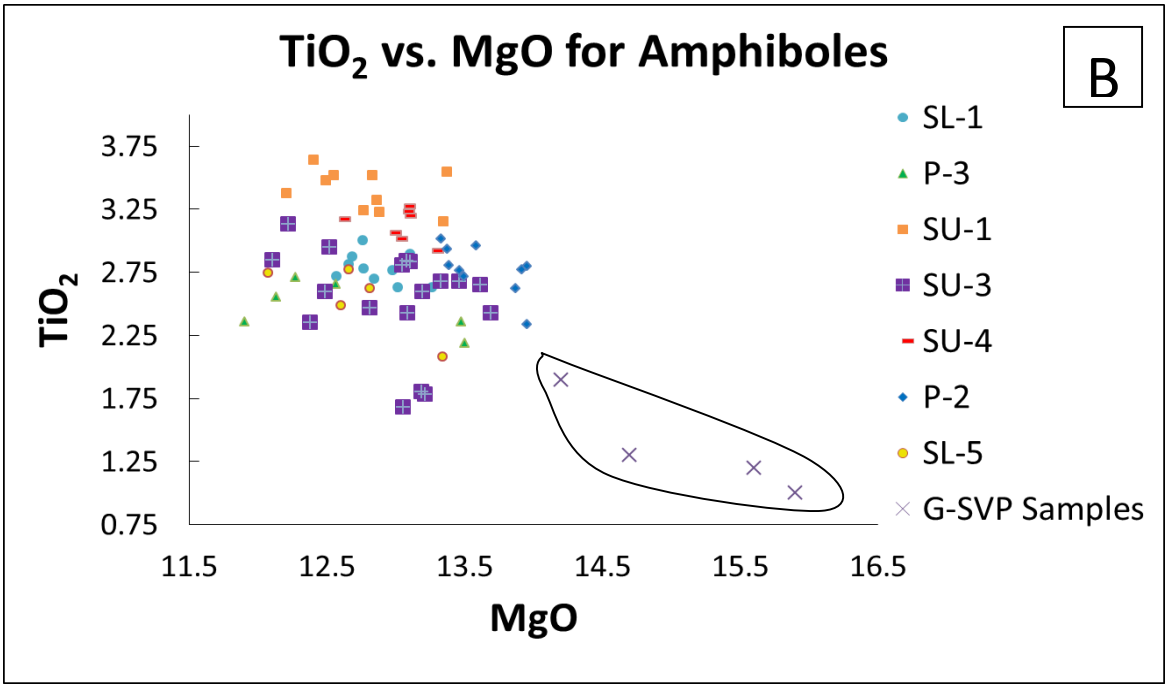

Fig. 15. MgO variation diagrams for FeO (panel A) and TiO_2 (panel B) showing abundances in amphibole phenocrysts from Sugarloaf andesites and dacite and also from rhyolites from the Goldfield-Superstition volcanic province (Dombroski, 2010) labeled here as G-SVP samples. Each plotted point represents a point on an amphibole grain analyzed by electron microprobe.

Biotite

One biotite phenocryst in the dacite (SL-5) was analyzed. The average composition is presented in Table 7. Sugarloaf biotite FeO and TiO_2 are plotted versus MgO in Fig. 16. Average values for G-SVP biotites (Dombroski, 2010) are plotted for comparison. Sugarloaf biotite has lower MgO than all but one G-SVP biotite (Fig. 16). The G-SVP biotite FeO concentrations form an inverse correlation with MgO, and the Sugarloaf biotite fits into that trend at the low-MgO end.

Table 7: Average composition of one biotite phenocryst in a dacite from Sugarloaf Mountain, central Arizona

	SL-5
SiO_2	34.2
TiO_2	4.7
Al_2O_3	15.0
FeO	16.2
MnO	0.05
MgO	13.6
CaO	<0.01
Na_2O	0.90
K_2O	9.2
Total	93.85
Mg#	0.46

Column is the average of 8 analytical points

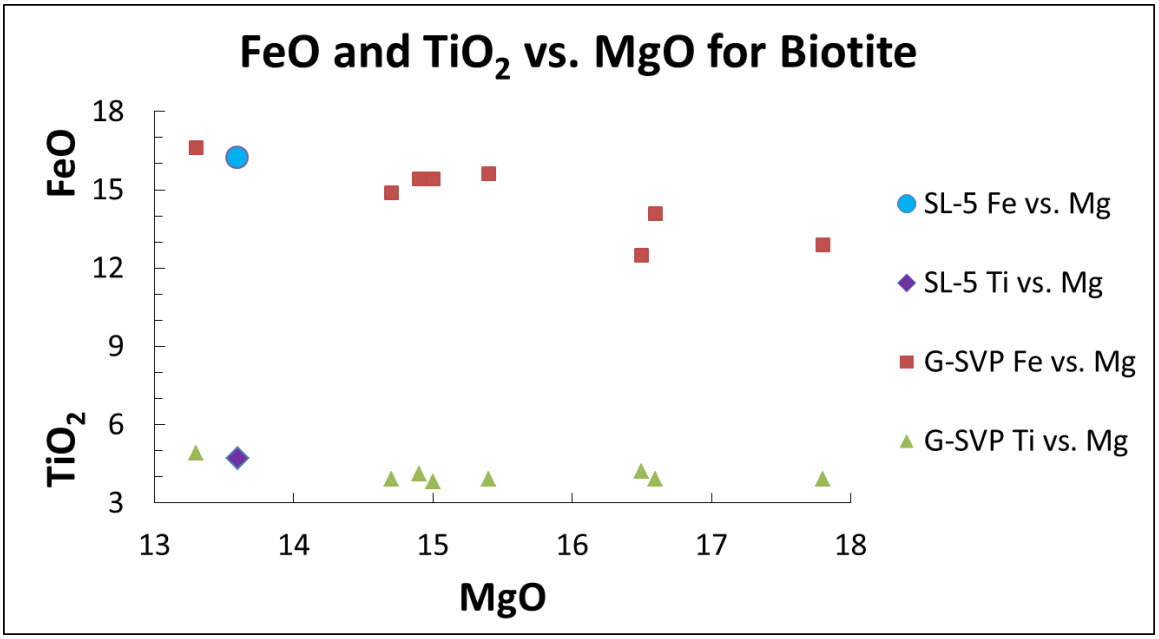

Fig. 16. MgO variation diagram for FeO and TiO_2 showing abundances in a biotite phenocryst from the Sugarloaf dacite and in biotite phenocrysts from rhyolites from the Goldfield-Superstition volcanic province (Dombroski, 2010) labeled here as G-SVP. Each data point represents an average of points on a biotite grain analyzed by electron microprobe.

DISCUSSION

Based on geochemistry and on modal mineralogy, two compositional groups make up the stacked, horizontal lava flows that constitute Sugarloaf Mountain. One group consists of intermediate-composition lavas that have phenocrysts largely of plagioclase, clinopyroxene, olivine, amphibole, quartz, and lesser amounts of biotite and orthopyroxene. These intermediate lavas are stratigraphically above the other group, which consists of alkalic basalt flows with phenocrysts of olivine and clinopyroxene. Each lava group has compositional variations among some of its major and trace elements and among some of its mineral compositions. All lavas have negative Nb-Ta anomalies, and some intermediate-composition lavas have negative Eu anomalies. Alkalic basalts compositionally similar to the Sugarloaf basalts are within 10 km of Sugarloaf at Stewart Mountain (Fig. 1A).

Understanding the petrogenesis of Sugarloaf Mountain lavas therefore must address: the origin of Sugarloaf intermediate-composition lavas with respect to their associated basaltic lavas; the causes of compositional variability among andesites and dacite as a group and among the basaltic lavas; the geochemical relationship of the intermediate-composition lavas to the basaltic lavas; some compositional characteristics of the Sugarloaf basaltic magma source materials; and the relationship of Sugarloaf basaltic lavas to nearby Stewart Mountain basalts of similar composition.

Origin of Sugarloaf andesites and dacite

Intermediate-composition lavas can originate by fractional crystallization of basaltic magma, assimilation of granitic country rock by a basaltic magma, magma mixing of basaltic and rhyolitic magmas, and by combinations of these three processes (Brophy & Dreher, 2000; Annen *et al.,* 2006; Hosono *et al.,* 2008; Macdonald *et al.,* 2008; Kent *et al.,* 2010). For example, at South Sister volcano, Oregon, Brophy & Dreher (2000) suggest that rhyolitic and andesitic magmas fractionally crystallized from a basaltic parent magma. Hosono *et al.* (2008) suggest that a parent basalt assimilated lower to middle crustal rock to produce high-K basalts and andesites in the Kyushu, Japan region. Kent *et al.* (2010) argue that Mount Hood andesites originated by magma mixing when mafic magma entered a shallow felsic magma chamber days before their eruptions. A combination of all three processes has been inferred at the Greater Olkaria Volcanic Complex, Kenya, by Macdonald *et al.* (2008) to explain the juxtaposition of basalts and andesites as well as disequilibrium features such as resorbed phenocryst rims and sieved plagioclase cores. I explore all of these processes for Sugarloaf intermediate lavas.

Fractional crystallization of Sugarloaf basalt to produce andesite and of andesite to produce dacite – major elements

Not all geochemical features of Sugarloaf lavas can be explained by fractional crystallization, but some may be. For example, MgO concentrations decrease and K_2O concentrations

increase as SiO_2 concentrations increase from basalts to andesites and from andesites to dacite. These relationships are normal for fractional crystallization of basalt to produce evolved compositions.

One method used to test differentiation by fractional crystallization of Sugarloaf basalt to produce Sugarloaf andesite was mass balancing using least-squares linear regression (Bryan *et al.,* 1969). Fractional crystallization of basalt to produce andesite was considered even though certain minerals, especially olivine and clinopyroxene, are present with similar compositions in both rock types. This overlap does not preclude a fractional crystallization relationship if convective mixing followed or occurred along with fractionation. I explored the highest-MgO Sugarloaf andesite (SL-4) as a possible daughter product of Sugarloaf basalts P-5 and SL-6. In the model, mineral compositions from or appropriate to Sugarloaf basalts were segregated from the parent melt.

The mass balancing model calculates the parent composition that mathematically could produce the daughter. After calculation, the differences for each major element between actual and calculated compositions are summed and squared. A sum close to zero implies a good fit, and a sum greater than 1 implies a poor fit. Table 8 shows that P-5 crystallized 4.3% olivine, 29.1% clinopyroxene, 38.5% plagioclase, 7.9% magnetite, and 2.1% ilmenite, with 18.2% as the calculated residual liquid (daughter). The fit is 1.36. The model for trachy-basalt SL-6 as a parent produces the same mineral assemblages but with the sum

of squares even higher at 4.50 (Table 8). The mass balancing models for major elements therefore suggest that fractional crystallization did not function as a single mechanism to produce the andesites.

Table 8: Least squares mass balancing for Sugarloaf basalts P-5 (MgO 7.72 wt. %) and SL-6 (MgO 7.13 wt. %) as parents to Sugarloaf andesite SL-4 (MgO 4.69 wt. %)

	Actual P-5 parent magma composition	Calculated parent magma (to yield SL-4 as daughter)
SiO_2	49.02	49.25
TiO_2	2.01	2.15
Al_2O_3	14.02	14.23
FeO	10.08	10.27
MnO	0.17	0.13
MgO	7.72	7.82
CaO	10.55	10.60
Na_2O	3.07	2.63
K_2O	1.41	0.77

These phases crystallize from P-5 parent in these percentages:	
Olv $Fo_{77.4}$	4.25
Cpx Mg#85	29.08
Pl $An_{47.4}$	38.49
Mt (75.3% FeO)	7.94
Ilm (48.1% FeO)	2.06
Residual (liquid)	18.18
Σr^2	1.36

	Actual SL-6 parent magma composition	Calculated parent magma (to yield SL-4 as daughter)
SiO_2	47.23	48.02
TiO_2	2.41	2.86
Al_2O_3	14.29	14.82
FeO	10.60	11.34
MnO	0.17	0.13
MgO	7.13	7.50
CaO	10.56	10.80
Na_2O	3.06	1.95
K_2O	2.07	0.88

These phases crystallize from SL-6 parent in these percentages:	
Olv Fo_{85}	2.72
Cpx Mg#81	25.97
Pl $An_{74.1}$	21.93
Spinel (60.5% FeO)	9.02
Ilm (48.1% FeO)	3.08
Residual (liquid)	37.28
Σr^2	4.50

Σr^2 is obtained by determining the difference between actual and calculated parent composition for each element, squaring the differences, and then summing all squared differences

Mass balancing does not evaluate fractional crystallization of basalt in terms of temperature, pressure, or oxygen fugacity. Therefore, as another evaluation of fractional crystallization that applies these magma parameters, I used MELTS modeling (Ghiorso & Sack, 1995; Asimow & Ghiorso, 1998) for the evolution of differentiated liquid in 5°C increments of crystallization for basalts SL-6 and P-5 under varying pressures and oxygen fugacities. Crystallization proceeded until the MgO concentration was lower than ≈4.7 wt. % (the highest andesitic MgO). I modeled pressures of 1 kbar and 8 kbar under redox conditions of FMQ-2 (slightly reducing) and FMQ+1 (slightly oxidizing). Oxygen fugacities between FMQ-2 and FMQ+1 are reasonable to consider for basalt crystallization (Mallmann & O'Neill, 2007; Mayfield *et al.,* 2011).

For both P-5 and SL-6 under all conditions evaluated, the MELTS modeling shows that when the daughter liquids reached MgO concentrations approximating that of SL-4 (≈4.7 wt. %), the SiO_2 concentrations remained basaltic (≈50 wt. %) (Tables 9–10; Figs. 17–18). The MgO vs. SiO_2 curves in Figs. 17 and 18 show that MgO reached and then passed 4.7 wt. % without SiO_2 coming close to an andesitic concentration (≈61.8 wt. %). Temperature of crystallization in the model output decreased ≈60–80°C between the beginning of crystallization and the commencement of andesitic MgO concentrations. These curves also show that when SiO_2 concentration did begin to increase significantly, MgO was less than half the andesitic value (Figs. 17–18).

Table 9: MELTS modeling for fractional crystallization of parent Sugarloaf basalt P-5 (MgO 7.72 wt. %) to daughter Sugarloaf andesite SL-4 (MgO 4.69 wt. %) under four conditions with varying pressure and fO_2. Minerals crystallized from the parent melt are presented as percentages of the magma system along with partial compositions for P-5 and four calculated residual daughter melts.

		Compositions resembling SL-4 under these conditions for P-5 crystallization							
	Parent P-5	FMQ-2; 1212 - 1132˚C 0.5 wt. % H_2O (1000 bar)		FMQ+1; 1188-1118 ˚C 0.5 wt. % H_2O (1000 bar)		FMQ-2; 1293 - 1228 ˚C 0.5 wt. % H_2O (8000 bar)		FMQ+1; 1293 - 1228 ˚C 0.5 wt. % H_2O (8000 bar)	
SiO_2	49.02%	50.12%		51.00%		48.95%		49.19%	
TiO_2	2.01	2.30		2.20		2.49		2.48	
FeO	10.08	9.04		7.04		9.78		7.67	
MgO	7.72	4.47		4.51		4.50		4.64	
K_2O	1.41	1.75		2.01		1.89		1.92	
Ol		Fo_{82-79}	6.10%	Fo_{78-85}	0.37%		-		-
Opx			-		-	$Mg\#_{79-81}$	0.78%		-
Cpx		$Mg\#_{77-81}$	11.10	$Mg\#_{75-81}$	0.87	$Mg\#_{83-84}$	23.75	$Mg\#_{72-81}$	26.10%
Pl		An_{72-73}	1.89	An_{66-69}	1.50		-		-
Fe-Ti ox			-	Usp_{27-32}	0.61		-		-
Whitlockite			-		-		0.25		0.16

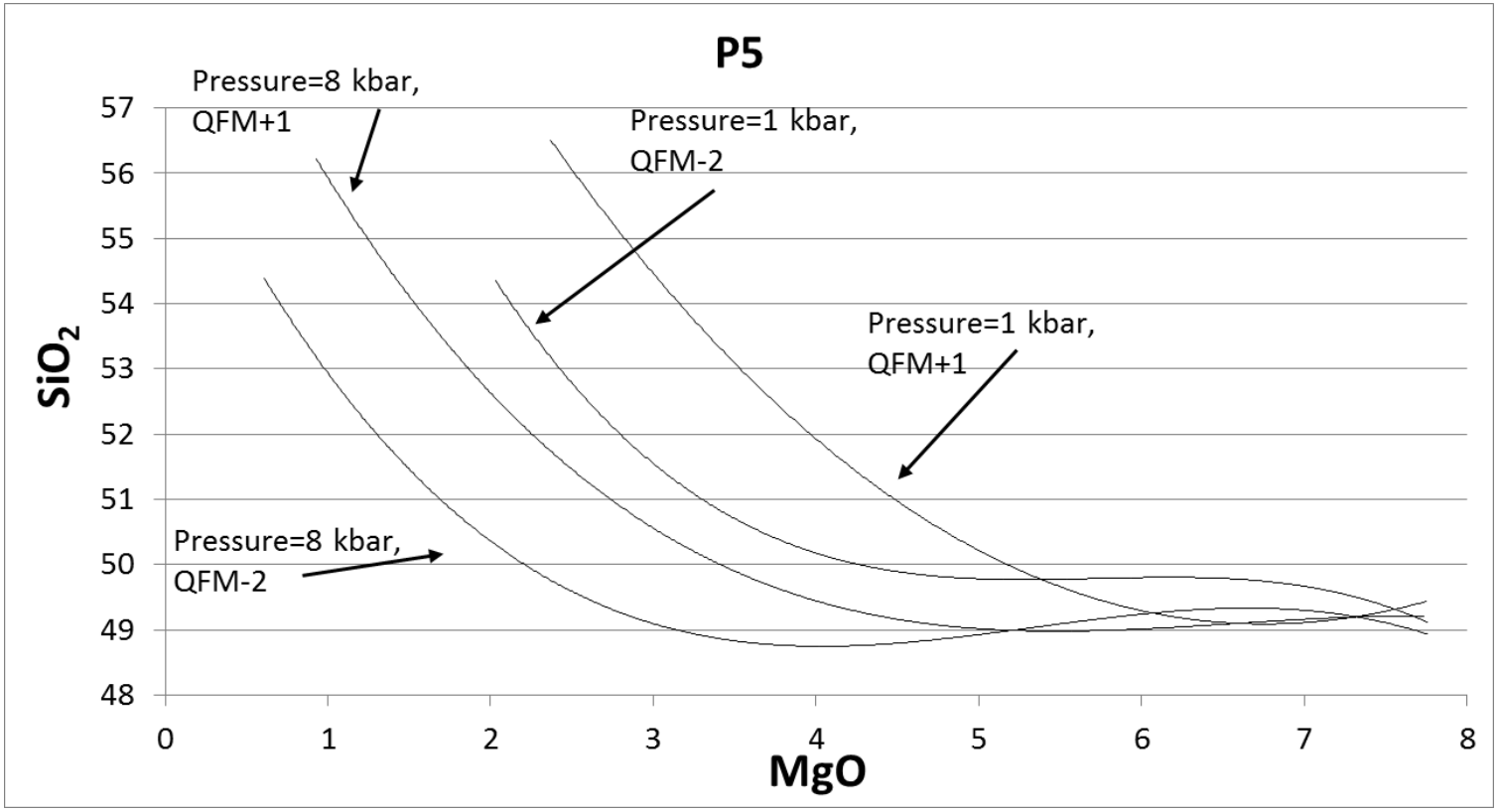

Fig. 17. Diagram showing lines of best fit for MgO and SiO_2 (wt. %) abundances during MELTS modeling for crystallization of Sugarloaf basalt P-5 (Table 9). An SiO_2 concentration high enough to resemble the Sugarloaf andesites is not achieved when MgO is ≈3.5–4.7 wt. % (andesitic).

Table 10: MELTS modeling for fractional crystallization of parent Sugarloaf basalt SL-6 (MgO 7.13 wt. %) to daughter Sugarloaf andesite SL-4 (MgO 4.69 wt. %) under four conditions with varying pressure and fO_2. Minerals crystallized from the parent melt are presented as percentages of the magma system along with partial compositions for SL-6 and four calculated residual daughter melts.

		Compositions resembling SL-4 under thse conditions for SL-6 crystallization					
	Parent	FMQ-2; 1202 - 1132 ˚C		FMQ+1; 1174 - 1124 ˚C		FMQ-2; 1276 - 1221 ˚C	FMQ+1; 1282 - 1222 ˚C
	SL-6	0.5 wt.% H_2O (1000 bar)		0.5 wt.% H_2O (1000 bar)		0.5 wt. % H_2O (8000 bar)	0.5 wt. % H_2O (8000 bar)
SiO_2	47.23%	48.09%		49.19%		47.35%	47.57%
TiO_2	2.41	2.63		2.37		2.91	2.89
FeO*	10.60	9.38		7.00		10.50	8.23
MgO	6.74	4.54		4.60		4.58	4.65
K_2O	2.07	2.42		2.67		2.70	2.75
Ol		$Mg\#_{80\text{-}81}$	5.10%	$Fo_{77\text{-}84}$	1.85%	-	-
Cpx		$Mg\#_{76}$	8.60	$Mg\#_{77\text{-}79}$	17.38	-	-
Spinel			-	$Usp_{28\text{-}33}$	2.65	-	-

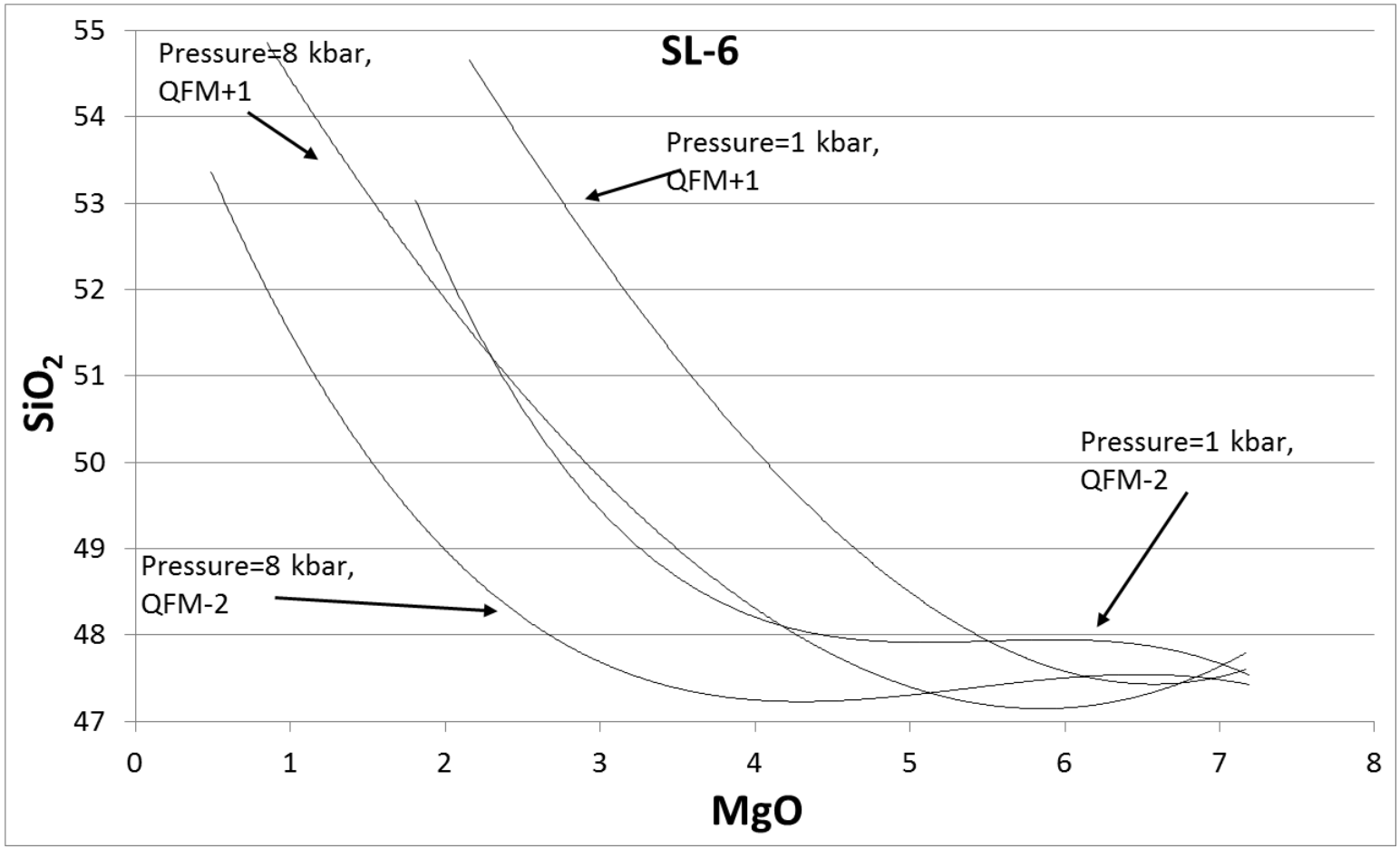

Fig. 18. Diagram showing lines of best fit for MgO and SiO_2 (wt. %) abundances during MELTS modeling for crystallization of Sugarloaf basalt SL-6 (Table 10). An SiO_2 concentration high enough to resemble the Sugarloaf andesites is not achieved when MgO is ≈3.5–4.7 wt. % (andesitic).

Even if fractional crystallization does not explain the presence of Sugarloaf andesites and dacite stratigraphically above Sugarloaf basalts, it may explain the range of chemical compositions present among the andesites and dacite. Between the andesites and the dacite, there is a decrease in MgO and increase in SiO_2 concentrations (Table 2). Therefore, mass balancing and MELTS models were also used to test the relationship between SL-4 (highest-MgO andesite) and SL-5 (dacite). In the mass balancing model, the melt composition for SL-4 crystallized 3.2% clinopyroxene, 7.2% amphibole, and 1.7% plagioclase, with the residual liquid having the composition of SL-5 (Table 11). This mineral assemblage and the low sum of squares value indicate that a crystallization relationship for the lower-MgO andesites and dacite by fractional crystallization is reasonable. Additionally, MELTS modeling was used to determine whether the SL-4 composition can evolve a dacitic composition through fractional crystallization under realistic conditions.

MELTS was used to create models of the andesite-dacite relationship under the same conditions applied to MELTS for basalt crystallization (Table 12). In the andesite-dacite models, a dacitic SiO_2 is reached after the calculated daughter liquids reach the actual dacite MgO of 3.5 wt. %. Namely, after ≈55 °C temperature decrease, the concentrations were ≈3.5 wt. % MgO but ≈62.3 wt. % SiO_2 (Fig. 19; Table 12) instead of the actual 63.9 wt. % SiO_2 of dacite SL-5. For example, at an oxygen fugacity of FMQ-2 and pressure of 1 kbar, the daughter liquid had concentrations of 62.4 wt. % SiO_2 and 3.4 wt. % MgO. Together, the reasonable results of the mass balancing andesite-dacite model (Table

11) and the failure of MELTS to relate the andesites with the dacite by fractional crystallization suggest that these rocks differ largely because of variation in the modal percentages of clinopyroxene, plagioclase, and amphibole.

Table 11: Least squares mass balancing for Sugarloaf andesite SL-4 (MgO 4.69 wt. %) as a parent to Sugarloaf dacite SL-5 (MgO 3.45 wt. %)

	Actual SL-4 parent magma composition	Calculated parent magma (to yield SL-5 as daughter)
SiO_2	61.81	61.66
TiO_2	1.18	1.14
Al_2O_3	13.74	13.59
FeO	5.70	5.61
MnO	0.09	0.09
MgO	4.69	4.46
CaO	5.74	5.79
Na_2O	3.24	3.33
K_2O	2.27	2.66
These phases crystallize from SL-6 parent in these percentages:		
Cpx Mg#79	3.24	
Amph Mg#65	7.17	
Pl $An_{44.3}$	1.74	
Residual (liquid)	87.90	
Σr^2	0.27	

Table 12: MELTS modeling for fractional crystallization of parent Sugarloaf andesite SL-4 (MgO 4.69 wt. %) to daughter Sugarloaf dacite SL-5 (MgO 3.45 wt. %) under four conditions with varying pressure and fO_2. Orthopyroxene crystallized from the parent melt is presented as percentages of the magma system along with partial compositions for SL-4 and four calculated residual daughter melts.

		Compositions resembling SL-5 under these conditions for SL-4 crystallization							
	Parent SL-4	FMQ-2; 1201 - 1146 ˚C 0.5 wt. % H_2O (1000 bar)		FMQ+1; 1190 - 1135 ˚C 0.5 wt.% H_2O (1000 bar)		FMQ-2; 1321 - 1266 ˚C 0.5 wt. % H_2O (8000 bar)		FMQ+1; 1313 - 1258 ˚C 0.5 wt. % H_2O (8000 bar)	
SiO_2	61.66%	62.42%		62.32%		62.42%		62.34%	
TiO_2	1.18	1.24		1.24		1.24		1.24	
FeO	5.70	4.77		3.67		4.88		3.82	
MgO	4.69	3.40		3.44		3.42		3.45	
K_2O	2.27	2.40		2.39		2.40		2.39	
Opx		Mg#80-82	5.05%	Mg#80-84	4.70%	Mg#80-83	4.51%	Mg#81-84	4.65%

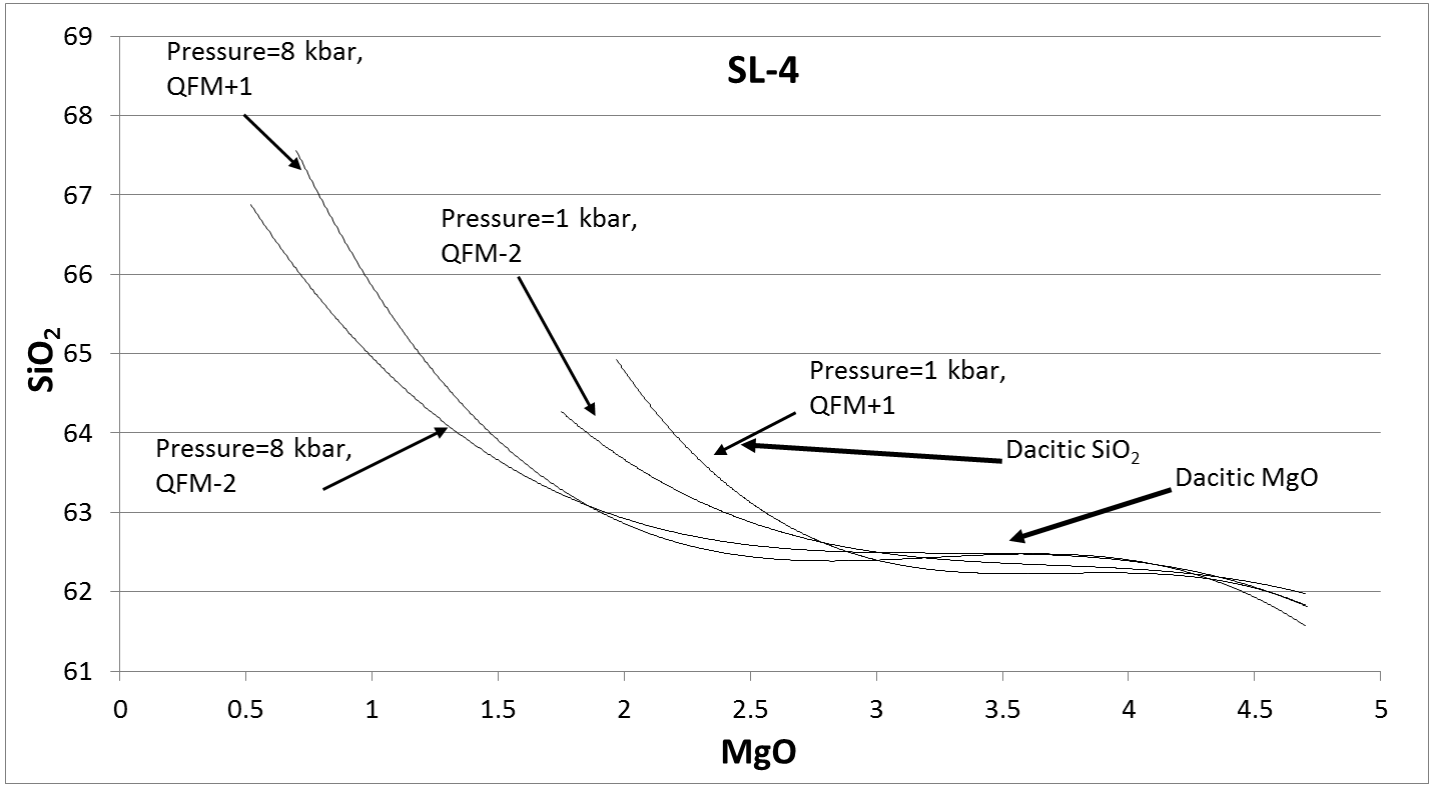

Fig. 19. Diagram showing lines of best fit for MgO and SiO_2 (wt. %) abundances during MELTS modeling for crystallization of Sugarloaf andesite SL-4 (Table 12). Daughter product SiO_2 concentrations high enough to resemble the Sugarloaf dacite (≈63.9 wt. %) are achieved, but only after the daughter MgO concentrations are less than ≈3.5 wt. % (dacitic).

Fractional crystallization of Sugarloaf basalt to produce andesite – trace elements

Mass balancing and MELTS modeling for major elements demonstrate the difficulty of the fractional crystallization process for producing Sugarloaf andesite from Sugaroaf basalt, but the models provide good results for fractional crystallization occurring within the group of intermediate lavas. To further explore whether fractional crystallization could relate the basalts to the andesites, the incompatible trace elements and K_2O abundances for these two compositional groups were examined. Some of these elements, such as K_2O, Ba, and Rb, increase as MgO decreases from basalt to andesite (Figs. 9–10). This is consistent with fractional crystallization of basalt, as basalt mineral assemblages do not readily incorporate these incompatible elements. Some other trace elements, such as Sc and Sr, are lower in the andesites and dacite than in the basalts. This, too, is consistent with fractional crystallization because the minerals clinopyroxene and plagioclase crystallize in basaltic magma and can incorporate Sc and Sr, respectively.

Many other incompatible trace elements, however, demonstrate the opposite trends of decreasing in abundance as MgO decreases from basalt to andesite. These include the rare earth elements Th, Nb, Ta, P, Sr, Hf, and Y, all of which are lower in the intermediate lavas than in the basalts (Figs. 9–10). For example, Ce decreases from 116 ppm in basalt P-5 to 96 and 77 ppm in andesite SL-4 and dacite SL-5, respectively. For the same samples, Zr decreases from 183 ppm to 165 and 151 ppm, respectively. Because there are no minerals that crystallize from basalt that incorporate these trace elements that

are lower in the evolved lavas than in the basalts, there must be a process other than fractional crystallization of basalt to account for the andesites and dacite.

Magma mixing and assimilation of wallrock

Another possibility for the origins of Sugarloaf intermediate lavas is that Sugarloaf basaltic magma incorporated crustal material that had relatively low incompatible trace element abundances but sufficient SiO_2 for the hybrid mixtures to have intermediate compositions. These characteristics can occur in a rock that is rich in quartz and feldspar. The SiO_2-rich, relatively low trace element material could be a rhyolitic magma or granitic country rock. If the SiO_2-rich end member was magma, it may have been produced by heat from basaltic magma emplaced into a region of the continental crust beneath Sugarloaf Mountain.

The presence of resorbed quartz, plagioclase, and amphibole in Sugarloaf andesites and dacite suggest that rhyolitic magma was crystallizing prior to mixing with basalt, and the elevated temperature resulting from the basalt mixing into rhyolite caused the rhyolite phenocrysts to be resorbed. Alternatively, these resorbed minerals could have been incorporated from country rock and exhibit the same resorption textures. Magma mixing or crustal assimilation could also explain some variation in mineral modes among and within certain Sugarloaf evolved samples. For example, andesite SU-1 contains both K-feldspar and plagioclase, and no K-feldspar was observed in the other andesites. Additionally, amphibole compositions differ among the andesites (Figs. 14–15; Table 6).

To evaluate this assimilation/mixing model, I explored the incorporation of representative upper crustal and Arizona granitic rocks into Sugarloaf basalts P-5 and SL-6. The upper crustal composition is the average in Rudnick & Gao (2003). The Arizona granitic material consists of a Stewart Mountain granite and a leucogranite, both from the Goldfield-Superstition volcanic province (unpublished data; R. Fodor, 2014). The results for mixing these three granitic compositions into basalt are in Table 13, which shows the proportions of basaltic and SiO_2-rich materials that produce compositions with major element abundances closely resembling those of andesite SL-4. The proportions of basalt in the mixtures range from 27 to 56% P-5 composition and from 25 to 53% SL-6 composition. These results are illustrated in Fig. 20, where the calculated hybrids' major element compositions are graphed against those observed for SL-4. The R^2 values for the best-fit linear curves are ≈0.99 to ≈0.999 for all major element graphs.

Selected trace elements are also calculated for the hybrids and compared to the actual SL-4 trace elements (Fig. 21). Even though trace element concentrations in the selected SiO_2-rich endmembers can vary much more widely than their major element concentrations, Fig. 21 shows that the calculated hybrids are similar to SL-4 in trace elements, with five out of the six calculated hybrids showing fits of 0.93 or higher. The fits are better for mixtures using basalt P-5 (fits ≈0.95–0.98) than trachy-basalt SL-6 (fits ≈0.86–0.93) which has higher incompatible element concentrations. Among the trace elements, Sr and Ba values are listed in Table 13 but not plotted on the graphs because they are both in

concentrations excessively high relative to other trace elements. Including Sr and Ba in the plots would therefore greatly reduce the R^2 value of best-fit linear curves through the overall trace element comparisons.

Table 14 shows major element results for assimilation of crystals that represent the phenocrysts in Sugarloaf andesites and dacite (plagioclase, K-feldspar, quartz, amphibole, and biotite) by basalts P-5 and SL-6. This simulates disaggregation of granitic wallrock crystals followed by melting and reaction. The percentages of the mixtures made up by each basalt and the minerals are presented as calculated hybrids in Table 14. For each calculated hybrid composition, basalt accounts for less than 50% of the mixture. The proportion of basalt used for the dacitic hybrid calculations (43–45%) is less than that used for the andesitic hybrid calculations (47–49%). This implies that more than 50% of the mixture components were crystals from wallrock. However, Sugarloaf andesites contain fewer than 25% phenocrysts. This disparity means that in order for this model to reflect the observed modes, more than half the xenocrysts must have melted. The R^2 values of the curves for actual versus calculated values in Fig. 22 are ≈0.99 to ≈0.999. These fits show that close approximations of the major elements in SL-4 and SL-5 can be produced by both P-5 and SL-6 compositions when they incorporate varying amounts of minerals (10–25% K-spar; 20–24% quartz; 9–16% plagioclase; 1–4% amphibole; 1–3% biotite) that are now present as phenocrysts in Sugarloaf intermediate lavas. However, rocks typically display positive Eu anomalies if they have incorporated large quantities of feldspar, but Sugarloaf

andesites actually have a slightly negative Eu anomaly. This model uses 19–36% feldspar, which may be sufficient to create a positive Eu anomaly, but none is observed for Sugarloaf lavas.

There are no noticeable compositional differences between hybrids created by basalt mixing with a rhyolitic magma and basalt assimilating SiO_2-rich country rock, as shown in Tables 13 and 14 and Figs. 20–22. Similarly, there are unlikely to be textural differences that distinguish the two processes. That is, during assimilation by basalt, granitoid rock partially melts, and unmelted minerals may react with the basalt, acquiring features such as those observed for quartz, feldspar, and amphibole in Sugarloaf intermediate lavas. These include Ca-rich plagioclase rims on some spongy plagioclase, and groundmass plagioclase richer in Ca (labradorite) than the spongy plagioclase phenocrysts (andesine). These reaction features and groundmass labradorite plagioclase laths will also result from mixing of basaltic and rhyolitic magmas when phenocrysts in the SiO_2-rich end member react with the basaltic magma.

Table 13: Hybrid magma compositions calculated by mixing basalts P-5 and SL-6 with average upper crust and two Arizona granite compositions for comparison with the actual composition of andesite SL-4

							Calculated Compositions (hybrids to simulate SL-4)					
	Basalt			Stewart Mt.**	GSVP**	Andesite	27% P-5	25% SL-6	41% P-5	38% SL-6	56% P-5	53% SL-6
	P-5	SL-6	Upper Crust*	granite	leucogranite	SL-4	73% UC	75% UC	59% SM	62% SM	44% G-S	47% G-S
SiO_2	49.02	47.23	66.60	70.85	78.20	61.81	61.85	61.76	61.90	61.87	61.86	61.79
TiO_2	2.01	2.41	0.64	0.48	0.06	1.18	1.01	1.08	1.11	1.21	1.15	1.31
Al_2O_3	14.02	14.29	15.40	14.02	12.10	13.74	15.03	15.12	14.02	14.12	13.18	13.26
FeO	9.07	9.54	5.04	2.98	0.60	5.13	6.13	6.17	5.48	5.47	5.34	5.34
MgO	7.72	7.13	2.48	0.95	0.16	4.69	3.89	3.64	3.73	3.30	4.39	3.85
CaO	10.55	10.56	3.59	2.22	0.53	5.74	5.47	5.33	5.64	5.39	6.14	5.85
Na_2O	3.07	3.06	3.27	3.05	2.47	3.24	3.22	3.22	3.06	3.05	2.81	2.78
K_2O	1.41	2.07	2.80	4.91	5.27	2.27	2.42	2.62	3.48	3.83	3.11	3.57
P_2O_5	0.71	1.00	0.15	0.17	0.02	0.59	0.30	0.36	0.39	0.49	0.41	0.54
Sr	969	1384	320	445	82.0	850	495	586	660	802	579	772
Ba	942	1262	628	934	161	2314	713	787	937	1059	598	745
Zr	183	237	193	208	61.0	165	190	204	198	219	129	154
Nb	33.7	41.5	12.0	12.9	4.3	22.3	17.9	19.4	21.4	23.8	20.8	24.0
La	55.9	83.0	31.0	44.0	37.0	56.3	37.7	44.0	48.9	58.8	47.6	61.4
Th	7.3	10.4	10.5	15.7	26.0	6.4	9.6	10.5	12.3	13.7	15.5	17.7
Hf	4.9	6.1	5.3	5.9	3.0	4.3	5.2	5.5	2.0	2.3	2.7	3.2
Ni	148	89.0	47.0	8.0	3.0	84.6	74.2	57.5	60.5	33.8	82.7	47.2

UC = upper crust; SM = Stewart Mt. granite, central Arizona; G-S = Goldfield-Superstition volcanic province granite

* from Rudnick & Gao (2003)

** unpublished data; R. Fodor (2014)

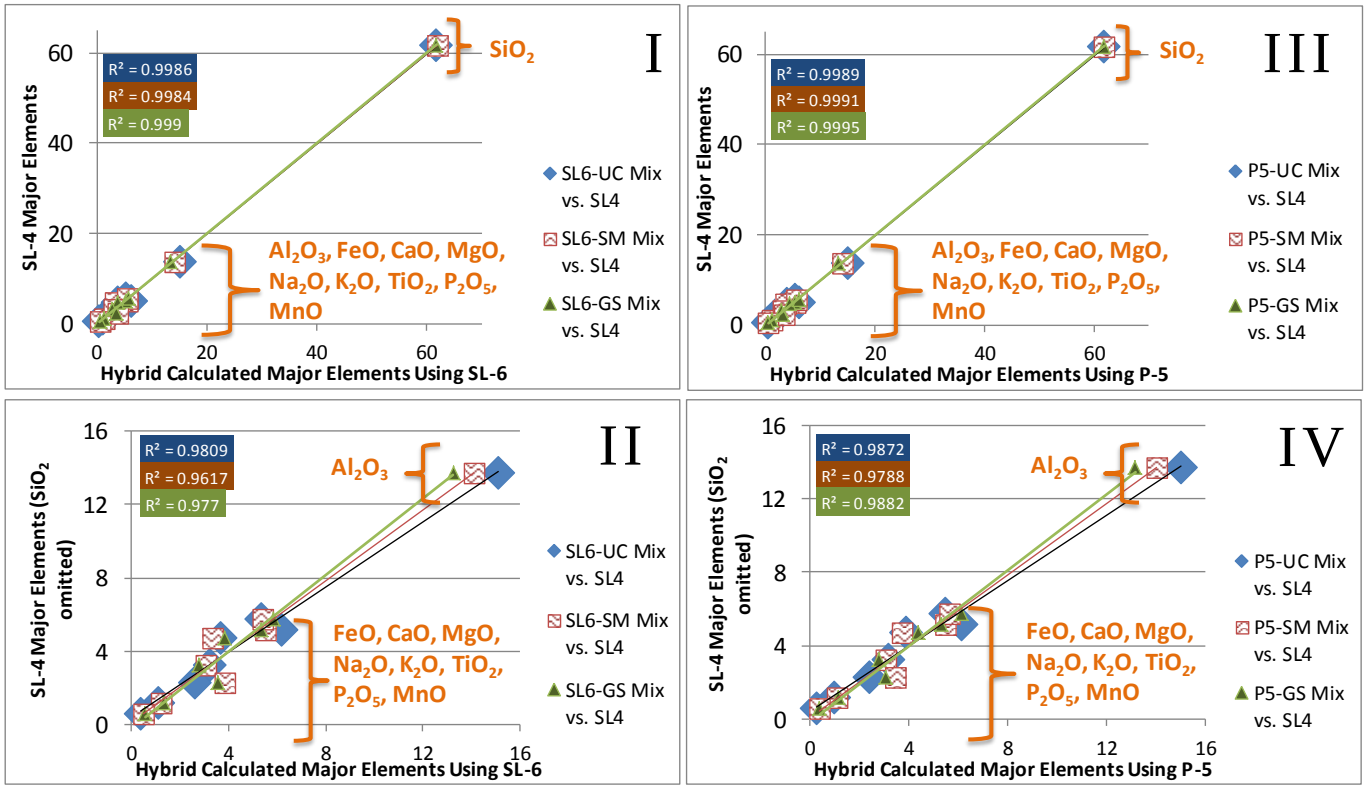

Fig. 20. Major element abundances calculated for hybrid magmas by mixing Sugarloaf basalts P-5 and SL-6 with crustal components (listed in Table 13) plotted against the actual Sugarloaf andesite SL-4 composition (Table 13) for comparison. Panels I and III show hybrids using SL-6 and P-5, respectively. Panels II and IV again show major element abundances for the hybrid magmas in Panels I and III, respectively, with SiO_2 omitted so that details of the calculated vs. actual major elements present at < 15 wt. % can be seen. The curve fits of $R^2 > 0.96$ illustrate the similarity of the calculated hybrids to SL-4. The crustal material mixed with P-5 and SL-6 are: UC (upper crust from Rudnick & Gao (2003)); SM (granite from Stewart Mountain); and GS (granite from the G-SVP).

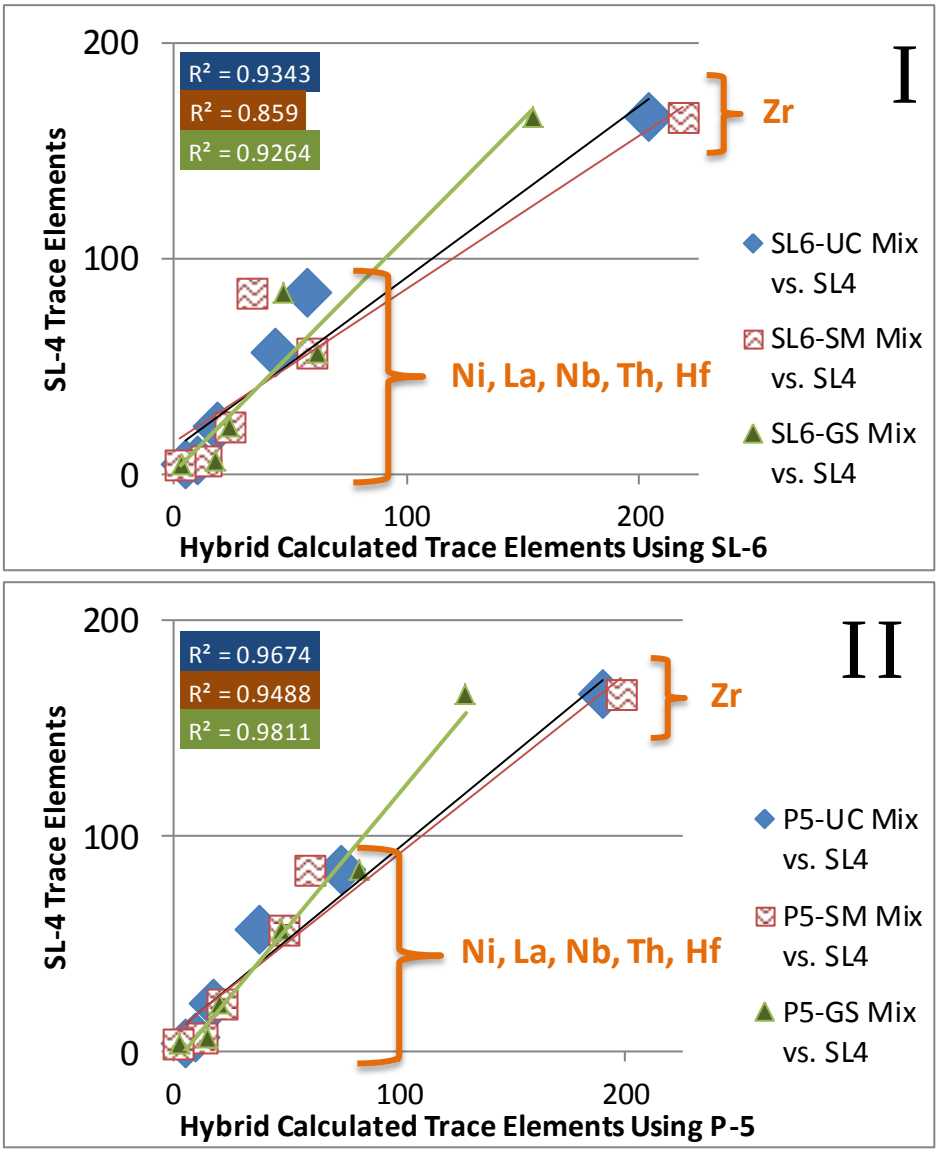

Fig. 21. Trace element abundances calculated for hybrid mixtures by mixing Sugarloaf basalts SL-6 (panel I) and P-5 (panel II) with crustal components listed in Table 13. These calculated hybrid mixtures are plotted against actual Sugarloaf andesite SL-4 for comparison (data from Table 2). The curve fit of $R^2 > 0.86$ for each graph illustrates the similarity of the calculated hybrid to SL-4. The crustal material mixed with P-5 and SL-6 are UC, SM, and GS as identified in Fig. 20 caption and Table 13.

Table 14: Hybrid magma compositions calculated by mixing quartz, feldspar, biotite, and amphibole into basalts P-5 and SL-6 for comparison with actual compositions of andesite SL-4 and dacite SL-5. The differences between actual compositions and calculated hybrids are listed.

	Basalts		Phenocrysts*					Andesite	Calculated Hybrids				Dacite	Calculated Hybrids			
	P-5	SL-6	Quartz	Amph	K-spar	Plag	Biotite	SL-4	A	Difference	B	Difference	SL-5	C	Difference	D	Difference
SiO_2	49.02	47.23	100.0	43.1	65.3	60.1	34.2	61.81	61.94	-0.13	61.89	-0.08	63.89	63.93	-0.04	63.91	-0.02
TiO_2	2.01	2.41		2.8			4.7	1.18	1.20	-0.02	1.33	-0.15	1.02	0.99	0.03	1.19	-0.17
Al_2O_3	14.02	14.29		11.3	19.4	24.9	15.0	13.74	13.42	0.32	13.40	0.34	13.72	13.53	0.19	13.12	0.60
FeO	11.20	11.78		13.0	0.08	0.26	16.2	6.33	6.32	0.01	6.40	-0.07	5.38	5.31	0.07	5.77	-0.39
MnO	0.17	0.17		0.18			0.05	0.09	0.09	0.00	0.09	0.00	0.09	0.08	0.01	0.08	0.01
MgO	7.72	7.13		13.6			13.6	4.69	4.58	0.11	4.04	0.65	3.45	3.73	-0.28	3.62	-0.17
CaO	10.55	10.56		12.1	0.03	5.7	< 0.01	5.74	6.36	-0.62	6.27	-0.53	4.82	5.18	-0.36	5.91	-1.09
Na_2O	3.07	3.06		2.2	4.8	7.7	0.90	3.24	3.27	-0.03	3.24	0.00	3.44	3.25	0.19	3.24	0.20
K_2O	1.41	2.07		0.37	10.0	0.78	9.2	2.27	2.08	0.19	2.42	-0.15	2.98	3.36	-0.38	2.98	0.00
P_2O_5	0.71	1.00						0.59	0.33	0.26	0.48	0.11	0.32	0.31	0.01	0.32	0.00
Total	99.88	99.70	100.00	98.65	99.61	99.44	93.85	99.68	99.58		99.57		99.11	99.66		100.13	

* Compositions representative of those observed in SL-4 and SL-5 (Tables 3 - 7)

A) Mix = 47% P-5, 10% K-spar, 20% quartz, 16% plagioclase, 3% biotite, and 4% amphibole

B) Mix = 49% SL-6, 11% K-spar, 21% quartz, 15% plagioclase, 2% biotite, and 2% amphibole

C) Mix = 43% P-5, 25% K-spar, 20% quartz, 9% plagioclase, 2% biotite, and 1% amphibole

D) Mix = 45% SL-6, 12% K-spar, 24% quartz, 16% plagioclase, 1% biotite, and 2% amphibole

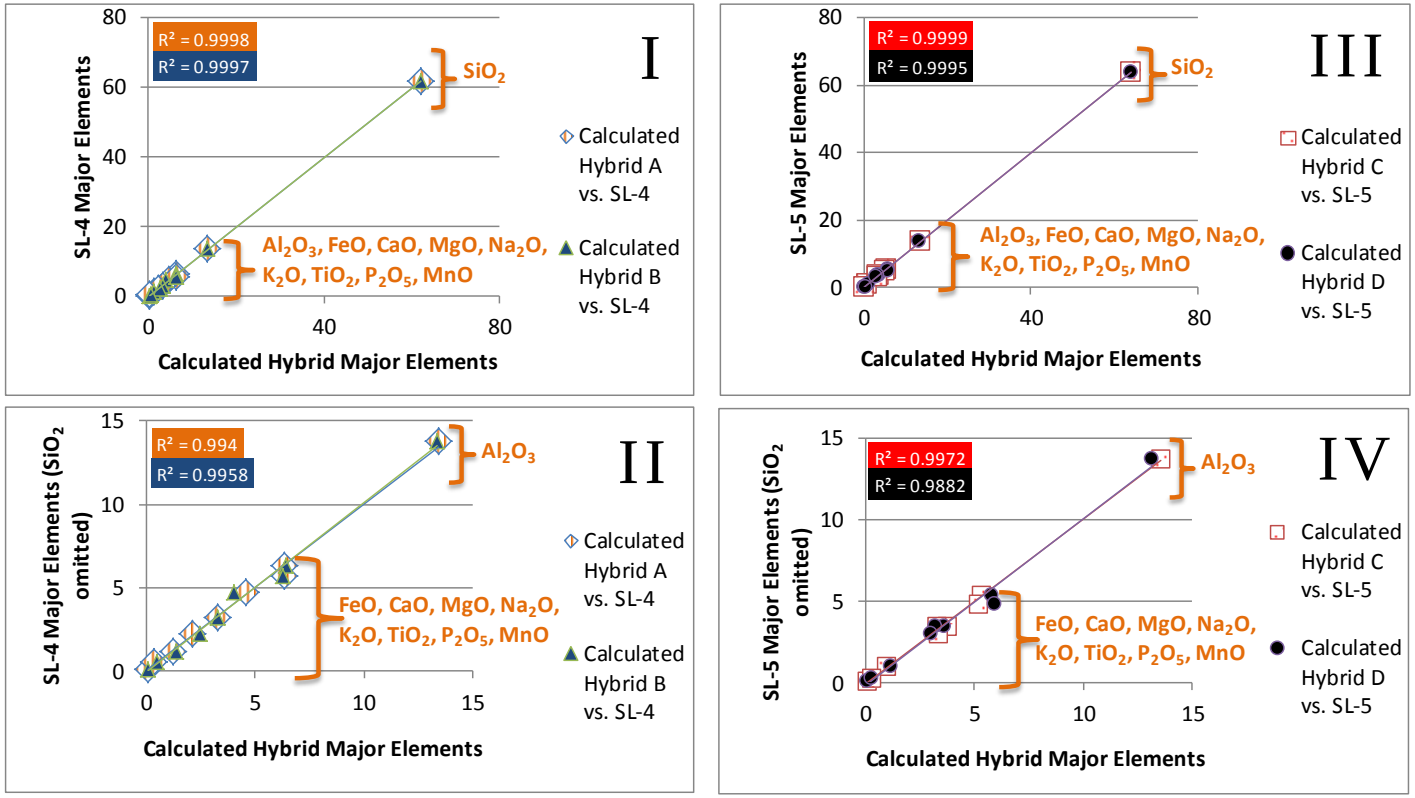

Fig. 22. Major element concentrations in hybrid magmas calculated by mixing Sugarloaf basalts P-5 and SL-6 with various amounts of minerals representative of those in Sugarloaf intermediate lavas. The hybrid compositions are labeled A, B, C, and D in Table 14, and the percentages of minerals used for each hybrid are listed in the Table 14 footnote. Panels I and II compare hybrids A and B to SL-4 and Panels III and IV compare hybrids C and D to SL-5. Panels II and IV show major elements with SiO_2 omitted, respectively for panels I and III, so that details of the calculated vs. actual major elements present at < 15 wt. % can be seen. Curve fits of $R^2 > 0.98$ illustrate the similarity of the calculated hybrids to SL-4 and SL-5.

Whether intermediate lavas result from magma mixing or assimilation of country rock, the petrographic characteristics of phenocrysts in the intermediate lavas will be identical. However, no granitoid xenoliths were observed in the intermediate lavas. If SiO_2-rich crustal rock assimilated and partially melted, it is likely that some rock fragments would remain as xenoliths in the lavas. It is possible that granitoid xenoliths are present in the Sugarloaf intermediate lavas without being present in the samples we studied. But because no granitoid xenoliths were observed, the most straight-forward interpretation is that magma mixing was the main process by which Sugarloaf intermediate lavas are related to Sugarloaf basaltic lavas.

This model for mixing between basaltic and rhyolitic magmas to produce andesites and dacite is consistent with models described in detail by Kent *et al.* (2010) for intermediate lavas at Mount Hood, Oregon and by Eichelberger (1978) for intermediate lavas at locations including the Ecuadorian Andes and New Zealand's Taupo Volcanic Zone. Namely, magma mixing is one of several possible origins for intermediate lavas occurring in volcanic fields that also contain basaltic lavas (Annen *et al.*, 2006) and Sugarloaf Mountain represents a relatively small volcanic field in which the intermediate lavas are related to the basalts by magma mixing. This instance further supports the origin of andesites by magma mixing processes that are known to have operated or to be currently operating in large volcanoes and volcanic provinces on a global scale.

Relationship between Sugarloaf trachy-basalt and alkalic basalts

The TAS diagram for Sugarloaf (Fig. 6) divides Sugarloaf basalts into trachy-basalt and alkalic basalts, and the trachy-basalt has higher incompatible trace element abundances (Figs. 8, 9A, and 10A; Table 2). These differences between the two basalt types occur at similar MgO concentrations among all Sugarloaf basalts (≈7.5 wt. %) (Fig. 8; Table 2). The incompatible element abundance differences can be explained by: (i) a different mantle source for each basalt type; or (ii) a single mantle source for both basalt types, with each type having been produced by a different degree of partial melting. Abundance ratios of highly incompatible trace elements in melts can help determine whether basalts have different or similar sources. This is because the ratios will remain constant during different degrees of partial melting from a single source, assuming that the incompatible elements are not fractionated during melting or subsequent melt differentiation. By contrast, abundance ratios will differ in basalt melts from different sources, regardless of the percentage of partial melting. Therefore, to evaluate trace element abundance ratios, several are plotted for the four basaltic samples (Fig. 23).

Some incompatible trace element ratios, such as Zr/Nb, Zr/Ba, La/Sm, and Th/La, are similar for the two basalt types (Fig. 23; Table 15), and this supports the possibility that they share a common mantle source. If so, then the two basalt types represent different degrees of partial melting, where the trachy-basalt, enriched in overall incompatible element abundances, represents a smaller percentage of melting. Using highly incompatible trace

elements, such as Ba, Nb, La, and P, which all have liquid-solid partitioning coefficients (K_Ds) approaching zero (e.g. 0.001), equilibrium melting can be applied to estimate relative differences in degree of partial melting required to yield the incompatible element abundances of each basalt type. Sugarloaf values can be input for the liquid concentration, C_L, in the equilibrium melting equation: $C_L/C_O = 1/(D(1-F)+F)$. There is not a known mantle composition for this region, but the original concentration, C_O, can be estimated as slightly enriched primitive mantle, using the enriched mantle source values shown in Table 16. If the K_Ds are assumed to be 0, then the equation used to calculate the percentage of partial melting, F, is $C_L/C_O = 1/F$. Solving for F (the percentage partial melting) for the trachy-basalt and the alkalic basalts will show their relative degrees of partial melting and help determine whether or not the trachy-basalt could represent a smaller degree of partial melting from a similar source.

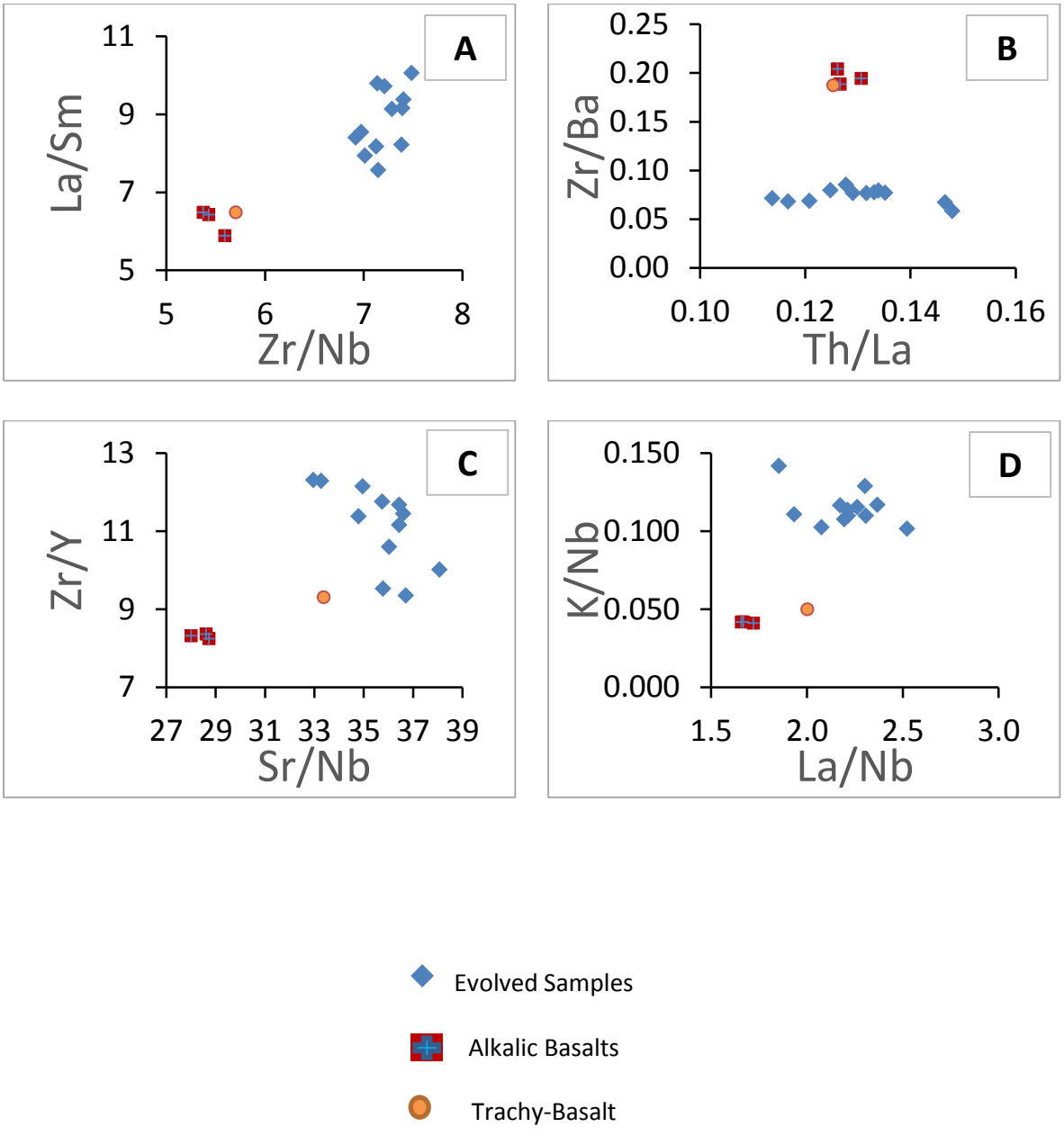

Fig. 23. Incompatible trace element ratio plots comparing Sugarloaf alkalic basalts, trachy-basalt, and evolved samples (andesites and dacite). Panels A and B show ratios that are similar for all Sugarloaf basalts. Panels C and D show trace element ratios that are different for the trachy-basalt and alkalic basalts.

Table 15: Selected trace element abundance ratios for three alkalic basalts and one trachy-basalt (SL-6) taken from Sugarloaf Mountain

	Alkalic			Trachy
Ratios	P-5	SU-5	P-4	SL-6
Zr/Nb	5.43	5.37	5.59	5.70
Zr/Ba	0.19	0.20	0.19	0.19
La/Sm	6.43	6.49	5.89	6.48
Th/La	0.13	0.13	0.13	0.13
Zr/Y	8.25	8.36	8.32	9.31
La/Nb	1.66	1.67	1.72	2.00
Sr/Nb	28.73	28.61	28.00	33.37
K_2O/Nb	0.04	0.04	0.04	0.05
Sr/Y	43.70	44.50	41.60	54.50
Rb/Y	0.94	0.97	0.98	1.40

Table 16: Equilibrium melting calculations using model enriched trace element abundances for the original concentration, C_O, and using Sugarloaf trachy-basalt (SL-6) and alkalic basalt (P-5) trace element abundances for the liquid concentration, C_L, to calculate the percentage of partial melting, F

	Model enriched mantle source	Trace element abundances		F (percent partial melt)	
	C_O	P-5	SL-6	P-5	SL-6
Ba	50.0	942.00	1262.00	5.3%	4.0%
Nb	1.8	33.73	41.47	5.3	4.3
La	3.3	55.90	83.00	5.9	4.0
P_2O_5	0.04	0.71	1.00	5.6	4.0

F calculated as $F = C_O/C_L$

Table 16 shows the percentage partial melting calculated using the equilibrium melting equation. These calculations estimate that the Sugarloaf trachy-basalt underwent partial melting of ≈4.0–4.3% while the alkalic basalts underwent greater partial melting of ≈5.3–5.9%. The higher alkalic basalt partial melting percentages show that for a reasonable mantle composition, differences between the trachy-basalt and alkalic basalt abundances of four highly incompatible trace elements could be produced by a smaller degree of partial melting from a common mantle source.

On the other hand, there are also incompatible trace element ratios for which the two basalt types are different. These ratios include Zr/Y, La/Nb, Sr/Nb, and K/Nb (Fig. 23). These differences in some trace element ratios suggest different mantle sources for each basalt type. Most of these ratios include Nb. A likely explanation for the coexisting basalt types is that they represent partial melting differences of a common enriched mantle source, but there was some compositional heterogeneity with respect to some trace elements, such as Nb and Y. The same scenario also could explain the differences between Sugarloaf basalts and some other regional basalts, namely the Stewart Mountain alkalic basalts. These regional basalts have slightly lower overall incompatible element abundances (Figs. 7–8), and their compositions could represent a slightly higher degree of partial melting of the mantle source for Sugarloaf basalts.

CONCLUSIONS

1) The lavas that make up Sugarloaf Mountain are bimodal as basalt and intermediate compositions. Sugarloaf basalts are both alkalic basalt and trachy-basalt compositions, and they each have olivine and clinopyroxene phenocrysts. The intermediate lavas are andesites and dacite, and their mineral assemblages include olivine, clinopyroxene, plagioclase, amphibole, quartz, ± orthopyroxene, ± biotite.

2) MELTS and mass balancing models to relate the basalts and andesites show that the two lava types cannot be related by fractional crystallization under various conditions of pressure and fO_2. Additionally, the lower abundances of many incompatible trace elements in andesites relative to those in basalts are inconsistent with a fractional crystallization relationship.

3) Mass balancing models suggest that the dacite may be related to the highest-MgO andesite by fractional crystallization of clinopyroxene, amphibole, and plagioclase. MELTS modeling, however, does not support this relationship under a variety of tested pressures and fO_2. Therefore, whether an intermediate lava is andesitic or dacitic, it is probably due to the variation in modal mineralogy.

4) Petrographic textures in Sugarloaf lavas include reaction rims and spongy oligoclase-andesine cores, thin Ca-plagioclase rims on Na-plagioclase cores, Ca-plagioclase groundmass laths, resorbed amphiboles, resorbed quartz grains (some with reaction rims), olivine and clinopyroxene phenocrysts, and a K-feldspar xenocryst in the intermediate composition lavas. All combined, these textures are consistent with a hybrid origin between basaltic magma and silicic rock or magma that contained at least Na-plagioclase, amphibole, quartz, and orthoclase.

5) Sugarloaf alkalic basalt and trachy-basalt as model parent magmas mixed with various compositions of silicic crustal magmas in proportions of 25 to 56% (basalt) and 44 to 75% (crust) create andesitic compositions resembling those of Sugarloaf andesite. For example, evaluating the hybrid composition as linear curves through data points for calculated hybrid vs. actual (SL-4) major-element values yield correlation coefficients of $R^2 \approx 0.96\text{-}0.99$.

6) Either basalt-rhyolite magma mixing or assimilation of SiO_2-rich country rock could produce Sugarloaf andesite chemical compositions. However, given the absence of lithic fragments in the andesites and dacite, the hybridization was most likely a mixing of basaltic and silicic magmas. The hybrid origin for Sugarloaf andesite and dacite lavas presented here are in the fashion of how Kent *et al.* (2010) and Eichelberger (2010) modeled andesite development at Mt. Hood, Oregon and Mt. Pinatubo, Philippines, respectively.

7) Sugarloaf Mountain alkalic basalts and trachy-basalt appear to be related by slightly different degrees of partial melting of a common source, enriched subcontinental lithosphere, that had some trace element heterogeneities. The nearby Stewart Mountain basalts likely had the same source but represent a slightly greater percentage of melting than Sugarloaf alkalic basalt.

8) The Sugarloaf Mountain and Stewart Mountain lavas are examples of small additions to continental crust in central Arizona resulting from partial melting of the upper mantle.

REFERENCES

Anderson, A. T. (1976). Magma mixing: petrological process and volcanological tool. *Journal of Volcanology and Geothermal Research* **1**, 3-33.

Annen, C., Blundy, J. D. & Sparks, R. S. J. (2006). The genesis of intermediate and silicic magmas in deep crustal hot zones. *Journal of Petrology* **47**, 505-539.

Asimow, P. D. & Ghiorso, M. S. (1998). Algorithmic modifications extending MELTS to calculate subsolidus phase relations. *American Mineralogist* **83**, 1127-1132.

Baldy, Tim (2014). Sugarloaf Mountain by tbaldy. *Panoramio.* 33°41'4.09''N and 111°31'29.17''W. December 7, 2014. June 5, 2015.

Beattie, P., Ford, C. & Russell, D. (1991). Partition coefficients for olivine-melt and orthopyroxene-melt systems. *Contributions to Mineralogy and Petrology* **109**, 212-224.

Brophy, J. G. & Dreher, S. T. (2000). The origin of composition gaps at South Sister volcano, central Oregon; implications for fractional crystallization processes beneath active calc-alkaline volcanoes. *Journal of Volcanology and Geothermal Research* **102**, 287-307.

Bryan, W.B., Finger, L.W. & Chayes, F. (1969). Estimating proportions in petrographic mixing equations by least-squares approximation. Science **163**, 926-927.

Burchfiel, B.C., Cowan, D.S. & Davis, G.A. (1992). Tectonic overview of the Cordilleran orogeny in the western United States. Ch. 8. Burchfiel, B.C., Lipman, P.W., and Zoback, M.L., eds., *The Cordilleran Orogen: Conterminous U.S.: Boulder, Colorado, Geological Society of America. The Geology of North America* **G-3**, 407-479.

Christiansen, R. L. & Yeats, R. S. (1992). Post-Laramide geology of the U.S. Cordilleran region. Ch. 7. Burchfiel, B.C., Lipman, P.W., and Zoback, M.L., eds., *The Cordilleran Orogen: Conterminous U.S.: Boulder, Colorado, Geological Society of America. The Geology of North America* **G-3**, 261-406.

Dombroski, B. (2010). Mineralogy, petrology, and geochemistry of Miocene silicic lavas and pyroclastic flows, Goldfield-Superstition volcanic province, central Arizona. Masters Thesis, North Carolina State University. 118 p.

REFERENCES

Eichelberger, J. C. (1978). Andesitic volcanism and crustal evolution. *Nature* **275**, 21-27.

Eichelberger, J. (2010). Volcanology: messy magma mixtures. *Nature Geoscience* **3**, 593-594.

Fodor, R. V., Johnson, K.G. & Dombroski, B.A. (2012). Intermediate-composition lavas, Goldfield-Superstition volcanic field, central Arizona: hybrids of mixed basaltic and silicic magmas. *2012 GSA Annual Meeting in Charlotte*.

Fodor, R. V. & Vetter, S. K. (2011). Miocene basaltic magmatism in the Goldfield-Superstition volcanic province, central Arizona: geochemistry, mineralogy, and petrology. *Rocky Mountain Geology* **46**, 1-41.

Ghiorso, M. S. & Sack, R. O. (1995). Chemical mass transfer in magmatic processes IV. A revised and internally consistent thermodynamic model for the interpolation and extrapolation of liquid-solid equilibria in magmatic systems at elevated temperatures and pressures. *Contributions to Mineralogy and Petrology* **119**, 197-212.

Glazner, A.F. & Bartley, J. M. (1984). Timing and tectonic setting of Tertiary low-angle normal faulting and associated magmatism in the southwestern United States. *Tectonics* **3**, 385-396.

Google Earth. Sugarloaf Mountain, central Arizona. 33°41'47.44"N and 111°31'51.25"W. March 14, 2015. May 13, 2015.

Green, T. H. & Watson, E. B. (1982). Crystallization of apatite in natural magmas under high pressure, hydrous conditions, with particular reference to 'orogenic' rock series. *Contributions to Mineralogy and Petrology* **79**, 96-105.

Hosono, T., Nakano, T., Shin, K. & Murakami, H. (2008). Assimilation of lower to middle crust by high alumina basalt magma as an explanation for the origin of medium-K volcanic rocks in southern Kyushu, Japan. *Lithos* **105**, 51-62.

Humphreys, E. D. (1995). Post-Laramide removal of the Farallon slab, western United States. *Geology* **23**, 987-990.

REFERENCES

Kent, A. J., Darr, C., Koleszar, A. M., Salisbury, M. J. & Cooper, K. M. (2010). Preferential eruption of andesitic magmas through recharge filtering. *Nature Geoscience* **3**, 631-636.

Leake, B. E., Woolley, A. R., Arps, C. E. S., Birch, W. D., Gilbert, M. C., Grice, J. D. *et al.* (1997). Nomenclature of amphiboles; report of the Subcommittee on Amphiboles of the International Mineralogical Association, Commission on New Minerals and Mineral Names. *American Mineralogist* **82**, 1019-1037.

Le Bas, M. J., Le Maitre, R. W., Streckeisen, A., & Zanettin, B. (1986). A chemical classification of volcanic rocks based on the total alkali-silica diagram. *Journal of Petrology* **27**, 745-750.

Lipman, P. W. (1992). Magmatism in the Cordilleran United States; Progress and problems. Ch. 9. Burchfiel, B.C., Lipman, P.W., and Zoback, M.L., eds., *The Cordilleran Orogen: Conterminous U.S.: Boulder, Colorado, Geological Society of America. The Geology of North America* **G-3**, 481-514.

Liu, M. (2001). Cenozoic extension and magmatism in the North American Cordillera: the role of gravitational collapse. *Tectonophysics* **342**, 407-433.

Macdonald, G. A. & Katsura, T. (1964). Chemical composition of Hawaiian lavas1. *Journal of Petrology* **5**, 82-133.

Macdonald, R., Belkin, H. E., Fitton, J. G., Rogers, N. W., Nejbert, K., Tindle, A. G., & Marshall, A. S. (2008). The roles of fractional crystallization, magma mixing, crystal mush remobilization and volatile–melt interactions in the genesis of a young basalt–peralkaline rhyolite suite, the Greater Olkaria Volcanic Complex, Kenya Rift Valley. *Journal of Petrology* **49**, 1515-1547.

Mallmann, G. & O'Neill, H.St.C. (2007). The effect of oxygen fugacity on the partitioning of Re between crystals and silicate melt during mantle melting. *Geochimica et Cosmochimica Acta* **71**, 2837-2857.

REFERENCES

Mayfield, A., Bohrson, W.A., Hunt, R. & Creamer, J. (2011). Documenting magma evolution of the Fossa delle Felci (Salina Island, southern Tyrrhenian Sea) volcanic sequence through integration of quantitative modeling and in situ chemical analysis. Geological Society of America *Abstracts with Programs* **43**, 58.

McIntosh, W. C. & Ferguson, C. A. (1998). Sanidine, single-crystal, laser-fusion 40Ar/39Ar geochronology database for the Superstition volcanic field, central Arizona. Arizona Geological Survey. 74 p.

Reubi, O. & Blundy, J. (2009). A dearth of intermediate melts at subduction zone volcanoes and the petrogenesis of arc andesites. *Nature* **461**, 1269-1273.

Roeder, P. L. & Emslie, R. (1970). Olivine-liquid equilibrium. *Contributions to Mineralogy and Petrology* **29**, 275-289.

Rudnick, R. L. & Fountain, D. M. (1995). Nature and composition of the continental crust: a lower crustal perspective. *Reviews of Geophysics* **33**, 267-309.

Rudnick, R. L., & Gao, S. (2003). Composition of the continental crust. *Treatise on Geochemistry* **3**, 1-64.

Shafiqullah, M., Damon, P. E., Lynch, D. J., Reynolds, S. J., Rehrig, W. A. & Raymond, R. H. (1980). K-Ar geochronology and geologic history of southwestern Arizona and adjacent areas. *Ariz. Geol. Soc. Dig*. **12**, 201-260.

Singer, K. I. (2009). Miocene magmatism in the southwestern Basin and Range province: mineralogy, petrology, and geochemistry of the Stewart Mountain basalt field, central Arizona. Masters Thesis, North Carolina State University. 56 p.

Singer, K. I. & Fodor, R. V. (2013). Petrology of Stewart Mountain basalt field in central Arizona, USA: A lithospheric source with small-scale trace element and isotopic heterogeneities. *Rocky Mountain Geology* **48**, 185-210.

Skotnicki, S. (1992). Geology of the Sycamore Creek region, Maricopa County, Arizona. Masters Thesis, Arizona State University. 126 p.

REFERENCES

Skotnicki, S. J. & Leighty, R. S. (1997). Geologic map of the Stewart Mountain Quadrangle, Maricopa County, Arizona. Arizona Geological Survey. 19 p.

Spencer, J. E., Richard, S. M., Reynolds, S.J., Miller, R.J., Shafiqullah, M., Gilbert, W.G. & Grubensky, M.J. (1995). Spatial and temporal relationships between mid-Tertiary magmatism and extension in southwestern Arizona. *Journal of Geophysical Research* **100**, 10,321-10,351.

APPENDICES

Appendix A

Petrographic descriptions of Sugarloaf lavas

Basalt descriptions

SU-5 is porphyritic; modal percentages for phenocrysts are ≈11 vol. % clinopyroxene and 7 vol. % olivine. Clinopyroxene phenocrysts are anhedral to subhedral and up to 1.5 mm in size but usually 0.5 mm or less. Olivine phenocrysts are subhedral and as large as 2 mm in size but 1 mm on average. Olivine is largely iddingsitized, with some grains having iddingsite only as a thin margin and some completely iddingsitized. The groundmass is intergranular and composed of plagioclase, olivine as iddingsite, clinopyroxene, Fe-Ti oxide, and interstitial feldspar.

P-4 is porphyritic; modal percentages of phenocrysts are ≈15 vol. % clinopyroxene, 7 vol. % olivine, and 3 vol. % opaque minerals. Clinopyroxene grains are subhedral and about 1 mm in size on average, but some grains are as large as 3 mm. Olivine grains are typically anhedral to subhedral and range from 0.5–2.5 mm in size. All olivine grains are iddingsitized, but fresh olivine remains in some cores. Much of the clinopyroxene occurs as glomerocrysts. Fe-Ti oxide is subhedral to anhedral and ≈1 mm in size. The groundmass is intergranular and composed of plagioclase, olivine as iddingsite, clinopyroxene, Fe-Ti oxide, and interstitial feldspar.

P-5 is porphyritic; modal percentages of phenocrysts are ≈11 vol. % clinopyroxene and 5 vol. % olivine. Clinopyroxene grains are subhedral, average less than 1 mm in size, and often occur in glomerocrysts. Olivine grains are anhedral to subhedral and about 0.5 mm to 1–2 mm in size. Some olivine grains are completely iddingsitized, while others have fresh areas. The groundmass is intergranular and composed of plagioclase, olivine as iddingsite, clinopyroxene, Fe-Ti oxide, and interstitial feldspar.

SL-6 is porphyritic; modal percentages for phenocrysts are ≈9 vol. % clinopyroxene and 2 vol. % olivine. Clinopyroxene grains are subhedral, have hourglass zoning and are up to 1 mm but more often 0.5 mm in size or less. Olivine grains are subhedral, partially iddingsitized, and ≈1 mm or less in size. The groundmass is micro-hyaloophitic with interstitial dark glass containing plagioclase microlites and rusty Fe-Ti oxides.

Basaltic andesite descriptions

SL-1 is porphyritic; modal percentages for phenocrysts are ≈3 vol. % plagioclase, 2 vol. % olivine, 1 vol. % amphibole, 1 vol. % quartz, 1 vol. % clinopyroxene, and trace orthopyroxene. Plagioclase grains are ≈1 mm in size and subrounded, some with reaction margins surrounded by a thin plagioclase rim, and some that are spongy throughout. Sanidine is present in trace amounts and exhibits highly resorbed rims. Olivine grains range from ≈1–2 mm in size, and some have iddingsite rims. Amphibole grains are subhedral, typically about 1 mm in size and subrounded. Quartz grains are subrounded, have reaction rims, and are ≈1.25 mm in size on average. Clinopyroxene is subhedral and ranges from 0.5–3 mm in size. The groundmass is glassy and contains microlites of plagioclase and Fe-Ti oxide. About 5% of this sample is vesicular.

SL-2 is porphyritic; modal percentages for phenocrysts are ≈5 vol. % plagioclase, 3 vol. % quartz, 1 vol. % olivine, 1 vol. % clinopyroxene, and 1 vol. % amphibole. Plagioclase grains are subhedral, spongy, and 0.5–4 mm in size. Quartz grains are anhedral, subrounded, ≈2 mm in size, and have reaction rims. Olivine grains are subhedral to near-euhedral, 1–2.5 mm in size, and have thin iddingsite rims. Clinopyroxene grains are subhedral and ≈1 mm in size. Amphibole grains are subhedral, subrounded and 0.5–1.5 mm in size. The groundmass is glassy and contains microlites of plagioclase and Fe-Ti oxide. About 5% of this sample contains small (≈0.5 mm or less) round vesicles.

SL-3 is porphyritic; modal percentages for phenocrysts and lithic fragments are ≈6 vol. % plagioclase, 3 vol. % lithic fragment, 3 vol. % clinopyroxene, 1 vol. % amphibole, 1 vol. % Fe-Ti oxides, 0.1 vol. % olivine, rare quartz with reaction rim, and rare biotite. Plagioclase grains are subhedral, andhedral and subrounded; 1–3 mm in size; and some have corrodal reaction rims or spongy cores. Clinopyroxene grains are subhedral, elongate and ≈1 mm in size. Amphibole grains are subhedral to subrounded, have opaque, oxidized rims and are 0.5–1.5 mm in size. Fe-Ti oxide grains are anhedral and up to ≈0.5 mm. The basaltic lithic fragment contains iddingsitized olivine, clinopyroxene and feldspar laths. Rare olivine grains are iddingsitized and ≈0.5 mm in size. A single observed biotite is surrounded by Fe-Ti oxide grains. The groundmass is glassy and contains microlites of plagioclase, Fe-Ti oxide, and clinopyroxene.

SL-4 is porphyritic; modal percentages for phenocrysts are ≈2 vol. % plagioclase, 2 vol. % clinopyroxene, 1 vol. % olivine, 1 vol. % quartz, 1 vol. % amphibole, and rare biotite. Plagioclase grains are subhedral, spongy, 0.5–2 mm in size and exhibit a calcic rim surrounding a core of attacked sodic plagioclase. Clinopyroxene grains are subhedral and 0.5–2 mm in size. Olivine grains are euhedral, slightly iddingsitized, and ≈1 mm in size. Quartz grains are anhedral, ≈2 mm in size and have reaction rims. Amphibole is subhedral, subrounded, and ≈1 mm in size. Periite is present as an accessory mineral. The groundmass is glassy and contains microlites of feldspar and Fe-Ti oxides.

SL-5 is porphyritic; modal percentages for phenocrysts are ≈6 vol. % plagioclase, 1 vol. % quartz, 1 vol. % amphibole, 1 vol. % olivine, 0.3 vol. % clinopyroxene, and rare biotite. Plagioclase grains are subhedral to subrounded and 0.5–2 mm in size. Most have spongy margins or cores, and some have thin (< 10 μ) rims of plagioclase that surround spongy margins. Quartz grains are subrounded, 1–1.5 mm in size and have reaction rims. Hornblende grains are subhedral, subrounded and ≈0.5 mm in size. Olivine is subhedral and 1–2.5 mm in size. Iddingsite is present in some olivine grains. Clinopyroxene grains are ≈1 mm in size. Rare biotite is ≈1 mm long and has jagged margins surrounded by a thin rim of plagioclase and Fe-Ti oxide grains. The groundmass is glassy and contains microlites of plagioclase and Fe-Ti oxide.

P-2 is porphyritic; modal percentages for phenocrysts are ≈2 vol. % plagioclase, 1 vol. % amphibole, 1 vol. % clinopyroxene, and 0.3 vol. % quartz. Plagioclase grains are subhedral, typically 1 mm but up to 3 mm in size, spongy, zoned and zebra-striped. Amphibole is subhedral, subrounded and ≈1 mm in size. Clinopyroxene is subhedral and ranges from 0.5–2.5 mm but typically less than 1 mm in size. There is one quartz phenocryst ≈1 mm in size. The groundmass is glassy and contains microlites of plagioclase and Fe-Ti oxides.

P-3 is porphyritic; modal percentages for phenocrysts are ≈3 vol. % plagioclase, 2 vol. % clinopyroxene, and 2 vol. % amphibole. Plagioclase grains are subhedral, spongy, and range from 1–3 mm in size. Clinopyroxene grains are subhedral and range from 0.5–3 mm in size. Amphibole grains are subhedral, subrounded and range from 0.5–1.5 mm in size. The groundmass is glassy and contains microlites of plagioclase and Fe-Ti oxides.

Andesite descriptions

SU-1 is porphyritic; modal percentages for phenocrysts are 6 vol. % plagioclase, 3 vol. % amphibole, 1 vol. % clinopyroxene, and 0.5 vol. % quartz. Plagioclase is subhedral, ranges from 0.5–2 mm and is twinned. Amphibole grains are subhedral and range from 0.5–3 mm in size. Clinopyroxene grains are augite, subhedral and range from 1–2 mm in size. Augite phenocrysts show inclined extinction, low birefringence, and zoning. Fe-Ti oxide phenocrysts are small and anhedral. The groundmass is glassy and contains microlites of plagioclase and Fe-Ti oxides. About 5% of this sample has vesicles.

SU-2 is porphyritic; modal percentages for phenocrysts are ≈9 vol. % clinopyroxene, 3 vol. % plagioclase, 0.2 vol. % quartz, and 0.1 vol. % amphibole. Clinopyroxene is anhedral to euhedral and ranges from 0.5–2 mm in size. Plagioclase grains are subhedral, range from 1–3 mm, and are spongy. Quartz grains are subrounded, anhedral, 1 mm in size, and have reaction rims. Amphibole ranges from 0.5–3 mm in size. The groundmass is glassy and contains microlites of plagioclase and Fe-Ti oxides. About 10% of this sample contains vesicles.

SU-3 is porphyritic; modal percentages for phenocrysts are ≈8 vol. % clinopyroxene, 5 vol. % plagioclase, 2 vol. % amphibole, and 1 vol. % quartz. Clinopyroxene is subhedral and ranges from 0.5–1.5 mm in size. Plagioclase grains are typically anhedral, range from 1–3 mm, and are zoned and spongy. Amphibole grains are subrounded, subhedral and range from ≈0.5–3 mm in size. Quartz grains are subrounded and anhedral, are ≈1 mm in size, and have reaction rims. The groundmass is glassy and contains microlites of plagioclase, Fe-Ti oxides, and olivine. About 5% of this sample contains vesicles.

SU-4 is porphyritic. Modal percentages for phenocrysts are ≈5 vol. % clinopyroxene, 5 vol. % plagioclase, 1.5 vol. % quartz, and 1 vol. % amphibole. Clinopyroxene grains are anhedral to near-euhedral and range from 0.5–4 mm in size. Amphibole grains are subhedral to near-euhedral and range from 0.5–2 mm in size. Plagioclase grains range from anhedral to subrounded, are ≈1 mm in size, and generally have reactive margins or spongy rims. Quartz is generally subrounded, ≈1–2 mm in size, and some have reaction rims. The groundmass is a dark glass and contains microlites of plagioclase, clinopyroxene, and Fe-Ti oxides. About 10% of this sample contains small (≈0.5 mm or less) round vesicles.

P-1 is porphyritic; modal percentages for phenocrysts are ≈3 vol. % plagioclase, 1 vol. % amphibole, 1 vol. % clinopyroxene, and 0.5 vol. % olivine. Plagioclase phenocrysts have spongy boundaries and are ≈3 mm and zoned or ≈3 mm and broken with some indications of zoning in large enough grains. Amphibole phenocrysts are ≈0.5 mm in size and identified as hornblende based on 120/60 angle. Clinopyroxene grains are subhedral and 0.5–4 mm in size. Olivine grains are ≈1 mm in size and show no crystal outline but pink birefringence and a rim that has altered to a yellow clay but not to iddingsite. The groundmass is glassy and contains microlites of plagioclase, Fe-Ti oxides and clinopyroxene. About 5% of this sample contains vesicles.

Appendix B

Table 17: Latitudes and longitudes for the locations of samples taken from Sugarloaf Mountain, central Arizona

	Latitude	Longitude
P-5	33°41'12.06"N	111°31'9.12"W
SU-5	33°41'15.20"N	111°31'17.20"W
SL-6	33°41'43.44"N	111°31'2.52"W
P-4	33°41'43.21"N	111°31'44.44"W
SL-4	33°41'40.42"N	111°31'16.41"W
SL-1	33°41'15.54"N	111°31'19.08"W
P-3	33°41'44.53"N	111°31'45.73"W
SU-2	33°41'40.00"N	111°31'35.91"W
SU-1	33°41'38.29"N	111°31'13.50"W
SL-2	33°41'19.92"N	111°31'14.70"W
SU-4	33°41'42.40"N	111°31'42.60"W
SU-3	33°41'41.70"N	111°31'40.80"W
SL-3	33°41'38.46"N	111°31'13.14"W
P-1	33°41'47.52"N	111°31'51.30"W
P-2	33°41'45.34"N	111°31'47.38"W
SL-5	33°41'41.16"N	111°31'18.42"W